Evaluation of polymeric nanocarriers for RNA delivery

Dissertation

zur Erlangung des Grades

"Doktor der Naturwissenschaften"

im Promotionsfach Pharmazie

am Fachbereich Chemie, Pharmazie und Geowissenschaften

der Johannes Gutenberg-Universität

in Mainz

vorgelegt von

Bettina Sarah Krieg

geboren in Mainz

Mainz, im September 2014

Die vorgelegte Dissertation wurde am Institut für Pharmazie und Biochemie der Johannes Gutenberg-Universität in Mainz zur Erlangung des Grades "Doktor der Naturwissenschaften" angefertigt.

Hiermit versichere ich eidesstattlich:

1. Ich habe die jetzt als Dissertation vorgelegte Arbeit selbst angefertigt und alle benutzten Hilfsmittel (Literatur, Apparaturen, Material) in der Arbeit angegeben.
2. Ich habe oder hatte die jetzt als Dissertation vorgelegte Arbeit nicht als Prüfungsarbeit für eine staatliche oder andere wissenschaftliche Prüfung eingereicht.
3. Ich hatte weder die jetzt als Dissertation vorgelegte Arbeit noch Teile davon bei einer anderen Fakultät bzw. einem anderen Fachbereich als Dissertation eingereicht.

Ort, Datum Bettina Krieg

Danksagung

Abstract

Therapeutic RNAs, especially siRNAs, are a promising approach for treating diseases like cancer, neurodegenerative disorders and viral infections. Their application, however, is limited due to a lack of safe and efficient delivery systems. Nanosized carriers with the ability to either complex or entrap RNA species are a promising option.

Such a carrier has to meet a lot of requirements, some of which are even partly contradictive. Understanding and controlling the interplay between the different demands would advance a strategic design at an early stage of therapeutic development.

This work is centered around a systematic evaluation of polyplexes, such carriers that are able to complex siRNA due to electrostatic interactions. Six structurally and chemically diverse candidates, poly-L-lysine brushes, block copolymers, cationic peptides, cationic lipids, nanohydrogels, and manganese oxide particles, were tested in a simultaneous fashion. The assays, mostly based on fluorescently labeled siRNA, ranged from the evaluation of polyplex formation and stability to *in vitro* parameters like cellular uptake and knockdown capability. The analysis from several perspectives offered insight into the interplay between the specifications of one polyplex. Assessing the different carriers under exactly the same experimental conditions also allowed conclusions about favourable traits and starting points for further optimization. This comparative approach also revealed weaknesses of some of the conventional protocols, which were therefore contrasted with alternative methods. In addition, *in vitro* knockdown assays were optimized and the impact of fluorescently labeled siRNA on knockdown efficiency was assessed.

A second class of carriers, which share the ability to entrap siRNA inside their matrix, are briefly addressed. Nanocapsules, dextran particles and liposomes were assessed for basic features like siRNA encapsulation and knockdown capability.

In an approach towards targeted delivery of RNA, liposomes were endowed with mitochondriotropic tags. Despite successful functionalization, no colocalization between the liposomal cargo and mitochondria was so far observed, which makes further optimization necessary.

Zusammenfassung

Therapeutische Ribonukleinsäuren, vor allem siRNA, stellen eine vielversprechende Behandlungsoption für eine Vielzahl von Krankheiten dar. Ihre Anwendung ist jedoch eingeschränkt aufgrund der Schwierigkeit, ein sicheres und effizientes Transportsystem zu finden. Der Transport von siRNA mit Hilfe nanometergroßer Polymere, die siRNA entweder einschließen oder komplexieren, stellt eine aussichtsreiche Strategie dar.

Ein solches Transportsystem muss eine Reihe von Anforderungen erfüllen, von denen einige sich sogar teilweise widersprechen. Ein strategisches Design solcher Systeme könnte vorangebracht werden, wenn es gelänge, das Zusammenspiel zwischen den verschiedenen Anforderungen zu verstehen und zu kontrollieren.

Diese Arbeit beschäftigt sich schwerpunktmäßig mit einer systematischen Evaluation von Polymeren, die mit siRNA aufgrund elektrostatischer Wechselwirkungen Polyplexe bilden. Dazu wurden sechs Kandidaten, Poly-L-Lysin Bürsten, Block Kopolymere, kationische Peptide, kationische Lipide, Nanohydrogele und Manganoxidpartikel, vergleichend untersucht. Die angewandten Tests überprüften Polyplexbildung und -stabilität sowie *in vitro* Parameter wie zelluläre Aufnahme und Knockdown Effizienz. Diese Analyse ermöglichte es, Stärken und Schwächen einzelner Polyplexe sowie Ansatzpunkte für deren Optimierung herauszuarbeiten.

Der Vergleich zeigte darüber hinaus Schwachpunkte einiger etablierter Protokolle, denen aus diesem Grund alternative Methoden gegenübergestellt wurden. Zudem wurden *in vitro* Knockdown Tests optimiert sowie der Einfluss von fluoreszenzgelabelter siRNA auf die Knockdown Effizienz untersucht.

Eine weitere Klasse von Trägern, deren Bindungsprinzip im Einschluss von siRNA besteht, wurde kurz gestreift. Dabei wurden Nanokapseln, Dextranpartikel und Liposomen im Hinblick auf siRNA Einschluss sowie Knockdown Effizienz untersucht.

Ein erster Schritt hin zu einem zielgerichteten Transport von RNA wurde unternommen, indem Liposomen mit mitochondriotropen Gruppen versehen wurden. Da bislang keine Kolokalisation der in die Liposomen eingeschlossenen Fracht mit Mitochondrien festgestellt werden konnte, ist eine weitere Optimierung nötig.

Contents

List of Figures

List of Tables

1 Introduction

1.1 RNA interference - a promising therapeutic strategy

RNA interference (RNAi) is a powerful cellular tool that is mediated by small interfering ribonucleic acids (siRNA) and causes specific gene silencing on a post transcriptional level. A short RNA strand that is complementary to a target messenger (m) RNA is incorporated into an enzymatic unit called RNA induced silencing complex (RISC), which leads to an efficient and specific degradation of the target mRNA. RNAi is one amongst the mechanisms that have broadened the view on RNA during the last decades. While Francis Crick's dogma of molecular biology from 1958 [1] regarded RNA mainly as a messenger between deoxyribonucleic acids (DNA) and protein, the essential role of RNA species like siRNA, micro (mi) RNA and piwi interacting (pi) RNA [2] in the regulation of gene expression has become evident by now and opened up new strategies for both basic research and therapeutic interventions. Especially siRNA has a great potential not only for loss of function studies, but also for treating diseases by the specific knockdown of pathogenic genes.

1.1.1 Short history of siRNA research

In 1990, Napoli and Jorgensen overexpressed an enzyme responsible for the blue color of petunia petals to intensify the coloring, but observed white petals instead [3]. They explained this outcome by a "cosuppression" of the endogenous gene, not being aware that they had actually encountered an RNAi effect. This effect was not understood until 1998, when Fire and Mello made the seminal observation that the injection of double stranded (ds) RNA in C. elegans causes a 100x more efficient gene silencing than the injection of a single strand targeting the same mRNA, which led to the elucidation of the RNAi mechanism [4]. They were awarded the Nobel Prize in Medicine and Physiology in 2006. In the following years, there were increasing signs that these

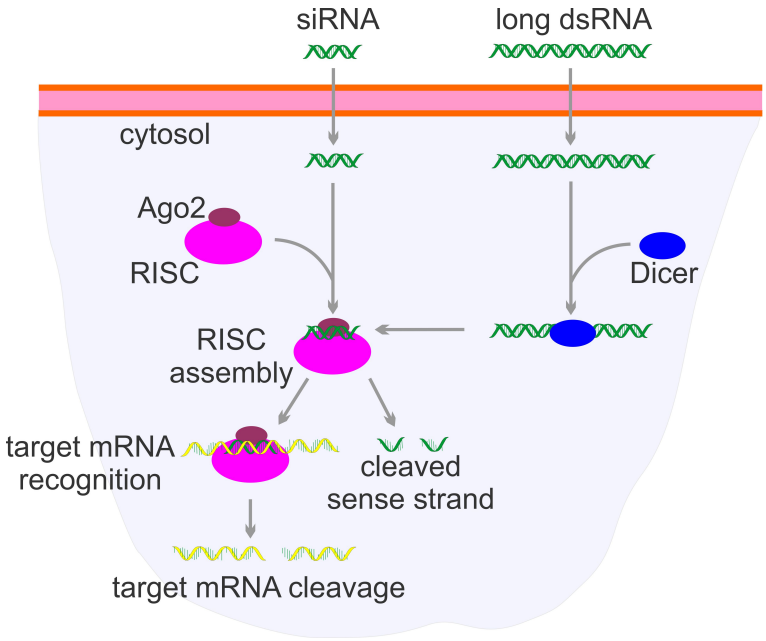

Figure 1.1: Essential components of the RNAi process, adapted from Whitehead 2009 [11].

dsRNAs are processed to 21-23 nucleotides long double strands that constitute a silencing intermediate [5, 6]. So far, a strong interferon response after the introduction of long dsRNA had prohibited any application in mammals. In 2001, Elbashir and Tuschl were the first to make RNAi work in mammalian cells, when they managed to circumvent this immune response by directly transfecting the small double strands, referred to as siRNAs [7]. The further elucidation of the RNAi mechanism included the identification of Dicer as the enzyme responsible for siRNA processing [6, 8], RISC as the enzymatic entity that mediates mRNA degradation [9] and the process by which the antisense strand is incorporated into RISC [10].

By now, RNAi has become a common method for *in vitro* gene function studies [12] and has already shown *in vivo* efficiency in mice [13] and humans [14]. In addition, a large range of RNAi based drugs have been developed and tested in clinical trials [15, 16].

1.1.2 Therapeutic potential of RNAi

Having a mechanism at hand that enables the specific silencing of a target gene opens up a broad range of applications. RNAi may also be advantageous over gene therapy, as it acts on a post transcriptional level, thereby circumventing riscs associated with the direct manipulation of DNA [17]. RNAi strategies that are currently in clinical

trials cover - among others - targets associated with cancer, cardiovascular diseases, macula degeneration, viral infections and asthma [15]. For example in cancer therapy, RNAi targeting cancer specific genes like the signal transducer and activator of transcription 3 (STAT3) or the vascular endothelial growth factor (VEGF) [18] appears promising. RNAi may also provide the possibility to drug yet "undruggable" targets [19]. Local administration of naked siRNA to the eye or the lung is currently in clinical trial (phase 1 and 2) [15]. Systemic siRNA delivery has also reached this status, in most cases with lipid nanoparticle formulations [15].

1.1.3 Rendering siRNA applicable

While the rational design of siRNA sequences is sufficiently advanced [20, 21], the bottleneck for a systemic application of siRNA is finding a strategy for its efficient delivery. Although uptake of naked siRNA has been reported for special cell types [22], it is in general inefficient because of the polyanionic character of siRNA and its size [23]. In addition, the very unstable siRNA has to be protected from e.g. degrading enzymes in the physiological environment before it reaches its target site [24].

Electroporation [25] or transfection with commercial available cationic lipids [26] are standard *in vitro* methods. Electroporation has been reported for *in vivo* transfection of dermal tissue [23], but this method is not available for a systemic application. *In vivo* use of the highly efficient cationic lipids has so far been hampered by their toxicity [27, 28].

Stable expression of small hairpin (sh) RNA has been achieved via viral transduction in mice [29, 30]. As, however, viral vectors for DNA delivery have shown severe and unpredictable side effects in clinical trials [31], they may not be the method of choice.

Chemical modification of siRNA is another way to improve *in vivo* features. Via modifications on the phosphate, the ribose or the bases, serum stability [32] and immunogenicity of siRNA [33, 34] can be controlled. Covalent attachment of e.g. lipids or cell penetrating peptides can mediate cellular uptake [35, 36].

A strategy that is intensively pursued at the moment is the application of polymeric nanosized carriers for siRNA delivery [37]. Carriers can either bind siRNA due to electrostatic interactions, forming so called polyplexes [38], or can entrap siRNA in their matrix [39]. Successful *in vitro* [40–43] and *in vivo* experiments [38, 44] are reported for various approaches. Still, a thorough understanding of the conditions that turn such a carrier into an efficient delivery vehicle is lacking.

It should be mentioned that the research on efficient DNA delivery also involves

polymeric carriers. However, a clear distinction should be made between these two kinds of nucleic acids. Structure, size, stability and site of action are just a few of the differences that require a specific optimization of the carrier for each payload [45, 46].

1.2 Polyplexes: characteristics and requirements

This section provides a theoretical background for the key issue of this work, the investigation of polyplexes. Studies are discussed that monitor the influence of specific polyplex features on biological activity (for siRNA: knockdown capability) and toxicity, parameters that determine if a polyplex is suitable for siRNA delivery.

Studies on DNA polyplexes are also considered, as most carriers are tested for both DNA and siRNA delivery, and systematic approaches are more abundant for DNA. It can be assumed that similar parameters are essential for both kinds of nucleic acids, while the optimal specification of one carrier will be cargo specific.

1.2.1 Polyplex formation

Polyplexes have to bind siRNA efficiently during transport to their site of action. For an *in vivo* application, this means stable binding is required in the blood stream and during cellular entry. siRNA has to be able to move inside a polyplex during the process of complexation, therefore polyplexes do not possess a distinct separation from their surrounding (see figure 1.2). Binding is determined by electrostatic interactions between the siRNA's negatively charged phosphates and the positively charged moieties of the carrier.

In the following, it will be necessary to refer to the uncomplexed forms of the different carriers in a standardized way, though being aware of their structural heterogeneity. Therefore the term monomer is used for the smallest unit of an uncomplexed carrier, may it be a small entity (e.g. a lipid or an oligopeptide), a polymer, or a particle.

To describe the binding conditions of a polyplex, several parameters have been introduced.

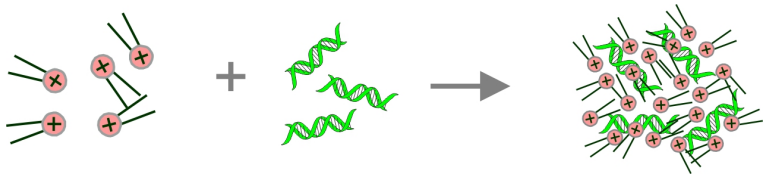

Figure 1.2: Scheme of the polyplex formation process exemplified by cationic lipids.

The m/m ratio represents the mass of the monomers in relation to the mass of siRNA in a polyplex [41]. While this parameter is a useful working tool, it does not make much statements about specific polyplex characteristics.

The molar ratio between monomers and siRNA is another way to calculate quantity proportions [47, 48].

A more meaningful parameter is the N/P ratio, the ratio of positive charges of the monomers (mostly conveyed by **N**itrogen containing moieties) and the negative charges of the siRNA (from its **P**hosphate backbone).

This ratio can be calculated for a polyplex from the following data:

- mass/mass ratio (m/m) of monomers and siRNA
- molecular weight (M_W) of a monomer and siRNA
- number of charges per monomer and siRNA

The minimal N/P needed for complete binding of siRNA reflects how efficiently a carrier can make use of its charges.

The N/P is considered to influence the structure of a polyplex. Studies have pointed out that the N/P has to be carefully controlled to optimize knockdown efficiency and biocompatibility. In a homologous series of arginine rich peptides, higher N/Ps led to less stable and bigger polyplexes, as the excess positive charges repulse each other [48]. A comparable effect was observed for poly(ethylene)glycol - poly(2-dimethylamino)ethyl methacrylate (PEG-pDMAEMA) derivatives, where excess positive charges did not contribute to polyplex formation but created an additional population of uncomplexed monomers that increased toxicity (see section 1.2.6) [49]. A similar observation was made for poly-L-lysine (PLL) and poly(amido amine) (PAMAM) in all-atomic molecular dynamics simulations [50]. In a study with poly(ethylene)imine (PEI), an improved knockdown effect was found at low N/P ratios [51]. This suggests that an N/P near charge neutralization is beneficial [49, 51].

1.2.2 Polyplex stability

Given that a carrier can bind siRNA at a certain N/P, the question about the stability of this binding arises. Polyplex stability is a particularly important parameter, as it balances two rather contradictive requirements [52, 53]:

During the transfection process, a polyplex has to first protect its cargo and, at the site of action, release it. Though the dissociation of a polyplex has been described as

the critical step during transfection [54, 55], it is clear that a certain degree of stability is equally essential.

These opposite requirements are well illustrated by a study that was carried out for a series of DNA - methacrylate polymers, where stability was determined by anion competition as well as nuclease resistance (see section 1.4.3) and its influence on transgene expression investigated. It was found that neither too low nor too high stability was beneficial [54]. A study addressing a comparable question by time resolved fluorescence spectroscopy observed a lower stability for poly(ethylene)imine (PEI) compared to PLL as tested by anion competition (see section 1.4.3). This coincided with a better transgene expression for PEI [55].

A study that regarded DNA and siRNA complexation in parallel approached the question of stability by systematically controlling a polymer's charge density. This parameter is defined by the number of charges and their spatial arrangement in the polymer [56]. The experimentalists compared pDMAEMA that contains one positive charge per monomer with poly(3,5-bis(dimethylaminomethylene)- p-hydroxyl styrene) (QNPHOS), a polymer that comprises two quaternized amines with two permanent positive charges per monomer. The higher charge density for QNPHOS led to enhanced stability as shown by heparin competition (see section 1.4.3), that also resulted in improved knockdown efficiency for siRNA. In contrast, QNPHOS could not mediate transgene expression after transfection of DNA, presumably because the polyplex was so stable that no release was possible any more [57].

In addition to charge density [58], the accessibility of charges in a polymer is also influencing its stability [59]. Controlling this parameter however seems difficult, as the steric conditions in a polymer are hard to predict and may also substantially change during complexation.

These studies suggest that polyplex stability has to be carefully balanced to guarantee both protection and release of the cargo.

1.2.3 Surface charge

The surface charge of a polyplex is usually positive. Its degree has frequently been found to be correlated with transfection efficiency [58–60] (see section 1.2.4). As polyplexes with positively charged surfaces can electrostatically interact with the negatively charged proteins on the cell membranes, their uptake is enhanced [11, 60] and their aggregation among each other is reduced due to mutual repulsion [58]. In contrast to these positive features, high surface charge is also connected with enhanced cytotox-

icity because it facilitates interactions with the various negatively charged molecules in a physiological surrounding [61]. A major danger *in vivo* is polyplex aggregation with serum proteins, which can lead to capillary clogging [61].

For determining the surface charge of a polyplex, its zeta potential is measured, which is defined as the electrical potential at the slip plane between a particle and the bulk solution [62].

Surface charge can be reduced by lowering the N/P [49, 63], a process that has to be carefully balanced for still ensuring an efficient complexation (see section 1.2.1). Another way is to shield the charge from the surrounding by pegylation [64]: Decorating the particle surface with poly(ethylene)glycol) (PEG) lowered toxicity [52, 60, 65] and additionally served the purpose of preventing unspecific effects [66] (see section 1.2.8), but also led to reduced polyplex stability [64].

A certain tradeoff always has to be accepted when determining the optimal surface charge.

1.2.4 Cellular uptake

Cellular uptake is the starting point for the intracellular journey of a polyplex. The extent to which this process takes place is referred to as transfection efficiency. A clear distinction has to be made between efficient transfection and the actual ability of a polyplex to mediate a biological effect (for siRNA the knockdown of a specific gene), as the further intracellular processing determines if the transfected siRNA finally reaches its site of action, the cytosol.

Polyplexes cannot directly permeate cell membranes [67]. So the first step towards So their cellular uptake mainly takes place via endocytosis [68, 69], the vesicular uptake of extracellular macromolecules [67]. This process does not need mediation via a receptor, as polyplexes with positive surface charge can interact with negatively charged membrane proteins [38]. While this general statement holds true for the majority of polyplexes, studies have also determined alternative uptake routes for specific carriers [26, 70]. In the case that multiple uptake routes are found for one carrier, it also needs to be clarified which of these routes or combinations of them are responsible for mediating knockdown [71, 72] or if, in the case that one route is blocked, a change to an alternative pathway is possible [73].

Four major routes for endocytic uptake have been described and are depicted in figure 1.3 [69]:

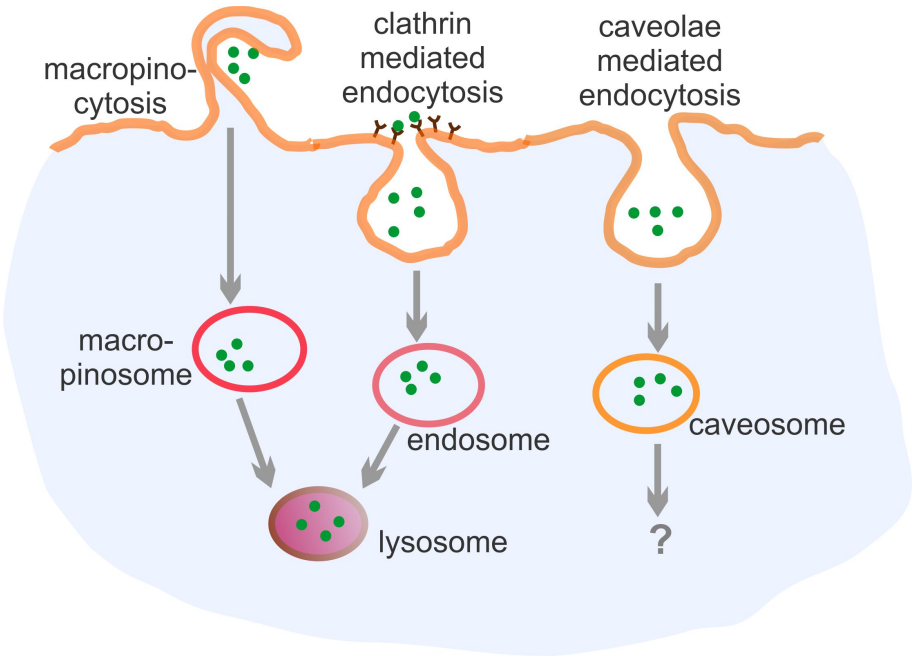

Figure 1.3: Uptake pathways, adapted from Agirre 2014 [74].

- clathrin mediated endocytosis
- receptor induced (clathrin mediated) endocytosis
- caveolae mediated endocytosis
- macropinocytosis
- in addition: clathrin and caveola independent endocytosis

Clathrin mediated endocytosis starts from the binding of a macromolecule to an adaptor molecule on the cell surface, e.g. the transferrin receptor [75]. In the following, clathrin coated pits invaginate and form vesicles with a diameter of about 100 nm, which pinch off from the plasma membrane [76]. While they are processed from early to late endosomes to finally fuse with lysosomes, their pH drops from 7.4 to 5.0. The main problem with polyplexes that enter via clathrin mediated endocytosis is that they may not be able to leave the endosomes, where they are destined for degradation [69].

By attaching a ligand for a receptor that is overexpressed on the surface of certain cell types, the targeting of special cell populations becomes possible (see section 1.2.8). In this case however, the uptake pathway is a priori determined to be clathrin mediated endocytosis, as this is the major route for receptor induced uptake [69].

Caveolae are small flask shaped membrane domaines that are rich in cholesterol and sphingolipids [77]. After association of macromolecules with these regions, caveosomes with a diameter of 50 nm pinch off, which are nonacidic and nondigestive. This process has the advantage that it does not end in lysosomes [77, 78].

Macropinocytosis is characterized by the formation of large vesicles up to 5 µm in diameter. Macropinosomes experience a drop in pH and destine their content for lysosomal degradation [69] but have been described as leaky, which facilitates the escape of their cargo [79].

Clathrin and caveola independent endocytosis summarizes a range of additional pathways that each rely on special uptake mechanisms [75].

This variety of pathways and fates that are connected with them shows that cellular uptake is only a prerequisite. It is rather the intracellular processing of polyplexes that determines if the desired biological effect (knockdown for siRNA, transgene expression for DNA) will occur [53], as, in the end, the cargo has to be available at its site of action, for siRNA the cytosol or for DNA the nucleus.

Attempts have been undertaken to modify carriers in order to promote one desired pathway. This can be achieved by endowing them with ligands [80, 81]. Another strategy is to influence the size of a polyplex. A study with latex beads stated that particles smaller than 200 nm are preferentially taken up via clathrin mediated endocytosis and larger particles of about 500 nm rather enter via the caveolar pathway [77]. This finding is quite contradictory to the size of 50 nm which has been mapped to caveosomes. However as it has been shown that also viruses enter via this pathway [69], it is evident that caveosomes can indeed engulf large particles.

1.2.5 Intracellular release

Cellular uptake involves the inclusion of polyplexes in vesicles, but siRNA can only be active if available in the cytosol [82], or in the nucleus [83], a case that is, however, not further discussed in this work.

The necessity of intracellular release out of these vesicles into the cytosol is evident [84, 85]. In the case of cellular uptake via endosomes, the escape from these compartments is also required for the reason that their cargo is destined for degradation in lysosomes (see section 1.2.4). Several mechanisms for endosomal escape are discussed [86].

Lipoplexes often consist of a cationic lipid, that ensures the complexation of the cargo, and a neutral helper lipid with fusogenic properties, e.g. 1,2-dioleoyl-sn-glycero-

3-phosphoethanolamine (DOPE). This helper lipid aids in adopting a non-lamellar hexagonal phase that promotes disorder of the endosomal membrane [87]. A second mechanism that is discussed for efficient lipoplex release into the cytosol is the so called "flip-flop" of anionic lipids that exchange places from the endosomal membrane into the lipoplex, thereby destabilizing both lipoplex and membrane [88].

The concept of a "proton sponge", though not definitely proven, is associated with polyplexes that possess a pH buffering capacity in the physiological range [89]. Such polyplexes with moieties like PEI or histidine with a pK_b between 7 and 9 are protonated during endosomal acidification. This buffering leads to further proton influx accompanied by their counterions into the endosomes, resulting in osmotic swelling and finally endosome disrupture [86]. It has been shown that attaching such moieties like histidine to otherwise non pH responsive carriers renders them endosomolytic [90]. pH dependent release triggers have also been developed for lipid carriers [91].

When discussing intracellular release, the impact of polyplex stability also has to be considered. Cytosolic availability requires not only endosomal escape, but also siRNA release from the polyplex, which can not take place if electrostatic interactions are too strong (see section 1.2.2).

1.2.6 Toxicity

For keeping toxicity as low as possible, polyplexes should be biocompatible, non immunogenic and, in the best case, even biodegradable [56]. High biological efficiency however is usually correlated with enhanced toxicity [92]. An increase in toxicity has been observed for high N/P ratios (see section 1.2.1) and high surface charge (see section 1.2.3). This also explains why the carrier alone is usually more toxic than its polyplex, as the incorporated nucleic acids reduce the overall charge [56].

Charge density has also been identified as a factor influencing toxicity [56].

Although a certain degree of toxicity may not be completely avoided, its level can be reduced by rendering the material as biocompatible as possible and keeping the administered doses low [26]. Again, the tradeoff between efficiency and toxicity has to be carefully balanced.

1.2.7 Size

In addition to controlling size to favour one cellular entry pathway (see section 1.2.4), studies have also tried to determine an optimal particle size for efficient transfection.

Studies with cationic lipids showed higher *in vitro* efficiencies for DNA lipoplexes with a diameter of 200 nm - 1 µm than for those of 100 nm in diameter [93]. One way to explain this could be the stronger sedimentation of larger particles that leads to better contact with the cells. Another explanation would be that larger lipoplexes preferentially enter via the more advantageous caveolar pathway because of their size (see section 1.2.4). The same correlation for polyplex size was found in an *in vitro* study for DNA-PEI-polyplexes with an optimal size of 70 kDa [94]. The findings of these studies are most probably not generally applicable, as the focus on merely size leaves apart all other features mediated by the material and the N/P of the polyplex.

When it comes to *in vivo* applications, the influence of size on biodistribution becomes another important factor [95]. A monodisperse size distribution is preferred [96, 97]. For a safe application, size changes in response to the surrounding conditions, e.g. the ionic strength [98], have to be controlled and aggregation of either particles among each other or with other proteins has to be avoided (see section 1.2.3).

An optimal carrier size between 10 - 50 nm for *in vivo* siRNA delivery has been proposed [99], as carriers of this size are too big for glomerular filtration (cutoff size of 10 nm [100]), but are still small enough to be endocytosed and not recognized by the reticuloendothelial system (RES) (cutoff size 100 nm [99]).

1.2.8 Functionalization

The functionalization of carriers opens up a range of possibilities for rendering polyplexes more efficient (see section 1.6). Even multifunctional approaches have been suggested, by endowing a carrier with a targeting ligand for cell specific uptake, a second shielding moiety like PEG to reduce unwanted interactions, and a third moiety

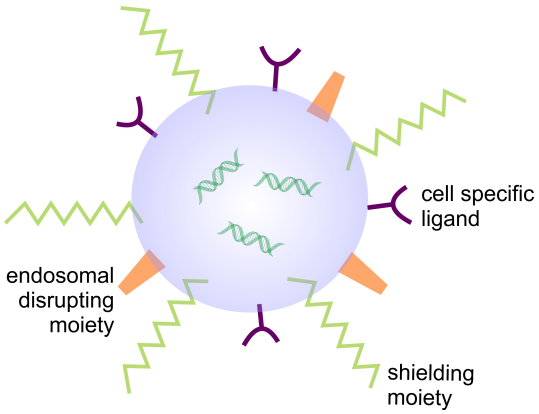

Figure 1.4: Scheme of a multifunctional carrier, adapted from Akhtar 2007 [67].

facilitating endosomal escape (see figure 1.4) [97]. For this purpose, a carrier needs functional groups that are amenable for covalent conjugation reactions, like amines for N-hydroxysuccinimide (NHS) ester chemistry or terminal alkynes for the Copper catalyzed azide alkyne cycloaddition (CuAAC) [101].

1.3 Polyplexes for siRNA delivery

Basically every polymer that possesses a certain number of positive charges should be able to interact with the negatively charged phosphate backbone of nucleic acids, forming a polyplex. One of the first materials employed for the purpose of gene delivery is PEI, that has been used in unmodified [102, 103] as well as modified (e.g. pegylated) [104–106] and targeted [107] versions. PLL is another carrier that is frequently used in many variations [108, 109]. PAMAM [92], polyvinylalcohol (PVA) [110], pDMAEMA [111], diaminobutane-dendrimer-(NH_2)64 (DAB) [111], chitosan [112], polycationic cell penetrating peptides (CPP) [41, 48] and cationic lipids like 1,2-dioleoyl-3-trimethylammonium-propane (DOTAP) [113] are only a few more of the materials that are able to form polyplexes.

The six positively charged carriers under investigation in this work each derive from a different class of material which makes the set chemically and structurally highly diverse. This section presents their material, build-up and key features as well as studies that have previously been conducted with these polyplexes.

1.3.1 Poly-L-lysine brushes

Creating macromolecules with special topologies employing cationic monomers as building blocks has been proposed as a strategy for DNA delivery with enhanced transgene expression and reduced cytotoxicity [114]. The poly-L-lysine polymers possess a polymethacrylate main chain on which side chains are grafted that consist of 55 PLL units each. As the positively charged side chains repulse each other, the molecule adopts a brush like shape [115]. siRNA was expected to arrange itself in the spaces between the side chains.

The PLL brushes have already shown the capability to complex plasmid DNA and have led to an efficient expression of eGFP plasmid in brain capillary endothelial cells - in contrast to linear PLL [116]. This suggested an uptake pathway apart from endocytosis for DNA-brush-complexes, as the lysines with a pK_b of 4 can not promote

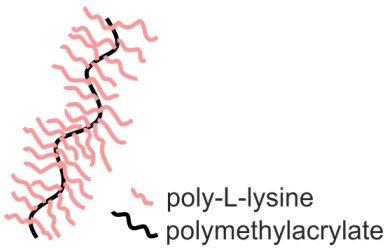

Figure 1.5: Scheme of poly-L-lysine brushes

endosomal escape. To enable this escape for PLL carriers, their modification with endosomolytic moieties is usually required (see section 1.2.5) [68, 90].

A study comprising a range of carriers found the highest toxicity for PLL (and PEI) [56]. The change in topology could not reduce cytotoxicity, as was shown by a direct comparison between linear PLL and PLL brushes [116], which makes low concentrations of this polyplex mandatory.

The PLL brushes were synthesized by xxxxxxxxxxxxxxxxx xxxxxxxxxxxxxxxx xxx [115].

1.3.2 Block copolymers

While most polymeric carriers rely on amines as cationic function, this polymer possesses guanidinium groups. It was designed to mimic cell penetrating peptides (CPPs), as their uptake is supposed to be mainly mediated by their arginine rich motifs [117], that also contain guanidinium moieties. Comparable polymers have already shown cellular uptake [118]. This polymer consists of the statistical copolymer N-(2-hydroxypropyl) methacrylamide-s-N-(3-aminopropyl) methacrylamide and a short terminal 3-guanidinopropyl methacrylamide block, (HPMA-s-APMA)-b-GPMA.

The HPMA moieties enhance water solubility and make the polymer less prone to serum aggregation, the APMA introduces an additional amino group for potential functionalization and the GPMA enables complexation of siRNA. The block copolymer was synthesized by xxxxxxxxxxx [119].

Figure 1.6: Scheme of block copolymers

1.3.3 Cationic peptides

These peptides do not try to mimic CPPs, but pursue a specific strategy to efficiently escape endosomes. The amphipathic, α-helical 26 residue long peptides contain 4 histidines and 4 lysines among alanines and leucines. While the lysines contribute to siRNA complexation, the histidines are able to mediate endosomal escape. With a pK_b of 8, protonation of histidine residues takes place during acidification in endosomes (see section 1.2.5), leading to peptide release from the polyplex that causes disorder of the endosomal membrane [41]. Polyplexes with the peptides have already proven their efficiency for plasmid [120] and siRNA transfection [41, 121] with tolerable toxicity and were kindly provided by xxx [41].

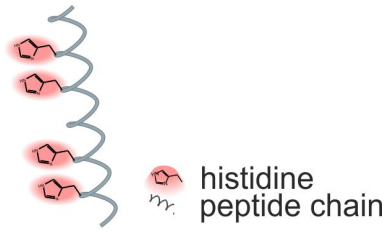

Figure 1.7: Scheme of cationic peptides

1.3.4 Cationic lipids

Cationic lipids are widely used as standard transfection agents for *in vitro* experiments. Their polyplexes are also referred to as lipoplexes. They are commercially available, highly efficient and have been optimized for different cargo like Lipofectamine^{TM} LTX for plasmid and Lipofectamine^{TM} RNAi max for siRNA delivery. The cationic lipid employed in this work is Oligofectamine^{TM}, which is preferably used for oligonucleotides. The formulations of these commercial products are mostly proprietary, it is however known that Lipofectamine^{TM} consists of 3 parts DOSPA (2,3-dioleyloxy-N-[2(spermine carboxamido) ethyl] -N,dimethyl-1-propanaminium trifluoroacetate) and 1 part DOPE

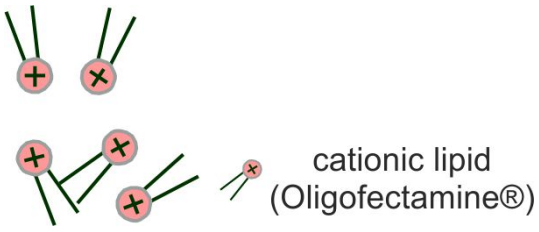

Figure 1.8: Scheme of cationic lipids

[93]. Employing a mixture of a cationic lipid (here the polycationic DOSPA) and an uncharged helper lipid with fusogenic properties (here DOPE) is a common strategy for promoting endosomal escape for lipid polyplexes. The flip-flop mechanism of anionic lipids from the endosomal membrane also supports intracellular release for lipoplexes (see section 1.2.5).

However, the toxicity of lipoplexes has to be carefully controlled before they can be rendered into safe *in vivo* agents [122]. This toxicity is mainly deriving from the polar head group and may be soothed by employing delocalized positive charges rather than quaternary or tertiary amines [27].

1.3.5 Nanohydrogel particles

These particles are formed from P(MEO_3MA)-b-P(PFPMA) block copolymers that consist of a block made from the hydrophilic monomer tri- (ethylene glycol)methyl ether methacrylate (MEO_3MA), that also conveys biocompatibility via its PEG moiety, and a second block of the hydrophobic pentafluorophenyl methacrylate (PFPMA). In dimethyl sulfoxide (DMSO), these polymers self-assemble into spherical structures with the PFPMA block in the core and the PEGylated MEO_3MA block on the surface. This spatial arrangement can be fixed by crosslinking the core with spermine linkers affording nanosized hydrogels. After this step, these nanohydrogels can be transferred to physiologic solvents like phosphate buffered saline (PBS) while keeping their spherical structure, even after complexation with siRNA, which results in preformed polyplexes [123, 124]. The positively charged spermine moities in the core serve in complexing siRNA. Nanohydrogels mediate cellular uptake of siRNA [123], their intracellular fate though has not yet become clear [125]. The nanohydrogels did not show toxictity at doses applied for knockdown studies [125].

The particles were synthesized by xxxxx xxxxx xxxxx xxxxx xxxxx xxxxx xxxxx [123].

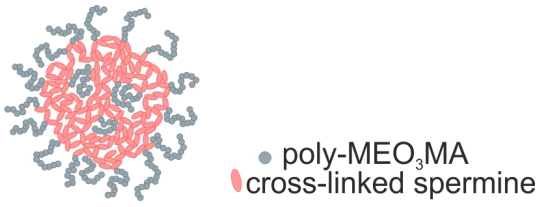

Figure 1.9: Scheme of nanohydrogel particles

1.3.6 MnO@SiO_2 particles

These particles are the only inorganic structures in the set and were initially developed for an application in magnetic resonance imaging. They are superparamagnetic core shell structures and consist of a manganese oxide (MnO) core that is encapsulated with a shell of silicon dioxide (SiO_2) functionalized with PEG and 3-aminopropyltriethoxysilane (APS) [126]. PEG conveys biocompatibility and APS mediates siRNA binding. In this case, the complexation takes places on the outer surface of the particle (in contrast to the nanohydrogels that possess amine functions located in the core), while the PEG chains are supposed to shield the siRNA from the surrounding. Their polyplexes are considered to be preformed like the nanohydrogels.

The particles were synthesized by xxxxx xxxxx xxxxx xxxxx xxxxx xxxxx xxxxx [126].

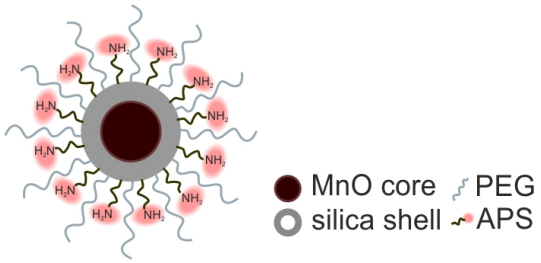

Figure 1.10: Scheme of manganese oxide particles

1.4 Methods for the evaluation of polyplexes

The evaluation of polyplexes comprises a range of methods each focussing on a specific feature. This section introduces the methods that are employed in this work and describes selective studies in which they have already been applied. Subsequently, the results section discusses strengths and weaknesses of each method in view of the conducted experiments, as well as differences between alternative methods.

Most of the methods require a fluorescent label on the siRNA [127, 128]. Some even employ a double labeling resulting in a Förster resonance energy transfer (FRET) effect that reveals the siRNA's integrity status [129–131].

1.4.1 Prerequisite: Fluorescently labeled siRNA

Förster resonance energy transfer

FRET is the physical process by which energy is transferred non-radiatively from an excited chromophore (the donor) to another chromophore (the acceptor) and has found numerous applications in the life sciences [132, 133]. FRET can overcome distances from 1 nm to 10 nm and declines with rising distance. The FRET efficiency, defined as the fraction of energy transferred, depends on the distance between donor and acceptor with an inverse 6th order law (see equation 1.1) [134]. The constant R_0 in the equation is the FRET pair specific Förster radius, the distance between the fluorophores with half maximal FRET efficiency.

$$E_{FRET} = \frac{1}{1 + \left(\frac{r}{R_0}\right)^6} \qquad \text{(equation 1.1)}$$

FRET is most efficient when the dipole moment of donor and acceptor are oriented parallel to each other [133]. The donor and acceptor dye (the FRET pair) also have to show an appropriate spectral overlap of the donor emission and the acceptor absorption spectrum (see figure 1.11 A). However, when donor and acceptor spectra are too close, crosstalk becomes an issue. This phenomenon occurs when the excitation and/or emission spectra of two or more fluorophores in a specimen overlap, which makes it difficult to isolate the activity of one fluorophore alone [135]. Crosstalk can be divided into cross excitation and bleedthrough [136]. Cross excitation arises when a second fluorophore is also excited by the wavelength that is employed for the fluorophore of interest. Bleedthrough takes place when a second fluorophore also emits in the channel that has been defined for the fluorophore of interest [136].

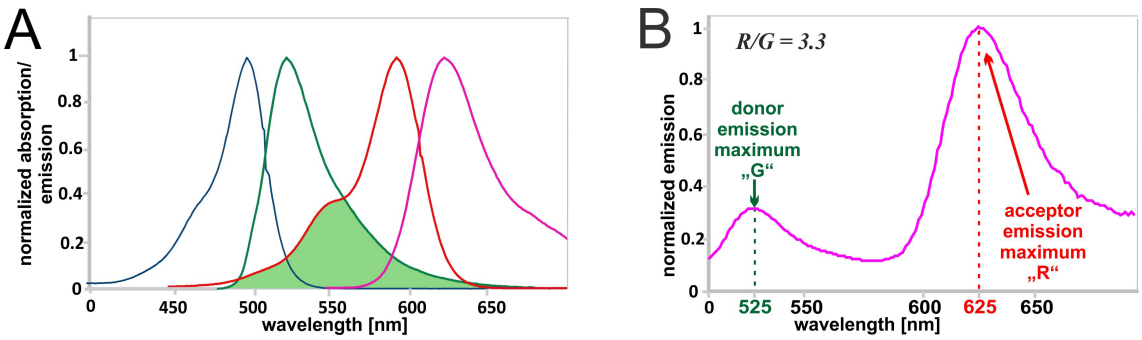

Figure 1.11: (A) Spectral overlap of the donor Atto 488 and the acceptor Atto 590 causing FRET, (blue) donor excitation spectrum, (green) donor emission spectrum, (red) donor excitation spectrum, (pink) donor emission spectrum, (green coloured area) spectral overlap, (B) spectrum of a Atto 488/Atto 590 FRET labeled probe at donor excitation (488 nm).

When it comes to monitoring FRET effects in e.g. microscopy or flow cytometry, three channels are defined. Especially the FRET channel is prone to be affected by bleedthrough of donor and acceptor emission.

- donor channel: donor emission at donor excitation
- FRET channel: acceptor emission at donor excitation
- acceptor channel: acceptor emission at acceptor excitation

Though FRET efficiencies can be determined via techniques like acceptor photobleaching, sensitized emission or donor quenching [137, 138], this work chooses an approach that is more easily accessible: The R/G ratio (red/green ratio) is defined as the quotient of the fluorescence intensity (FI) at acceptor emission maximum and that of the donor emission maximum at donor excitation (see equation 1.2 and figure 1.11 B). This value rises with increasing FRET effect and is able to compare samples within one experimental setup [130, 131, 139].

$$R/G_{\text{donor ex}} = \frac{FI_{acceptor\ emission\ max}}{FI_{donor\ emission\ max}} \qquad \text{(equation 1.2)}$$

FRET labeled siRNA

In the context of siRNA delivery, cellular uptake [140], intracellular distribution [131], tissue distribution [141], and *in vivo* delivery [142] are only a few examples for processes that can be monitored with fluorescently labeled siRNA. For these applications, a single label on the siRNA is sufficient.

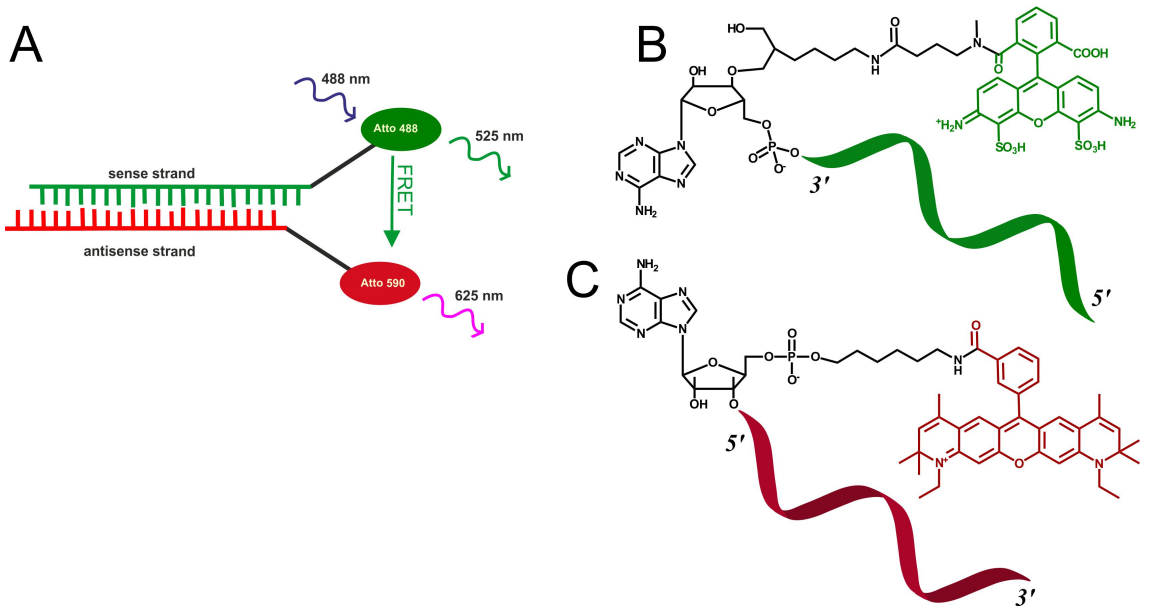

Figure 1.12: (A) Scheme of a double labeled siRNA, (B) structure of an oligonucleotide labeled on the 3'-terminal nucleotide with Atto 488, (C) structure of an oligonucleotide labeled on the 5'-terminal nucleotide with Atto 590.

Involving a second fluorophore in the monitoring of siRNA has been proposed in several variations, as the resulting FRET effect yields additional information apart from the localization signal.

One option is labeling the carrier with a donor and the siRNA with an acceptor dye. This causes FRET while the polyplex is intact [88]. Another option is the incorporation of two differently labeled siRNAs into one polyplex: one siRNA single labeled with a donor dye, the other one with an acceptor dye, which also undergo FRET, while they are both situated in the polyplex [143]. These kinds of labeling monitor polyplex integrity, but do not reveal the integrity status of the siRNA.

In this work, double labeled siRNAs are employed, that possess one fluorescent label on each strand (see figure 1.12 A). The fluorophores are attached to a terminal nucleotide via an alkane chain spacer (see figure 1.12 B). Sense strands are labeled on the 3'-, antisense strands on the 5'-end. As the position of the dyes in the duplex is close enough for the occurence of FRET, this effect breaks down when the two strands are separated or degraded. As a result, the monitoring of siRNA integrity becomes possible.

While siRNA labeling enables detailed studies on various features of the siRNA itself and its polyplex, the effects resulting from such a chemical modification also have to be considered. Attaching fluorophores to an siRNA has an impact on its biological

activity. For example, the stability of the duplex ends determines which strand is chosen as the antisense strand during RISC incorporation [144]. Modifications on the riboses have already shown to be able to stabilize or destabilize distinct regions in the duplex, thereby influencing the biological activity of siRNA [145]. For base modifications, effects on duplex stability have also been reported [146]. To get a clearer picture of the impact of fluorescently labeled siRNA, their effects on knockdown efficiency are investigated in section 3.6.

Fluorescence quenching in polyplexes

A reduction in fluorescence intensity of labeled siRNA during complexation is frequently observed [51, 147–151]. It can decrease to 10% compared to uncomplexed siRNA (see section 3.1).

Two explanations for this phenomenon appear in the literature. One is that quenching is caused by high salt concentrations [152, 153]. In a polyplex solution, ions are densely compacted inside a polyplex and the counterions, often Cl^- or Br^-, are presumably accumulated close to it. Therefore the local ion concentration inside a polyplex is much higher compared to the rest of the solution. This concentration can only be estimated, but probably reaches a level at which salt quenching is effective. The Stern Volmer equation (see equation 1.3) quantifies the reduction in fluorescence intensity in dependence on the salt concentration, with [Q] being the concentration of the quencher and K_{SV} the Stern Volmer constant.

$$F_0/F = 1 + K_{SV} * [Q] \qquad \text{(equation 1.3)}$$

Two kinds of quenching mechanisms can be distinguished. Dynamic quenching results from collisions between fluorophore and quencher. Static quenching occurs when fluorophore and quencher form a non fluorescent complex. The Stern Volmer correlation is linear in case that only one quenching mechanism is present. For most salts, both mechanisms contribute to the quenching [152].

The second explanation is the self quenching of fluorophores that are situated in close proximity to each other. siRNA and therefore its fluorophores condense during complexation to an extent that is dependent on the carrier as well as the N/P ratio. This effect has found applications in investigating complex formation (see section 1.4.2).

1.4.2 Methods for evaluating polyplex formation

Running a polyplex on a gel is the most basic and most frequently conducted way to assess the binding capability of a carrier [26, 41, 57]. This method has also been described for the investigation of protein - nucleic acids investigations [154]. siRNA that has not been complexed moves towards the anode, while complexed siRNA stays in the loading pocket as the size of the polyplex prohibits its migration. In addition, polyplexes mostly possess a net positive charge (see section 1.2.1), which also prevents migration in the direction of siRNA.

Thermophoresis is a relatively new method. It is based on the movement of molecules in a temperature gradient that is detected via their fluorescent label. Therefore two lasers focus on one spot in the sample solution, one to heat up the spot, the other to detect changes in fluorescence intensity. While fluorescence correlation spectroscopy (FCS, see below) monitors the diffusion, a parameter that is dependent on merely the hydrodynamic radius (R_h), thermophoresis detects thermodiffusion. This movement is influenced not only by size, but also by charge and solvation shell of a molecule, which makes this effect hard to predict [127, 155]. The method has been developed for the determination of dissociation constants (K_D) of proteins and ligands [155]. Its application is constantly expanding and already covers nucleic acids. With this method, thermal stability of DNA has been determined [156], RNA has been separated by size [157] and, in this work, siRNA polyplexes are investigated.

Self quenching of fluorophores occurs when labeled siRNA is densely complexed in a polyplex (see section 1.4.1). For strongly quenching polyplexes, changes in fluorescence intensity are mapping the process of complex formation. The titration of pDMAEMA with Rhodamine labeled oligonucleotides at increasing N/Ps revealed a decreasing fluorescence intensity before N/P 2, which rose constantly afterwards (see figure 1.13) [150], indicating that fluorophore density first increases and above a certain N/P decreases. A quenching curve of a comparable shape for PEI polyplexes was employed to define the optimal N/P for transfection studies [51]. These curves are in accordance with molecular dynamics simulations for arginine rich peptides that found a molecular reorganization process with less stable and bigger polyplexes at rising N/Ps due to the repulsion of excess positive charges [48] (see section 1.2.1).

FCS [128] confirms polyplex formation by adressing the size of a polyplex. This method monitors fluorescence fluctuations that are caused by the diffusion of labeled molecules. Fitting these fluctuations with an autocorrelation curve yields the diffusion time of the fluorescent molecule. As diffusion times are dependent on the size of a

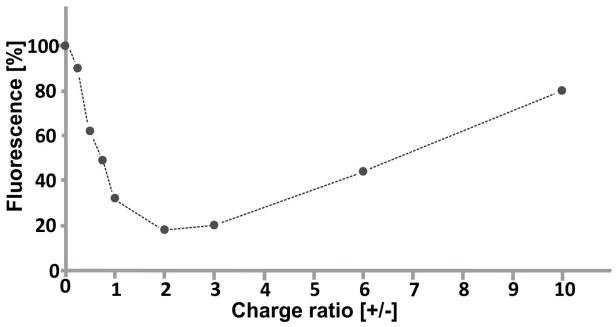

Figure 1.13: Changes in fluorescence intensity of rhodamine labeled oligonucleotides in pDMAEMA polyplexes at rising N/P ratios, adapted from Van Rompaey 2000 [150].

molecule, an R_h can be derived.

When labeled siRNA is employed to monitor polyplex formation, an increase in R_h of the fluorescent species after complexation in comparison to the R_h of an siRNA only sample indicates successful complexation, as the fluorescent label is then situated on a much bigger entity, the polyplex.

Apart from this basic setting, FCS has been applied for the investigation of polyplexes during formulation [111], in biological fluids [158], during cellular uptake and intracellular release [159].

1.4.3 Methods for evaluating polyplex stability

Polyplex stability, sometimes also referred to as binding strength [48, 57, 160], is a versatile term, which is used for the different concepts of stability that are present in the literature.

Determining dissociation constants (K_D) via isothermal titration calometry has served as a means to assess polyplex stability from a thermodynamic point of view [51, 161–163]. An example for a study that regards polyplex stability under kinetic aspects is the investigation of intracellular unpacking kinetics undertaken via FRET labeling of carrier and DNA [164] (see section 1.4.1). Though such biophysical analyses are not applied frequently, they could contribute to a better understanding of phenomenons that are encountered during the application of standard methods for assessing polyplex stability (see section 3.2.2).

Such methods usually consider polyplex stability in a more application-related way, by regarding this feature as resistance against the various conditions that are encountered in an *in vivo* surrounding. In this context, polyplex stability has been determined with regard to specific challenges like competing polyanions [48, 54, 59, 64],

blood serum [59, 165] or nucleases [59, 160].

To assess polyplex stability by the extent to which other negatively charged macromolecules can destabilize a polyplex, molecules like heparin [48, 54, 57, 59, 64, 113, 166], chondroitin sulfate, hyaluronic acid or poly-L-aspartic acid [55] have been employed. The stability in the presence of such macromolecules is relevant, as sulfated glucosaminoglycans are present in the extracellular environment [59].

Nuclease resistance is another stability criterion, as the polyplex is challenged by the presence of various digestion enzymes during its journey through the blood stream and inside the cell. The basic procedure for testing this feature comprises incubation of the polyplex with nuclease, inactivation of the enzyme and analysis on a gel [109]. A more precise readout via FRET is obtained when employing double labeled oligonucleotides (see section 1.4.1). This approach has first been described for microscopic studies on intracellular integrity of nucleic acids [167] and has then been transferred to nuclease resistance studies for polyplexes [160]. The nuclease resistance protocol applied in this work extends the established setup to real time monitoring of siRNA integrity and fitting of a decay curve [129–131, 168].

1.4.4 In vitro methods for evaluating cellular uptake

Basic *in vitro* methods comprise confocal laser scanning microscopy (CLSM) and flow cytometry. Both methods require fluorescent labels on the siRNA. CLSM is a standard method for tracing cellular uptake and intracellular distribution of siRNA [36, 140, 169]. FRET microscopy has been applied to study intracellular integrity of nucleic acids [88, 130, 131, 167, 170, 171]. While microscopy discloses intracellular conditions, it usually only evaluates a small number of cells, which may hamper quantifications and representativeness for the whole cell population.

Flow cytometry is able to quickly analyze the fluorescence of ten thousands of cells, however without yielding information about intracellular distribution. Though high cell numbers are considered, this method is also not appropriate for quantification. Firstly, it is not able to distinguish between internalized fluorescent molecules or those sticking on the cellular membrane [26]. Secondly, it does not consider changes in fluorescence intensity that may be due to the intracellular milieu, the prevalent pH, self quenching of huge amounts of siRNA compacted in small vesicles and quenching of siRNA while still in the polyplex.

An alternative method has been proposed as a means for an unbiased quantification. It includes thorough washing steps to remove siRNA bound on the membrane, cell

lysis with TritonX (TrX), and sodium dodecyl sulfate (SDS) treatment to release siRNA from the polyplexes. As a readout, fluorescence in cell lysate is determined and normalized to the protein content [172].

1.4.5 In vitro methods for evaluating knockdown capability

The measure for the actual outcome of siRNA delivery is the knockdown of a target gene. *In vitro* reporter gene assays make a first statement about knockdown capability and allow a judgement if further *in vivo* testings could be promising. Apart from luciferase systems [42, 92], eGFP knockdown is a convenient method with an easy read out via flow cytometry or fluorescence in cell lysate [173, 174].

1.4.6 Testing strategies

A common approach for the evaluation of polyplexes is focusing on one class of material and optimizing one specific parameter. This kind of studies have been conducted for e.g. the PEG content of PAMAM [92], the number of cationic amine functions in PVAs [110], the length of arginine-rich peptides [48], the molecular mass of branched PEI [103] and the grafting of PLL brushes [109].

This approach facilitates a rational design as it controls the specific influences of one parameter while keeping all other parameters constant. However, when it comes to the comparison of different materials, establishing a connection between such studies is difficult. Above all, a direct comparison would require all experiments to be carried out under standardized conditions [175]. Furthermore, the outcome of a study for one material can not be directly transferred to other materials, as specifications do not apply for each carrier in the same way [176].

It is also important to not only focus on one specific parameter, as the whole set of parameters displayed by one carrier determines its overall behaviour.

Studies that compare different materials however are relatively rare and restricted to a limited number of materials and features tested in parallel [57, 59, 177]. A comprehensive and systematical screen of a range of materials would be able to take the whole set of features of one carrier into account and may thus be able to elucidate promising candidates for siRNA delivery.

1.5 Particles with siRNA entrapping capability

A second class of nanocarriers is constituted by particles that are able to entrap siRNA. They do this by either forming a shell around an siRNA solution or by embedding siRNA into their matrix. As their binding principle differs much from that of polyplexes, these particles were assessed separately.

1.5.1 Nanocapsules

Nanocapsules consist of a preferably biodegradable polymeric shell, which encapsulates cargo in an aqueous phase. Poly(lactide-co-glycolide) (PLGA) [178], poly(L-lactide) PLLA [178], PEG-PLGA [179] or hydroxyethyl starch [180] have served as materials for the preparation of capsules.

Nanocapsules containing siRNA and are made of poly(n-butylcyanoacrylate) (PBCA) were prepared via an inverse miniemulsion process with subsequent anionic polymerization by xxxxx xxxxx xxxxx xxxxx xxxxx xxxxx xxxxx [181]. Previous batches of PBCA capsules containing Cyanine 5 (Cy5) labeled oligodeoxynucleotides (ODN) have shown uptake in mesenchymal stem cells (MSC) [182]. Here, initial tests for siRNA delivery with these capsules were carried out.

Figure 1.14: Scheme of nanocapsules

1.5.2 Dextran particles

Apart from core shell structures like liposomes or capsules, particles can also enclose siRNA in their matrix. Such particles often make additional use of positively charged materials to add electrostatic interactions as a second binding principle [42]. For example, siRNA - DOTAP polyplexes have been emulsified in an acid degrable matrix and could sucessfully transfect macrophages [183].

siRNA containing particles made from acetal-modified dextran endowed with spermine moieties (spermine-Ac-Dex) were obtained via a double emulsion water/ oil/

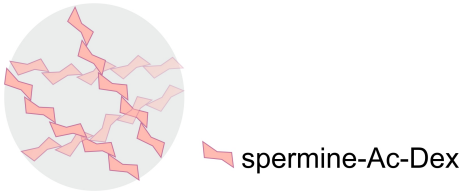

Figure 1.15: Scheme of dextran particles, adapted from Cohen 2011 [42].

water evaporation method. The acetals render the particles biodegradable in a pH dependent manner and the positively charged spermines assist in the binding of siRNA. Dextran particles have already shown knockdown capability in HeLa luc cells with minimal cytotoxicity [42]. These formulations were provided by xxxxx xxxxx xxxxx [42].

1.5.3 Liposomes

Liposomes are vesicular structures of a lipid bilayer that encloses an aqueous phase. They either transport hydrophilic cargo in the inside or lipophilic cargo settling in the bilayer. Liposomes are created by either extrusion [184], sonication [185], detergent dialysis [186] or centrifugation [129]. Their characteristics are influenced by the choice of lipids. Employing pegylated lipids is a common method to render liposomes "stealth like", which means reducing their immunogenicity and enhancing their circulation time, thereby making cellular uptake more difficult [187]. Their endosomal release can be facilitated by incorporating fusogenic lipids (see section 1.2.5) [188]. Liposomes are also suited for functionalization, so that moieties that enhance cellular uptake, e.g. cell penetrating peptides [189] or targeting ligands [190] can be attached. Positively charged lipids like DOTAP are often involved in the transport of negatively charged cargo like siRNA. In this case, a differentiation must be made between liposomes incorporating the siRNA [129] or empty liposomes that are mixed with siRNA [191], the latter formulation rather being a lipoplex (see section 1.3).

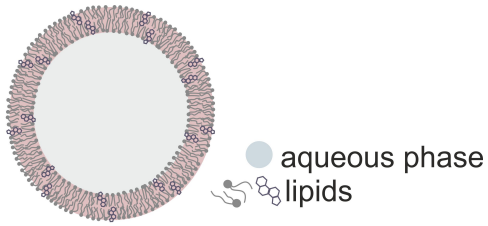

Figure 1.16: Scheme of liposomes

In this work, liposomes were prepared by dual centrifugation (DC), a method that produces siRNA containing liposomes on a small scale under sterile working conditions. In a special centrifuge, samples experience a second counter clockwise rotation around their own axis in addition to the main rotation. The resulting shear forces lead to the formation of vesicles, consisting mostly of unilamellar liposomes. Liposomes prepared with this technique have shown high encapsulation efficiencies up to 60%, stability for more than three months and ability to protect siRNA cargo from degradation [129]. Cellular uptake is inefficient for pegylated ("stealth") liposomes, but can be enhanced by applying special lipid compositions and surface functionalization [101].

1.6 Targeting RNA to mitochondria

Strategies for the targeted delivery of therapeutic agents aim at enhancing the efficiency of the treatment and reducing unwanted side effects [85]. Two subcategories of targeted delivery can be distinguished. One is the cell type specific targeting, that spares side effects in non target tissues [14, 61, 141, 192]. The second category is intracellular targeting, that comes into play when a therapeutic agent is supposed to inside a specific cellular organelle [193]. For example, the targeting of tRNAs to mitochondria is a therapeutic approach for certain mitochondrial diseases.

1.6.1 Mitochondrial diseases

Mitochondria are the sites of oxidative phosphorylation, a process that results in adenosine triphosphate (ATP) synthesis [194]. ATP provides energy necessary for the cell's metabolism. In addition, mitochondria are the sites of the citric cycle [194] and are involved in purin and pyrimidine synthesis [195], apoptosis [196] and cell signalling [197]. These central roles implicate mitochondrial involvement in various physiologic and pathogenic processes. Mitochondrial dysfunction has been related with e.g. ageing and tumorigenesis [198].

The class of mitochondrial diseases that is regarded in this work results from inherited DNA mutations.

Mitochondria descend from prokaryotic ancestors and therefore possess their own genome. However, only 1% of mitochondrial proteins are encoded and synthesized by the mitochondria themselves. The genes of the majority of mitochondrial proteins have been transferred to the nucleus, are synthesized in the cytosol and imported into mitochondria [197]. While 22 transfer (t) RNAs are mitochondrially encoded [199], additional tRNAs are also imported [200, 201].

This means that mitochondria can be affected by mutations in the mitochondrial as well as in the nuclear genome [202]. In most cases, a mutated and an unmutated DNA population are present together in one cell ("heteroplasmy"). In order to affect mitochondrial processes, the fraction of the mutated population has to exceed a certain threshold, which has been found to be more than 90% in some cases [203]. After passing this threshold, a broad range of neurologic and myopathic symptoms arise, and mostly several organ systems are involved [203].

An example for a nuclear derived mitochondrial disorder is the mutation in the nuclear POLG gene, which encodes for a mitochondrial DNA polymerase, resulting

in mitochondrial DNA deletions [196]. Mutations of the mitochondrial DNA lead to diseases like MERRF (myoclonic epilepsy with ragged red fibers), which has mainly been associated with a mt8344A-G transition in a gene encoding for mt $tRNA^{Lys}$ [204], MELAS (mitochondrial encephalomyopathy with lactic acidosis and stroke-like episodes), mainly associated with a mt3242A-G transition in a gene encoding for mt $tRNA^{Leu}$ [205, 206], or LHON (Leber hereditary optic neuropathy), associated with mutations in genes encoding for nicotinamide adenine dinucleotide (NADH) dehydrogenase [203]. These attributions of specific mutation sites to a certain disease, however, do not capture the whole image, as also other mutation sites are discussed as a cause for these diseases [207], atypical or even mixed clinical features can arise from one mutation [208, 209], and again, the level of heteroplasmy has to be taken into account.

1.6.2 RNA delivery to mitochondria

For tRNA affecting mitochondrial disorders like MERRF and MELAS, approaches have been developed to replace diseased tRNAs. One strategy employs the nuclear encoding of engineered tRNAs. Karicheva et al. [205] achieved nuclear expression of transgenic tRNAs that were imported into mitochondria and subsequently aminoacylated, thereby improving mitochondrial functions. Sieber et al. [201] constructed a fusion protein consisting of an RNA binding domain and a motif that targets mitochondria. This construct was able to transport RNA species into isolated mitochondria, which may be a starting point for a system for tRNA delivery.

Nanocarriers have been proposed for DNA delivery to mitochondria. Cells were transfected with a modified DNA oligomer conjugated to a peptide with a mitochondrial localization signal [210]. To enhance the delivery of this construct, PEI [211] or liposomes [212] were employed. This concept may also be applicable for RNA delivery.

1.6.3 Design of targeted carriers

Targeting of nucleic acids to mitochondria can be achieved by imitating cellular strategies like the attachment of a peptide with a mitochondrial localization signal (see section 1.6.2).

Furthermore, synthetic molecules with mitochondriotropic properties have been identified [213], among them triphenylphosphonium (TPP) [214, 215], Rhodamine 123 [216], Cyanine 5 (Cy5) [182, 217] and dequalinium [218] (see figure 1.17 A-D).

These molecules display common structural features: They are amphiphilic, which

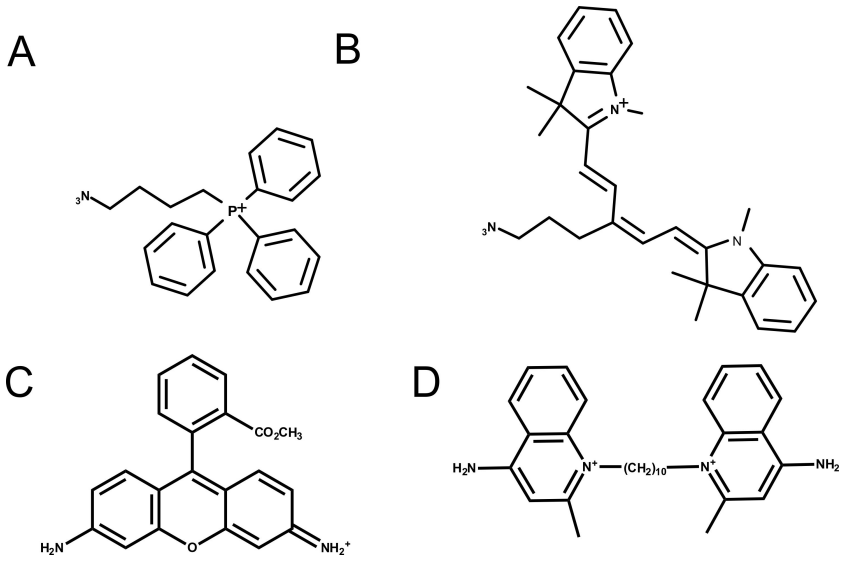

Figure 1.17: Mitochondriotropic compounds: (A) TPP shown as its azide, (B) Cy5 shown as its azide, (C) Rhodamine 123, (D) dequalinium.

means they possess both a lipophilic moiety and hydrophilic, positively charged part. This charge is attenuated in its hydrophilicity as it is delocalized over at least three atoms [215]. The lipophilicity enables the molecules to interact with membranes. The delocalized positive charge attracts the molecules to mitochondria. This can be explained by the mitochondrial membrane potential of about 160 mV (negative inside) [219, 220] that is caused by the constant outward transport of protons by the respiratory chain.

The self assembling dequalinium derivatives have served as carriers for DNA delivery to mitochondria [218] .

The other moieties have been attached to carriers in order to deliver diverse cargo to the mitochondria. Lipids were functionalized with Rhodamine 123 and incorporated into liposomes, which were loaded with Paclitaxel, a drug that enhances the apoptotic activity of mitochondria [221]. These formulations showed enhanced cytotoxicity towards cancer cells than unfunctionalized liposomes. In another study, TPP functionalized liposomes were loaded with Ceramide, a lipid also involved in mitochondrial apoptosis induction. The TPP liposomes were able to inhibit tumor growth more efficiently than their unfunctionalized counterparts [214]. Liposomes endowed with octaargine moieties showed delivery of GFP to mitochondria [185]. Though the positive charges of octaarginine are not delocalized, it may still interact with the mitochondrial membrane, giving the carrier the possibility to deliver its cargo.

To suggest a therapeutic approach for the treatment of diseases like MELAS and

MERRF, first approaches towards the preparation of mitochondrially targeted liposomes for tRNA delivery were conducted.

As can be seen in figure 1.18, such a formulation needs to fulfil several requirements, from cellular uptake (1) to intracellular release in its intact form (2) towards accumulation at mitochondria and finally delivery through the two mitochondrial membranes into the organelle (3).

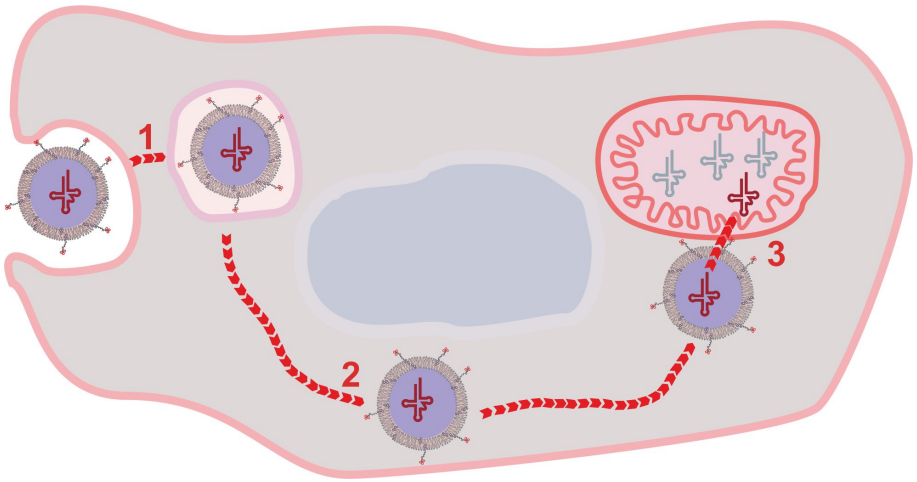

Figure 1.18: Targeted delivery of tRNA to mitochondria with a functionalized liposome.

2 Goal of the work

Polymeric nanocarriers are a promising option for the systemic application of RNA, especially siRNA. Various materials and designs have been proposed for this purpose. Still, a thorough understanding of the characteristics that constitute a successful carrier is hard to obtain, as such a carrier needs to fulfil a lot of requirements, which are even partly contradictive.

The goal of this work was to develop a systematic approach for the elucidation of favourable features for siRNA carriers. This was to be achieved by screening a range of candidates. In order to ensure that similar requirements apply among these carriers, only those that are able to bind siRNA due to electrostatic interactions were included in the screen. Attention was drawn to choose chemically and structurally diverse candidates for obtaining a broad spectrum of characteristics.

It was envisaged to subject this set of carriers to a sequence of assays. Each of the assays should focus on one specific feature. As this screen should serve in an early stage of development, criteria started from the two basic features, polyplex formation and polyplex stability. Subsequent *in vitro* tests comprised cellular uptake, intracellular integrity and knockdown capability. Conclusions about favourable features were to be obtained by comparing the carriers among each other as well as considering the interplay of features displayed by one carrier.

Taking into account that the testing system may also serve in further standardized screens, an emphasis was laid on method development as well as the comparison of alternative approaches. Thereby special attention was drawn to the optimization of *in vitro* knockdown assays, as they constitute key components in siRNA delivery studies.

Expanding the scope of this work also beyond polyplexes, a second class of carriers was additionally considered, though to a lesser extent. Three particles with the ability to entrap siRNA inside their matrix were assessed in a separate study, thereby focussing mainly on siRNA encapsulation and knockdown capability.

To also recognize the importance of targeted delivery of RNA, first advances into the functionalization of liposomes with mitochondriotropic moieties were undertaken.

3 Results & Discussion

3.1 Characterizing polyplex formation

The comparative evaluation of polyplexes constitutes the core of this work and comprises their examination from various perspectives. To follow a systematic approach, six cationic carriers were screened simultaneously. The formulations were assessed from their behaviour in polyplex formation and stability to *in vitro* experiments. This section presents and compares methods to monitor one essential requirement for these systems, polyplex formation. At first, basic procedures for working with siRNA are introduced.

3.1.1 Prerequisite: Hybridization of siRNA

siRNA single strands were obtained from commercial suppliers, comprising a range of sense and antisense strands for targeting the enhanced green fluorescent protein (eGFP). Though all sense and antisense strands, respectively, share the same sequence, the differences between them lie in the position and the kind of fluorescent label attached. These oligonucleotides form a modular system that enables the hybridization of an siRNA duplex with tailor-made labels for the envisaged application. For example, a FRET labeled siRNA can be assembled by choosing a sense strand with the donor dye on the 3'-, and an antisense strand with the acceptor dye on the 5'-end (see figure 3.1 and section 1.4.1). Dye pairs for FRET labeled siRNA have been optimized before by xxx [168].

Hybridizations were carried out in phosphate buffered saline (PBS) starting from single stranded (ss) RNA stock solutions. The concentrations of these stocks were determined by the supplier via UV absorption. In most cases, however, these declarations were obviously not accurate enough, as an equimolar hybridisation on the basis of the declared concentrations led to excess ss RNA. Therefore a titration became mandatory. For this purpose, the volume of sense strand was kept constant and different $\text{volume}_{\text{antisense}}/\text{volume}_{\text{sense}}$ ($v_{\text{antisense}}/v_{\text{sense}}$) ratios were established by varying

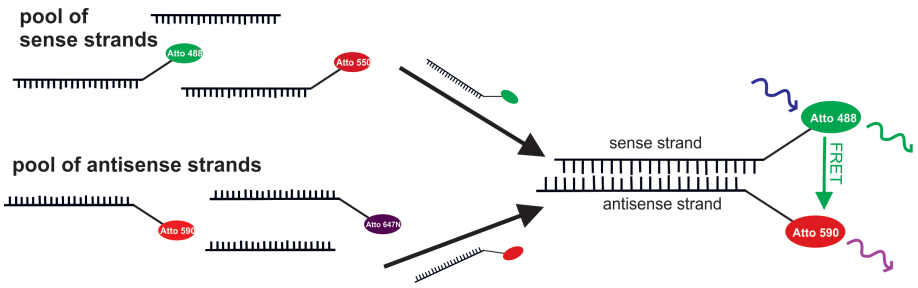

Figure 3.1: Hybridization of siRNA: Choosing sense and antisense strand with the appropriate fluorescent labels for obtaining a FRET labeled siRNA.

the volume of antisense strand in order to obtain the $v_{antisense}/v_{sense}$ which yielded a hybridization without excess ss RNA, signifying the input of equimolar amounts of both strands. Figure 3.2 shows the polyacrylamide gel electrophoresis (PAGE) analysis of the hybridization of a construct with labels on both strands, resulting in a FRET labeled double stranded (ds) RNA (see section 1.4.1). In this case, the optimal $v_{antisense}/v_{sense}$ ratio was 1.2/1, as for this sample signals for excess single strands were minimal.

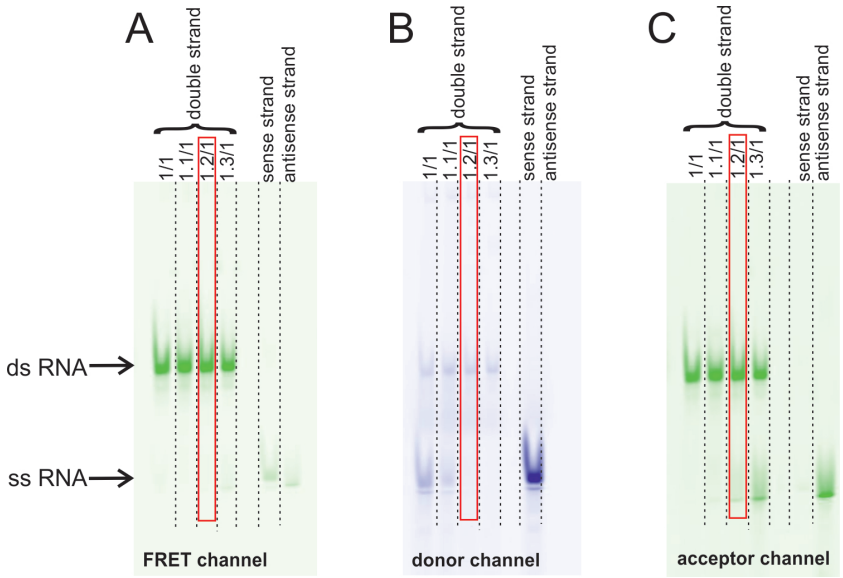

Figure 3.2: Non denaturating PAGE analysis of ds RNA hybridization with titrating the $v_{antisense}/v_{sense}$ ratio for quantitative formation of a Atto 488/ Atto 590 labeled ds RNA. (A) FRET channel: Ex 488, Em 670BP30, (B) donor channel: Ex 488, Em 520BP40, (C) acceptor channel: Ex 532 nm, Em 670BP30. Optimal $v_{antisense}/v_{sense}$ ratio 1.2/1.

3.1.2 Prerequisite: Purification of siRNA

Purity of all materials should be self-evident for any kind of experiment. Nevertheless, stock solutions of HPLC grade labeled oligonucleotides from commercial suppliers contained excess free dye to an extent varying from batch to batch. This can cause a bias for methods like FCS and thermophoresis. In these techniques, the different molecules under investigation are all endowed with the same fluorescent tag. Excess free dye thus constitutes an unwanted additional fluorescent species that interferes with the signals detected for the actually investigated molecules.

A method for purifying oligonucleotides needs to ensure the complete removal of free dye, high yields and the feasibility of upscaling.

The suitability of gel extraction was evaluated first. A labeled ds RNA was analyzed on a non denaturating PAGE, followed by excision, elution and precipitation of the ds RNA band. PAGE analysis showed that the additional band of free dye was not present any more after the purification (see appendix, figure A1). However, the time demanding procedure coupled with a low yield of 28% and a limited possibility for scaling up were the reasons for not further pursuing this method.

Another attempt was undertaken with reversed phase high performance liquid chromatography (RP HPLC), a standard procedure for oligonucleotide purification. The established protocol of ion pair chromatography with acetonitrile/triethylammonium acetate (TEAA) buffer as eluent system and a gradient of increasing fractions of acetonitrile was applied on a labeled ss RNA, which resulted in two fluorescent peaks. Even after optimizing the gradient, the elution times still differed by only one minute, which made a reliable separation impossible (see appendix, figure A2).

ds siRNA and a dye molecule differ widely in size, as can be concluded from their molecular weights (M_W) (14 kDa and about 600 Da, respectively). This made size exclusion chromatography (SEC) a promising option. A Superdex^{TM} 200 column was attached to the HPLC, expecting an efficient separation of free dye as well as excess ss RNA, which would make the ratio titration step obsolete (see section 3.1.1).

A ds RNA with Atto 488 attached to the sense strand was loaded on the column and eluted at a flow rate of 0.5 mL/min in PBS. Figure 3.3 shows that ds RNA and excess ss RNA eluted about 3 min apart from each other. The ds RNA peak at 32.0 min was clearly visible (see figure 3.3 A and C). A second peak at 34.8 min was detected when labeled ss RNA only was loaded (see figure 3.3 B), ds RNA was hybridized at a ratio effecting excess labeled ss RNA (see figure 3.3 A), or seen only in the absorption chromatogram when ds RNA was hybridized with slight excess of unlabeled ss RNA

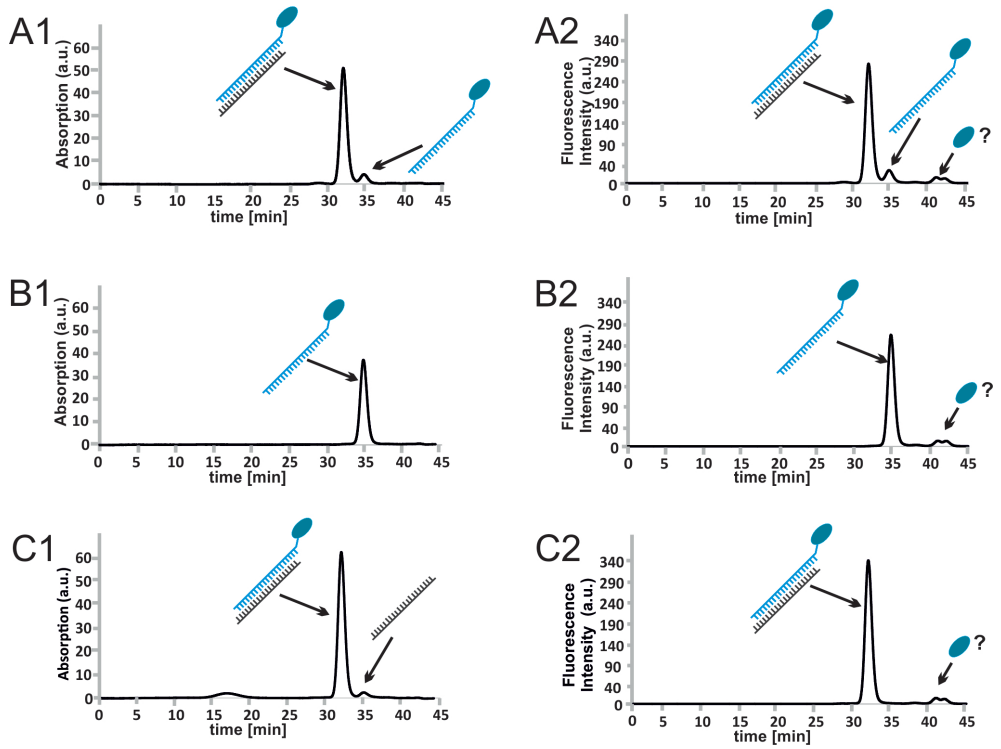

Figure 3.3: Purification of Atto 488 labeled ds RNA by SEC. Chromatograms for (A) ds RNA at a ratio effecting excess labeled ss RNA, (B) labeled ss RNA only, (C) duplex at a ratio effecting excess unlabeled ss RNA. (1) absorption at 254 nm and (2) fluorescence at Ex 490 nm, Em 520 nm, flow rate 0.5 mL/min.

(see figure 3.3 C). Reducing the flow rate to 2.5 min was tested once, but not further pursued, as the doubled elution time did not lead to a significantly better resolution (see appendix, figure A3).

A small double peak is detected at about 41 to 42 min in the fluorescence chromatograms, which may display the free dye. A further investigation of this peak was spared as PAGE analysis of the ds RNA fraction clearly showed the successful purification (see figure 3.4 A).

As an additional proof, fluorescence spectra of FRET labeled ds RNA were recorded at donor excitation (for PAGE analysis of these constructs see appendix, figure A4). The R/G ratio, an indicator for the extent of FRET (see section 1.4.1) increased from 2 to 10, after excess free donor dye had been removed (see figure 3.4 B and C).

The method permitted a loading of up to 3000 pmol ds RNA per run. As a work up, the purified fractions of several runs were united and concentrated.

Although two separate peaks for the ds and the ss RNA were present, excess ss RNA was to be kept as low as possible. The difference in elution times was sufficient enough

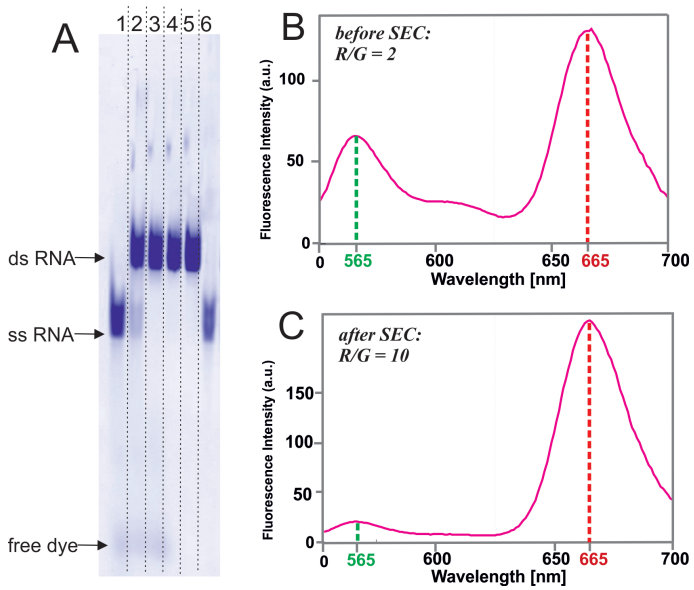

Figure 3.4: Analysis of SEC purification. (A) Non denaturating PAGE analysis of SEC purified ds RNA labeled with Atto 488. Loaded on the gel are (1) unpurified ss RNA, (2) unpurified ds RNA with excess of labeled ss RNA, (3) unpurified ds RNA at optimal ratio, (4) purified ds RNA with former excess ss RNA, (5) purified ds RNA of optimal ratio, (6) purified labeled ss RNA. Detection at Ex 488 nm, Em 520BP40. (B) Spectrum at donor excitation (543 nm) of an Alexa 555/Atto 647N labeled siRNA before and (C) after the purification.

to separate a small excess fraction. At rising peak areas for the ss RNA, the two peaks might overlap due to their proximity. The separation range of 10 kDa to 600 kDa for the employed Superdex^{TM} 200 is obviously not optimal for these two species of 14 kDa and 7 kDa. A way to improve conditions may be the change to a better suited column, e.g. the Superdex^{TM} 75 with a separation range of 3 kDa to 70 kDa.

To summarize, SEC was able to efficiently remove excess free dye, which was proven by PAGE analysis and an improved R/G ratio in the case of double labeled ds RNA (see figure 3.4). Also a scale up was easily achieved.

3.1.3 Polyplex formation under non equilibrium conditions

Polyplexes originate from electrostatic interactions between positively charged carriers and negatively charged siRNA. As such interactions are per se dynamic, they principally allow a dissociation of siRNA. While this possibility falls under the scope of polyplex stability, which is addressed in section 3.2, this section focuses on the formation process itself.

The six cationic carriers in the presented screen comprised poly-L-Lysine brushes,

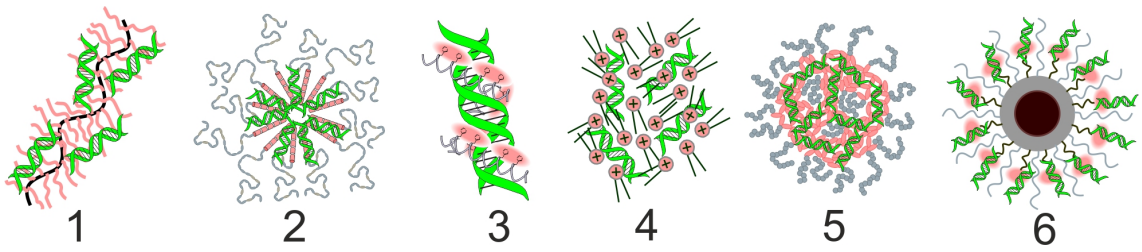

Figure 3.5: Schemes of the polyplexes under investigation. siRNA complexed with (1) poly-L-lysine brushes, (2) block copolymers, (3) cationic peptides, (4) cationic lipids, (5) nanohydrogel particles, (6) MnO@SiO_2 particles.

cationic block copolymers, cationic peptides, cationic lipids, nanohydrogel particles and manganese oxide (MnO@SiO_2) particles (see figure 3.5), which are all described in detail in section 1.3.

When screening potential candidates for their ability to complex siRNA, an electrophoretic mobility shift assay (EMSA) is typically applied, which simply means analyzing polyplexes on a gel (see section 1.4.2).

The major information drawn from an EMSA is the minimal m/m ratio ($mass_{carrier}$ per $mass_{siRNA}$) that is necessary for an almost complete complexation. The thus resulting N/P ratio (see section 1.2.1) shows how efficiently a carrier can employ its positive charges.

Polyplexes were prepared in PBS by adding Alexa 555/ Atto 647 N labeled siRNA to the carrier solutions. After a maturation time of 20 min, samples covering a range of m/m ratios were analyzed on an agarose gel. Figure 3.6 displays EMSA analyses for the six carriers. Table 3.1 compiles binding ratios, whereupon cc_1 and cc_2 correspond to the minimal m/m for almost complete complexation and the ratio with twice as much amount of carrier, respectively. Subsequent experiments will refer frequently to these two ratios. In addition, the fluorescence signals of the uncomplexed siRNA bands were quantified and a five parametric dose-response curve was fit to calculate an m/m ratio for 50% binding (BR_{50}).

cc_1 ratios covered a large range from 2/1 for PLL brushes to 100/1 for block copolymers. These ratios should be considered together with the respective N/P values. This parameter was available for four of the polyplexes. The N/P for the lipid Oligofectamine™, which has a proprietary composition, was approximated by that of Lipofectamine™ [93]. For MnO@SiO_2 particles, a value could not be obtained as the amines are attached via a surface modification, a process that can not be assessed in a quantitative manner.

Table 3.2 calculates N/P ratios among other characteristics for the carriers. N/P

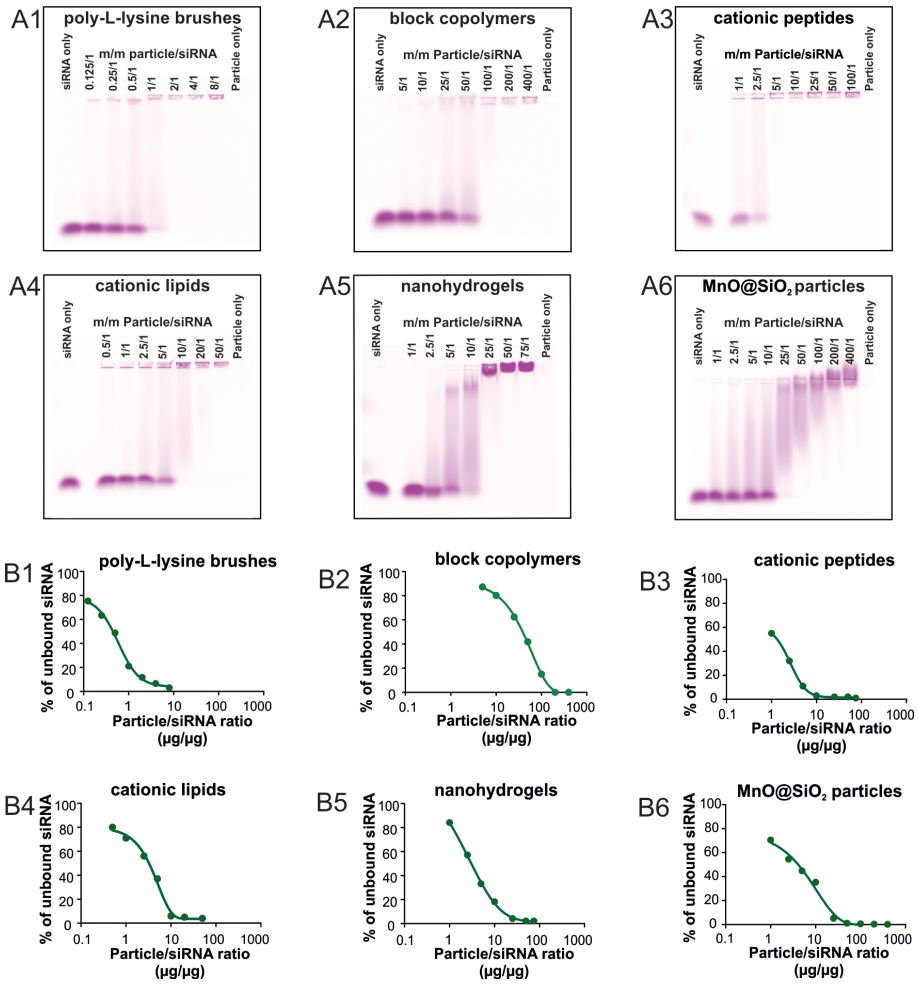

Figure 3.6: EMSA analysis of polyplex formation with Atto 555/ Alexa647N labeled siRNA. (A1-6) FRET channel: Ex 532 nm, Em 670BP30 for (1) poly-L-lysine brushes, (2) block copolymers, (3) cationic peptides, (4) cationic lipids, (5) nanohydrogels, (6) $MnO@SiO_2$ particles. (B1-6) Fluorescence signal of free siRNA was quantified and fit with a 5 parametric dose-response curve.

ratios at cc_1 for block copolymers and nanohydrogels as well as their m/m ratios are much higher compared to PLL brushes and cationic peptides, which implicates that the latter two may possess better accessible charges and/or their spatial arrangement in the polyplex is more efficient. In addition, highly charged polyplexes have been associated with enhanced toxicity due to nonspecific interactions with serum or tissue components [65] that can be caused by the presence of uncomplexed polymer [49] (see sections 1.2.1 and 1.2.3 for details). All these considerations favour the formation properties of cationic peptides and PLL brushes.

From the data listed in table 3.2, first assumptions about size and structure of the polyplexes can be derived. The average number of siRNA molecules per monomer at

Table 3.1: Binding ratios of polyplexes

carrier	cc_1	cc_2	BR_{50}[a] values for EMSA	MST
PLL brushes	2/1	4/1	0.6	0.6 (0.5[b])
block copolymers	100/1	200/1	43.8	50.4 (55.0[b])
cationic peptides	5/1	10/1	2.5	2.5
cationic lipids	10/1	20/1	4.1	7.1
nanohydrogels	25/1	50/1	1.8	14.6
MnO@SiO_2 particles	25/1	50/1	7.3	118

[a]mass/mass ratio at which 50% of siRNA is bound
[b]BR_{50} value from fluorimetric titration curve

Table 3.2: Charge ratios of polyplexes

carrier	N/P at cc_1	M_W [g/mol] of monomer	number of charges per monomer	siRNA per monomer at cc_1	number of charges per mass
PLL brushes	3	$9.9*10^6$	50000	367	0.005
block copolymers	30	30000	24	0.02	0.0008
cationic peptides	3	2800	5	0.04	0.002
cationic lipids	14[a]	n.a.	n.a.	n.a.	n.a.
nanohydrogels	29	$36.6*10^6$	125500	105	0.003
MnO@SiO_2 particles	n.a.	n.a.	n.a.	n.a.	n.a.
siRNA		14000	42		0.003

[a]N/P of Lipofectamine™ as an approximation for Oligofectamine™

cc_1 shows that for the PLL brushes and nanohydrogels, each monomer binds more than 100 siRNA molecules. The monomers of these two carriers also possess the highest M_W and the highest number of charges per monomer. Thus one polyplex could consist of one monomer decorated with a large number of siRNAs. This is evident for the nanohydrogels as preformed particles, but may also apply for the PLL brushes, in case they do not aggregate. On the other hand, copolymers and cationic peptides, possessing a roughly 1000x lower M_W, show a rather theoretical value of less than one siRNA per monomer at cc_1, which indicates that one polyplex must contain a number of monomers far exceeding that of siRNA. This issue will be further discussed in the context of size determination (see section 3.1.6).

The ratio of positive charges per mass is best able to reflect charge density, a parameter that has been correlated with improved siRNA carrier properties [57]. PLL brushes possess the highest value, copolymers the lowest, but the range is quite small. Clear correlations, however, are generally hard to establish, as a lot more determinants have an impact. For example, charge distribution and spacial accessibility of charges

within the carrier also play a role, but are difficult to quantify.

So far, the overall ability of the carriers for siRNA binding has been regarded. A second feature is also visible in the EMSA, which already hints at the feature of polyplex stability, a parameter that will come into focus in section 3.2. Electrophoresis is a non-equilibrium method, as an electrical field applies opposite forces on the carriers and the siRNA, trying to pull siRNA out of the polyplex. A smear between the pocket and the band of undetained siRNA indicates to what extent polyplexes dissociate under these conditions. As this smear is most prominent for nanohydrogels and MnO@SiO_2 particles, the stability of these polyplexes is judged to be rather low.

This adds an interesting piece of information and raises the question if different binding characteristics would be observed under equilibrium conditions.

3.1.4 Polyplex formation under equilibrium conditions

Microscale thermophoresis (MST) monitors the differential movements of labeled molecules in a temperature gradient [155]. This method is working under equilibrium conditions, as nothing else than two laser beams interfere with the sample solution (see section 1.4.2). It is conventionally applied for binding studies between proteins and their ligands. As polyplexes also result from interactions between a macromolecule and a small binding partner and thermophoretic properties of siRNA change upon complexation, thermophoresis turned out to be applicable. It thereby became possible to contrast the outcome of the EMSA with an equilibrium method.

A constant amount of Alexa 555/ Atto 647N labeled siRNA was added to a dilution series of the carrier, transferred to capillaries and analyzed. Compared to the EMSA, sample preparation consumed less amount of siRNA (225 ng versus 1 µg) and carrier (28 µg versus 50 µg). Figure 3.7 shows the Hill fits for each carrier. Inlays depict the primary binding curves. They partly lack the desired smoothness, as the same type of capillary was used for each carrier to grant identical experimental conditions. Still, a Hill fit yielded EC_{50} values which were interpreted as 50% binding ratios (BR_{50}) and added to table 3.1.

These values could be applied to compare the outcomes of the two methods. They largely correspond for four of the carriers. Exceptions are nanohydrogel particles and MnO@SiO_2 particles, which were already classified to possess comparatively low stability by the EMSA. This leads to the conclusion that polyplexes with high stability stay intact under non-equilibrium conditions like an electrical field. In contrast, siRNA is permanently removed from more unstable polyplexes under these conditions.

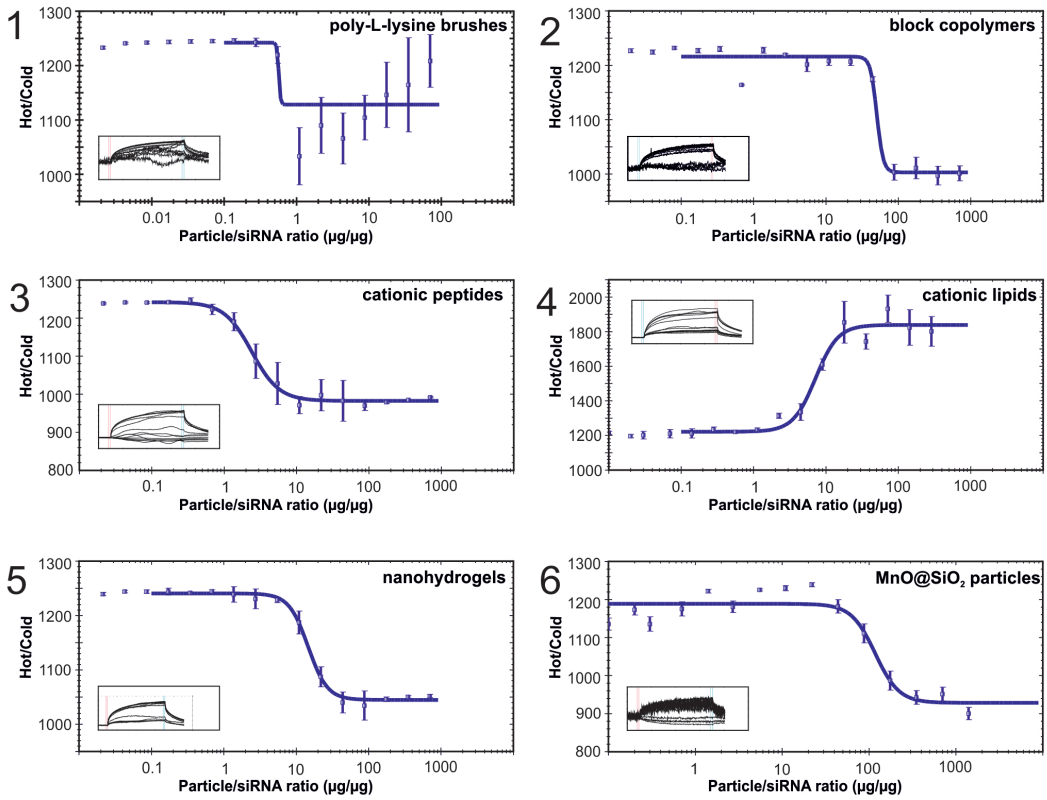

Figure 3.7: Thermophoretic analyis of polyplex formation. Hot-cold mode evaluation and Hill fit of polyplexes titrated from m/m 0.02 to 700 (n=5). (1) poly-L-lysine brushes, (2) block copolymers, (3) cationic peptides, (4) cationic lipids, (5) nanohydrogels, (6) MnO@SiO_2 particles. The inlays depict the primary binding curves of one measurement series.

The higher cc_1 for these carriers under equilibrium conditions results from constant rebinding, as in this case no siRNA is pulled away.

Which method is better suited to study polyplex binding depends on the settings to be investigated. A physiological environment may be best represented by non equilibrium conditions, as siRNA that is not stably bound will permanently be removed e.g. by RNase digest, challenges from other macromolecules or, at best, RISC incorporation [11].

As a last remark, which also leads to the next section, interpretation of EMSA data is conceptually identical for all carriers while thermophoresis data needs to be explained differently in the case of fluorescence quenching. To briefly touch the issue, polyplexes of PLL brushes and block copolymers quench siRNA fluorescence in a concentration dependent manner. So the fluorescence intensities in the binding curves rather map to quenching effects than to the actual thermophoretic behaviour. This

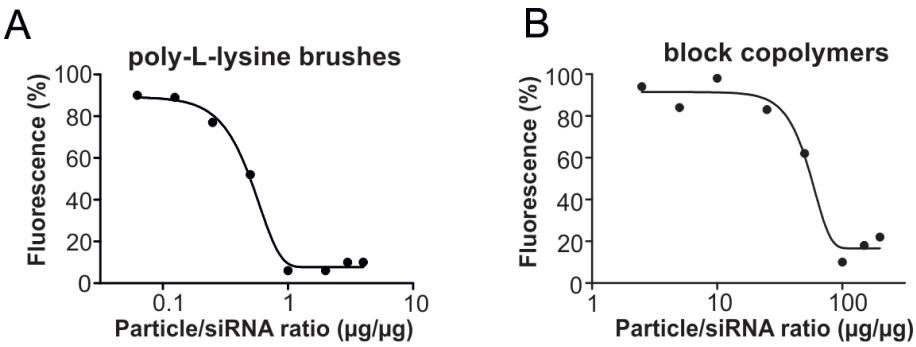

Figure 3.8: Fluorimetric determination of binding curves for (A) PLL brushes, and (B) block copolymers. siRNA was titrated with the respective carriers at different m/m ratios in a fluorimeter, siRNA 1 µM. The acceptor signal was normalized to uncomplexed siRNA and fitted with a 5 parametric dose-response curve.

was affirmed by an additional fluorimetric titration, that yielded binding curves (see figure 3.8) that largely correspond to those obtained by thermophoresis (see figure 3.7). As these curves aimed at determining the BR_{50} value, titration was not exceeded far after complete complexation. Therefore the reorganization effect discussed in section 1.4.2 is not covered, though it is already indicated for the block copolymers in the slight rise after m/m 100.

3.1.5 Monitoring polyplex formation via fluorescence quenching

Fluorescence intensities of labeled siRNA change after complexation (see section 1.4.1). The extent of this effect depends on the carrier and the m/m ratio. PLL brushes and copolymers caused almost complete quenching at cc_1 (see figure 3.9 A) regardless of the fluorophores attached to the siRNA (see appendix, figure A5). Although this effect has been observed for polyplexes of different kinds of nucleic acids and also found applications before [51, 148, 150, 151, 172] (see section 1.4.2 for details), control experiments were carried out to confirm that this extreme quenching is indeed due to the complexation itself. Figure 3.9 A shows the quenched spectra compared to siRNA only for PLL brushes and block copolymers, figure 3.9 B proves that heparin release (see section 3.2.1) completely reestablishes fluorescence intensities as well as initial R/G values for both carriers. This indicates that neither siRNA is degraded nor fluorophores are affected by the complexation. To rule out that precipitation of the polyplex is the reason for the loss of fluorescence in PLL brushes and block copolymer polyplexes, a part of the polyplex solutions was transferred to a second cuvette, where initial fluorescence could also be recovered by addition of heparin (see

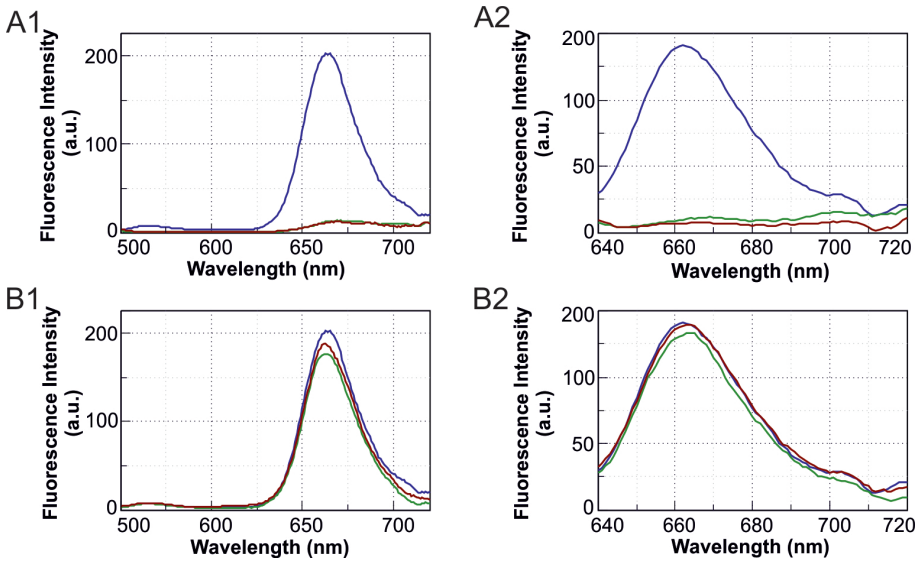

Figure 3.9: Fluorescence quenching of PLL brushes and block copolymers. Emission spectra of 1 µM Alexa/ Atto 647N labeled siRNA (blue) only, (green) PLL brushes at cc_1 and (red) block copolymers at cc_1 before (A1 at donor, A2 at acceptor excitation) and after (B1 at donor, B2 at acceptor excitation) addition of heparin at z^-_{Hep}/z^-_{RNA} 20.

appendix, figure A6).

Table 3.3 summarizes the percentage variations of siRNA fluorescence intensities in the polyplexes for cc_1 and cc_2. While the impact of cationic peptides, cationic lipids and MnO@SiO_2 particles was less pronounced, nanohydrogels even caused a boosted fluorescence intensity.

A definite explanation for the degree of quenching in a polyplex is hard to find, as several factors simultaneously effect the resulting fluorescence intensity. As discussed in detail in section 1.4.1, high salt concentrations [152] as well as proximity of fluorophores (closely connected to charge density) [150] can both cause fluorescence quenching. Structure and material of the carrier plays another important role, most

Table 3.3: Fluorescence intensity of siRNA in polyplexes

	fluorescence intensity [%][a]	
carrier	at cc_1	at cc_2
PLL brushes	7	11
block copolymers	5	12
cationic peptides	101	125
cationic lipids	41	46
nanohydrogels	234	290
MnO@SiO_2 particles	72	63

[a]Acceptor signal in polyplexes normalized to siRNA only

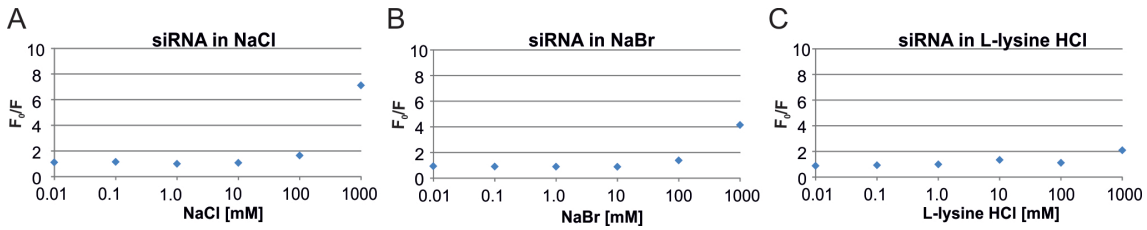

Figure 3.10: Fluorescence quenching caused by NaCl, NaBr and L-lysine HCl. siRNA was added to salt solutions with concentrations up to 1 M. F_0/F represents the ratio of acceptor fluorescence intensity of siRNA in PBS and in the respective salt solution, siRNA 0.4 µM. (A) NaCl, (B) NaBr and (C) L-lysine HCl.

prominent in the fluorescence boost for nanohydrogels.

Only the influence of salt concentration can be studied independently. When siRNA was titrated with rising concentrations of different salts, quenching was most prominent in 1 M solutions of NaCl or BrCl and weaker, but still observable, in L-lysine HCl (see figure 3.10). The salt concentration in a polyplex is assumed to be particularly high as the counter ions presumably accumulate inside and in close proximity to the polyplex (see section 1.4.1). For example, the counter ion of the poly-L-lysine brushes, Br^-, was estimated to possess a 1 M concentration in polyplexes that were prepared according to the protocols applied in this work. This means that the highly concentrated salt ions contribute to the quenching that was observed.

The degree of quenching in a polyplex is often unpredictable and can lead to biased results. Protocols should therefore be adjusted, e.g. when quantifying cellular uptake of siRNA [172] (see section 3.3.2).

On the positive side, this feature can serve as a measure for assessing the degree (see section 3.1.4 and figure 3.8) or the process of complexation [150], and may even offer a way to monitor release after cellular uptake.

3.1.6 Determination of polyplex size

Polyplex size is an important criterion as it affects a range of biological parameters, among them safety and body clearance [222]. It was determined via fluorescence correlation spectroscopy (FCS) (see section 1.4.2).

The measurements were carried out by xxxxx xxxxx xxxxx xxxxx xxxxx xxxxx xxxxx xxxxx. Following the same principle as in the thermophoresis experiments, the label on the siRNA was employed to monitor changes between free and complexed siRNA. FCS yielded R_h for polyplexes at cc_1 between 18 nm and 60 nm, which are clearly increased in comparison to the R_h of 3 nm for uncomplexed siRNA (see ta-

Table 3.4: R_h for monomers and polyplexes at cc_1

carrier	R_h of monomer [a]	R_h of polyplex[b]
PLL brushes	57 nm [115]	60 nm
copolymers	3.4 nm	29 nm [119]
cationic peptides	n.a.	highly polydisperse
cationic lipids	n.a.	highly polydisperse
nanohydrogels	24 nm [123]	22 nm
MnO@SiO_2 particles	9 nm [126]	18 nm
siRNA only	2.7 nm	

[a]determined by DLS
[b]determined by FCS

ble 3.4).

Dynamic light scatterering (DLS) measurements for the monomers, partly already published, were carried out by cooperation partners. These values are also added to table 3.4 in order to allow a comparison between the sizes of the monomer and the respective polyplex.

For the nanohydrogels, the concept of preformed particles was confirmed, as sizes did not change after complexation. MnO@SiO_2 particles doubled their size, but it can still be assumed that they also kept their preformed structure as the deposition of siRNA in the outer shell might have caused a certain increase in R_h. Also PLL brushes appeared to consist of one monomer per polyplex at cc_1, as discussed in 3.1.3. For this carrier, a static light scattering (SLS) analysis was additionally conducted by xxxxx xxxxx xxxxx. She assessed R_h directly after complexation and 24 h later for two m/m ratios slightly higher than cc_1 (see table 3.5). Changes in R_h and size in both directions over time were observed, indicating a strong dependance on m/m ratio and a maturation process during which brush polyplexes aggregate and disaggregate. This pilot experiment shows the potential of time dependent size determination to illuminate the complexation process and to define an optimal polyplex maturation period when it comes to applications like cell transfection experiments.

In contrast, cationic peptide and cationic lipid polyplexes form micrometer sized

Table 3.5: R_h for poly-L-lysine brush polyplexes over time determined by SLS

m/m	R_h after preparation	R_h after 24 h
2.3	190 nm	310 nm
2.8	120 nm	55 nm

aggregates that are too big and polydisperse to be amenable for a characterization by FCS. Sizes in the micrometer range have already been reported for cationic peptide polyplexes [41].

FCS could additionally yield information about the number of siRNA molecules per polyplex, a question that has already been approached by stoichiometric calculations in section 3.1.3. The intensity of a fluorescence peak induced by a polyplex would in general be proportional to the number of siRNA molecules it contains. Due to the quenching and boosting effects (see section 3.1.5), however, this analysis could not be conducted.

Size also offered a first hint about the pathway which is relevant for cellular uptake. Endocytosis is assumed to be the major pathway for the four polyplexes in the nanometer range (see section 1.2.4). For cationic peptides and cationic lipids, e.g. macropinocytosis seems more likely. The formation of undefined aggregates however renders a safe *in vivo* use problematic (see section 1.2.7). The cationic lipids are only intended for *in vitro* experiments, whereas the structure of the cationic peptides needs to be optimized to enable a therapeutic application.

3.2 Characterizing polyplex stability

During therapeutic application of a polyplex, the emphasis shifts from its formation to its dissociation. Polyplexes are supposed to stay intact in the blood stream and during cellular entry. Cargo must then be released at the site of action, for siRNA this is the cytosol. While special features have been developed to trigger release in the desired environment (see section 1.2.5), the carriers in this screen, with the cationic peptides being the only exception, do not possess such a functionality. Therefore the investigations into release processes presented here are based on the pure concept of polyplex stability. Viewed from this perspective, formation and dissociation become two sides of the same coin. Polyplex stability must be sufficient for cargo transportation and at the same time constrained to still enable release. The following assays aim at classifying the stability of the six carriers by challenging the polyplexes with factors that compromise their integrity.

3.2.1 Dissociation by anion competition

Heparin competition is a method for assessing the extent to which polyplexed siRNA can be displaced by another negatively charged macromolecule (see 1.4.3). Polyplexes at cc_1 and cc_2 were incubated with increasing heparin concentrations and analyzed in parallel on a gel and via thermophoresis. The z^-_{Hep}/z^-_{RNA} ratio defined the amount of negative charges of heparin per amount of negative charges of siRNA and was expected to be a parameter for a polyplex' strength to resist molecules that also compete for the same binding sites. Figure 3.11 shows the outcomes for the EMSA, figure 3.12 for the thermophoretic analysis, the determined z^-_{Hep}/z^-_{RNA} values for complete and 50% release are compiled in table 3.6. These values however did not differ distinctively among the carriers. Only a slight aberrance for cationic lipids and cationic peptides was found, where a small fraction of siRNA remained inaccessible for heparin (see figure 3.11 A3 and A4). Apart from this, displacement starting from a z^-_{Hep}/z^-_{RNA} of about 5 rather appeared as a feature that applies to siRNA polyplexes in general. A marginal note: Heparin competition for PLL brush - plasmid polyplexes yielded a z^-_{Hep}/z^-_{DNA} for complete release of 25 [116], as the larger size of a plasmid compared to siRNA presumably requires stronger forces for its replacement.

Differences in stability between the polyplexes were already observed in EMSA experiments (see section 3.1.3). The heparin assay, however, did not reflect this observation, thus yielding fewer information compared to other methods.

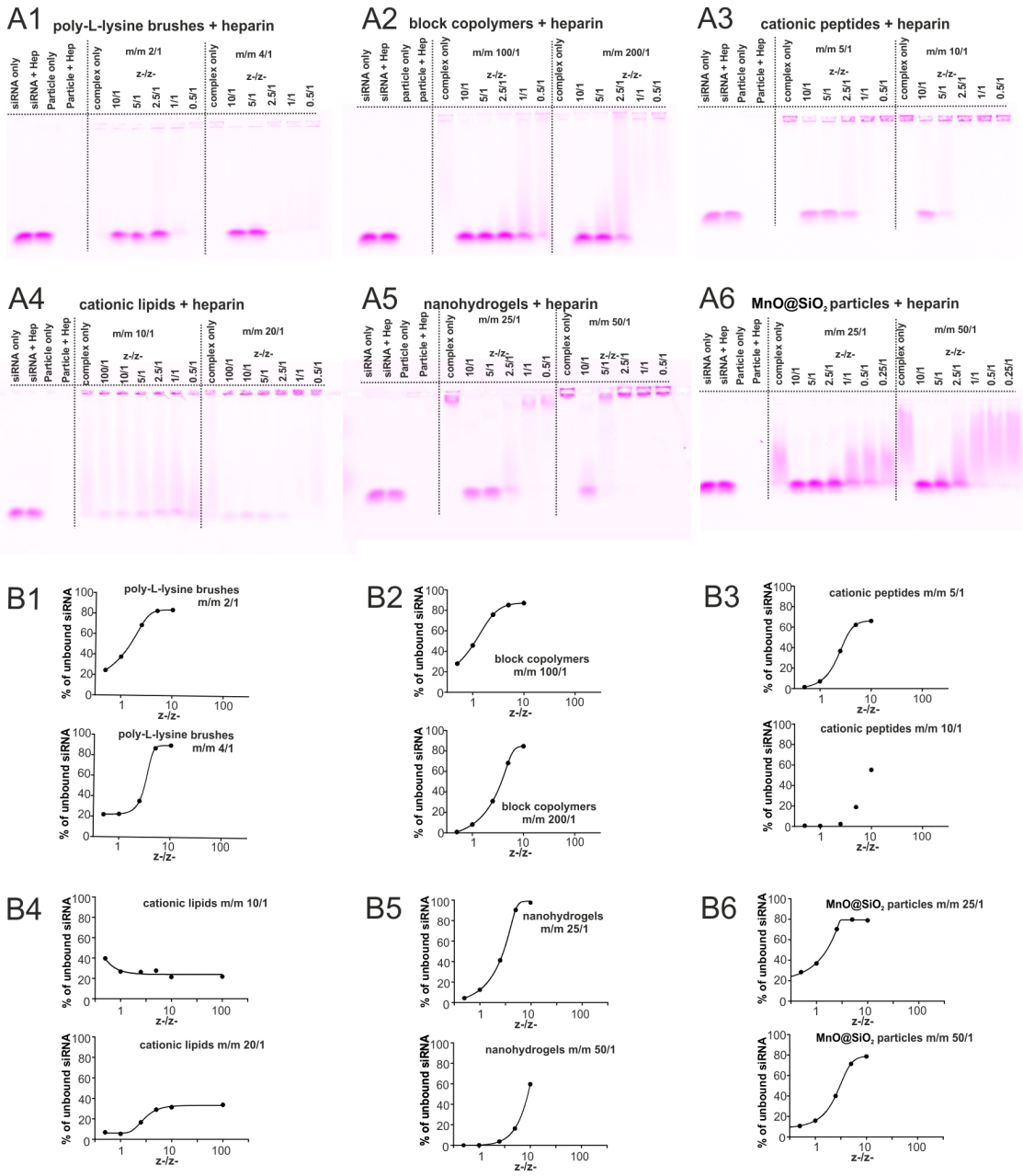

Figure 3.11: EMSA analysis of determination of z^-_{Hep}/z^-_{RNA} values for release from polyplexes by heparin at cc_1 and cc_2. (A1-6) EMSA for (1) PLL brushes, (2) block copolymers, (3) cationic peptides, (4) cationic lipids, (5) nanohydrogels, (6) MnO@SiO_2 particles. (B1-6) fluorescence signal of free siRNA quantified and fit with a 5 parametric dose-response curve.

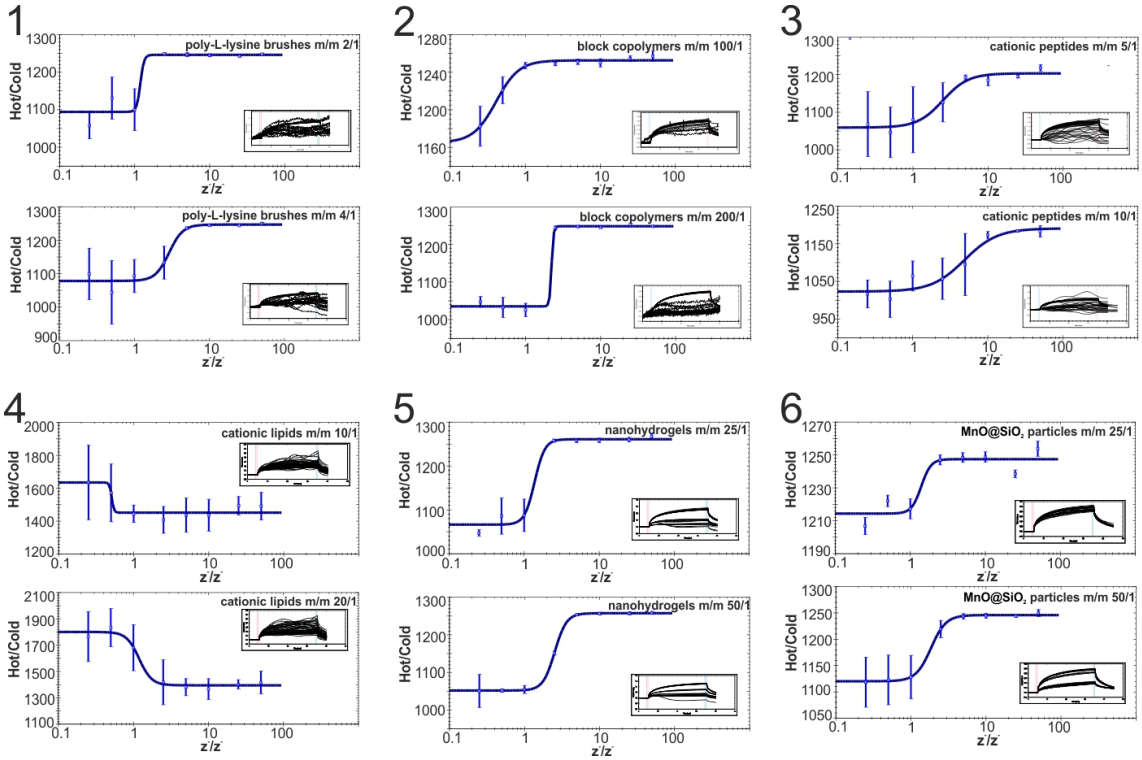

Figure 3.12: Thermophoretic analysis of heparin competition. Determination of z^-_{Hep}/z^-_{RNA} values for 50% release from polyplexes at cc_1 and cc_2 by thermophoresis of (1) PLL brushes, (2) block copolymers, (3) cationic peptides, (4) cationic lipids, (5) nanohydrogels, (6) MnO@SiO_2 particles.

Table 3.6: z^-_{Hep}/z^-_{RNA} values for heparin competition

	z^-_{Hep}/z^-_{RNA} values for cc_1			z^-_{Hep}/z^-_{RNA} values for cc_2		
carrier	complete release[a]	EMSA50[b]	MST50[c]	complete release[a]	EMSA50[b]	MST50[c]
PLL brushes	2.5	1.3	1.2	5	3.3	2.8
block copolymers	2.5	1.1	0.4	5	3	2.2
cationic peptides	5	2.3	2.5	10	n.a.	4.9
cationic lipids	n.a.	0.5	0.5	n.a.	2.8	1.2
nanohydrogels	5	2.8	1.4	10	n.a.	2.5
MnO@SiO_2 particles	2.5	1.6	1.4	5	2.7	1.8

[a] z^-_{Hep}/z^-_{RNA} ratio for complete release determined by EMSA
[b] z^-_{Hep}/z^-_{RNA} ratio for 50% release determined by EMSA
[c] z^-_{Hep}/z^-_{RNA} ratio for 50% release determined by MST
n.a. not available

3.2.2 Stability against nuclease digest

A nuclease digest was set up ot imitate key components of a physiological environment in the cuvette (see section 1.4.3). In doing so, it took up the concept of non-equilibrium conditions (see section 3.1.4). Polyplexes were exposed to RNase V1, while siRNA integrity was monitored in real time. The pace at which siRNA was degraded indicated the degree of unbound or only weakly protected siRNA and therefore permitted conclusions about the stability of a polyplex. A double label on the siRNA enabled the monitoring of its integrity via FRET. More precisely, the R/G value (see section 1.4.1) was read out. A calibration employing samples with defined fractions of double labeled siRNA connected the R/G value with the actual integrity level. An exponential decay fit finally provided a value for the mean lifetime of the siRNA (see figure 3.13). This assay was developed [129, 130, 168] and carried out by xxxxx xxxxx, who kindly provided the data.

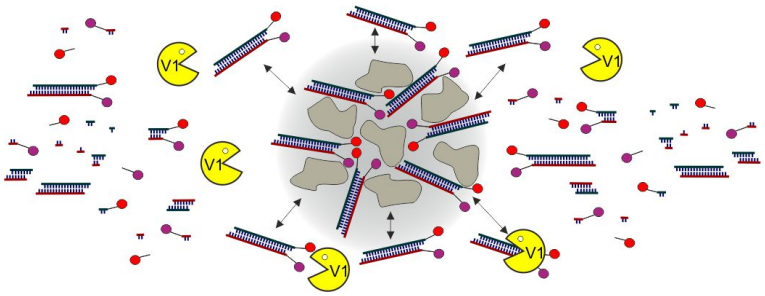

Figure 3.13: Scheme of the nuclease digest assay

Polyplexes at cc_1 and cc_2 with Alexa 555/ Atto 647N labeled siRNA were subjected to this assay. Figure 3.14 shows graphs of the integrity levels versus time. Mean lifetimes are compiled in table 3.7. The black curve added to each graph shows a reference digest of free siRNA, which was completely degraded within the first five minutes. Cationic peptides (3) and cationic lipids (4) showed a flat descent in siRNA integrity for cc_1 and siRNA was kept almost completely intact during the observation period of 2 h at cc_2. In contrast, integrity decayed quickly for nanohydrogels (5) and $MnO@SiO_2$ particles (6) at both ratios. Interestingly, degradation stalled at a level of 30 - 40% for nanohydrogels and 10 - 20% for $MnO@SiO_2$ particles, respectively (see below). This outcome reproduced the data obtained by EMSA (3.1.3) quite well, as the nuclease assay also classified these two particles as weak binders. Additionally, the smear on the gel was more pronounced for $MnO@SiO_2$ particles compared to the nanohydrogels and nuclease digest identified a higher fraction of strongly bound siRNA

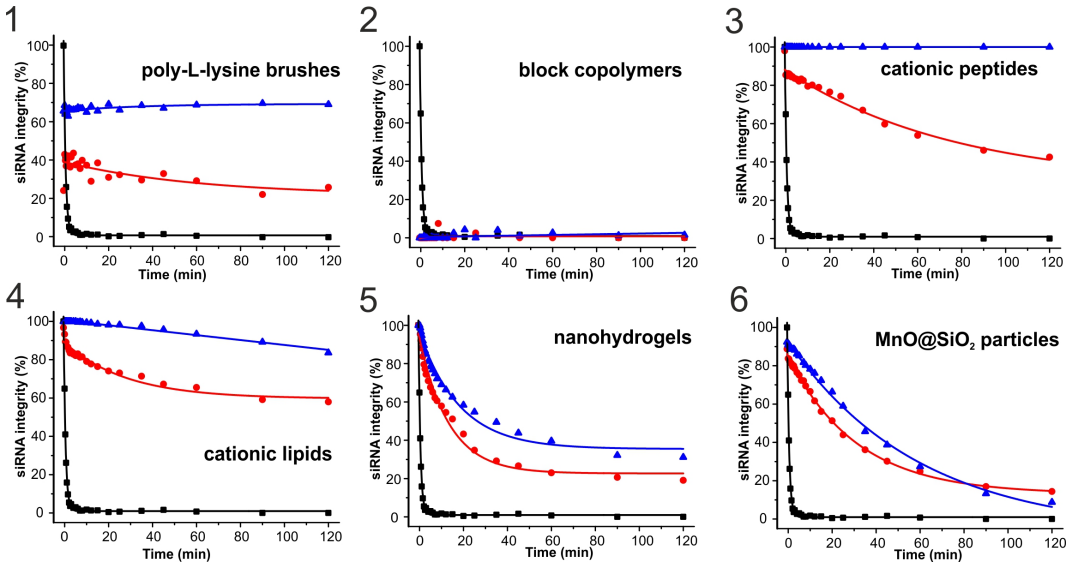

Figure 3.14: Nuclease digest assay. Polyplexes at ratios (red) cc_1, (blue) cc_2 and (black) naked siRNA were exposed to RNase V1. Upon degradation of free or released siRNA, changes in FRET were used to determine siRNA integrity levels for the polyplexes over time. (1) poly-L-lysine brushes, (2) block copolymers, (3) cationic peptides, (4) cationic lipids, (5) nanohydrogels, (6) MnO@SiO_2 particles.

for the latter.

The biphasic degradation profiles for nanohydrogels, MnO@Si_2 particles and, to a smaller degree, for cationic lipids at cc_1, may hint at a certain fraction of siRNA in the polyplex with a higher stability, which would mean that the stability even differs within one polyplex.

Data obtained for PLL brushes and block copolymers were difficult to analyze, as the almost quantitative fluorescence quenching rendered meaningful interpretation of R/G values impossible. Therefore, the standard evaluation was obviously inadequate, as can be seen in figure 3.14 (1 and 2). An alternative analysis was based on donor fluorescence, as degradation is always accompanied with a strong increase of this signal.

As siRNA that is prone to degradation is not complexed any more, fluorescence should be unquenched and thus a rise in donor signal observable. While this rise was obvious for siRNA only, neither PLL brushes nor block copolymers showed such an effect (see figure 3.15). As this means that for both cc ratios no degradation was present, the stability of these two polyplexes was classified to be even higher than that of cationic peptides and cationic lipids.

Including N/P ratios (see section 3.1.3) into the consideration, a huge gap in these values (3 and 30, respectively) was present for the two strong binders, PLL brushes and block copolymers. In a study with arginine rich peptides of varying length, a

Table 3.7: Nuclease resistance assay

	for ratio cc_1		for ratio cc_2	
carrier	mean lifetime[a]	degradation $time_{20}$[b]	mean lifetime[a]	degradation $time_{20}$[b]
siRNA only	1 min	<1 min	/	/
PLL brushes	61 min	n.a.	n.a.	n.a.
block copolymers	n.a.	n.a.	n.a.	n.a.
cationic peptides	78 min	11 min	>2h	>2h
cationic lipids	28 min	10 min	>2h	>2h
nanohydrogels	13 min	3 min	18 min	6 min
$MnO@SiO_2$ particles	31 min	2 min	59 min	8 min

[a]mean lifetime of intact siRNA
[b]time after which 20% of siRNA is degraded
n.a. not available

decreasing stability was observed with increasing N/P [48]. As far as N/P ratios were known, this was not the case in this assay, which suggests that such a relation might only exist within a homologous series of materials.

To summarize, this assay established characteristic decay curves for the six polyplexes and was able to classify PLL brushes and block copolymers as polyplexes with high, cationic peptides and cationic lipids with intermediate and nanohydrogels and $MnO@SiO_2$ particles with low stability.

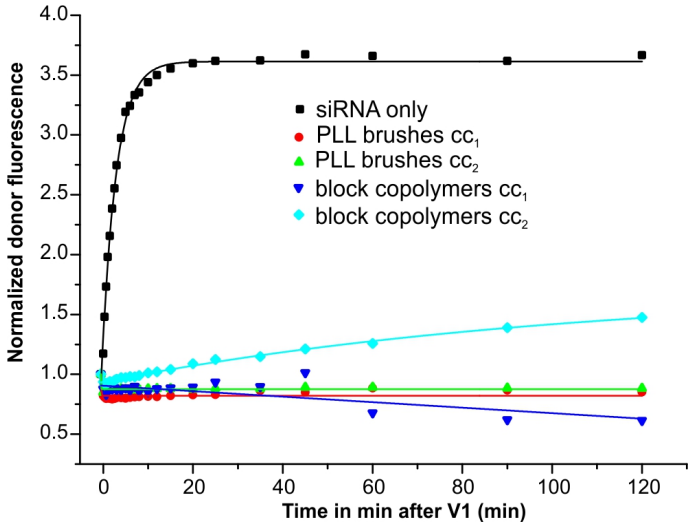

Figure 3.15: Normalized donor fluorescence during degradation of the strong quenchers poly-L-lysine brushes and block copolymers. The almost constant donor fluorescence signals for the polyplexes signify remaining integrity of the complexed siRNA in contrast to the quick increase for siRNA only, which is instantly degraded.

3.3 In vitro uptake and integrity of polyplexes

So far, assays have been conducted on a gel or in a cuvette. They all assessed characteristics of a rather biophysical nature with the aim to look into basic requirements and make predictions about a carrier's suitability for therapeutic application. In this section, *in vitro* experiments examine polyplex uptake and intracellular distribution (see section 1.4.4). A special interest lay in intracellular release, as this feature is a prerequisite for knockdown capability. The use of double labeled siRNA allowed the simultaneous monitoring of intracellular siRNA integrity. Due to a lack of the initial material, a second batch synthesis of block copolymers, nanohydrogels and MnO@SiO_2 particles was employed for all *in vitro* studies.

3.3.1 Intracellular distribution

Confocal laser scanning microscopy (CLSM), a standard method for the analysis of cellular uptake, which also allows the monitoring of FRET (see section 1.4.4), was applied first.

HeLa cells were incubated with polyplexes containing Alexa 555/ Atto 647N labeled siRNA at cc_1 and a final siRNA concentration of 40 nM. Images of living cells were acquired after 4 h. Microscopy of FRET labeled probes requires a careful adjustment of the settings to keep a bleedthrough of donor and acceptor dye into the FRET channel (see section 1.4.1) to a minimum. Controls with single labeled siRNAs show that this bleedthrough could not be completely avoided for spots with high fluorescence intensities. Still, FRET intensities are distinctively higher for double labeled constructs than for the single labeled controls (see figure 3.16).

While block copolymers and MnO@SiO_2 particles showed very weak signals, uptake was clearly visible for PLL brushes, cationic peptides, cationic lipids and nanohydrogels (see figure 3.17). The remarkable difference lay in the flooding of fluorescence in the whole cell for the cationic lipids and the fluorescence spots detected for the other polyplexes. These patterns indicated intracellular release for the cationic lipids, while the other polyplexes seem to be enclosed in vesicles. Interestingly, no release was detected in the cationic lipid's donor channel, which may be a sign for intact siRNA having escaped the endosomes. Though the cationic peptides should also be able to enter the cytosol, the CLSM images did not show a flooding. This may mean that only a massive intracellular release can be monitored by CLSM, while small fractions of siRNA escaping endosomes remain undetected.

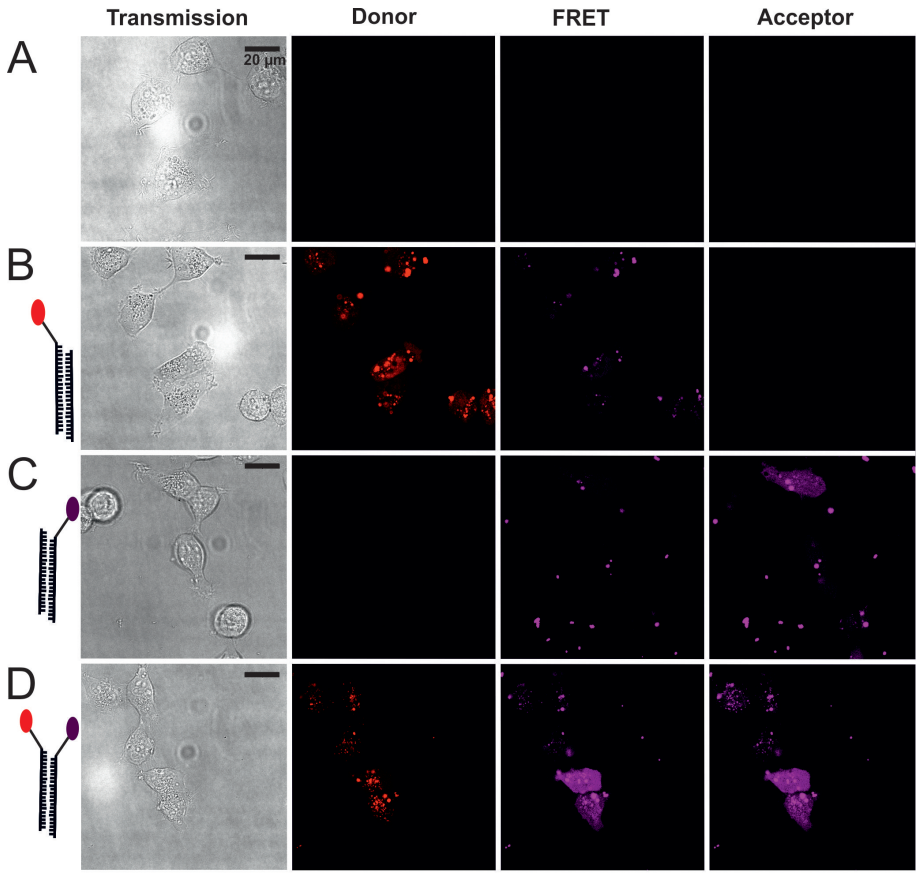

Figure 3.16: Confocal images of control samples, siRNA 40 nM transfected with Oligofectamine. (A) untransfected cells, (B) Alexa 555 (donor only) labeled siRNA, (C) Atto 647N (acceptor only) labeled siRNA, (D) Alexa 555/ Atto 647N labeled siRNA, transmission, donor, FRET and acceptor channel shown.

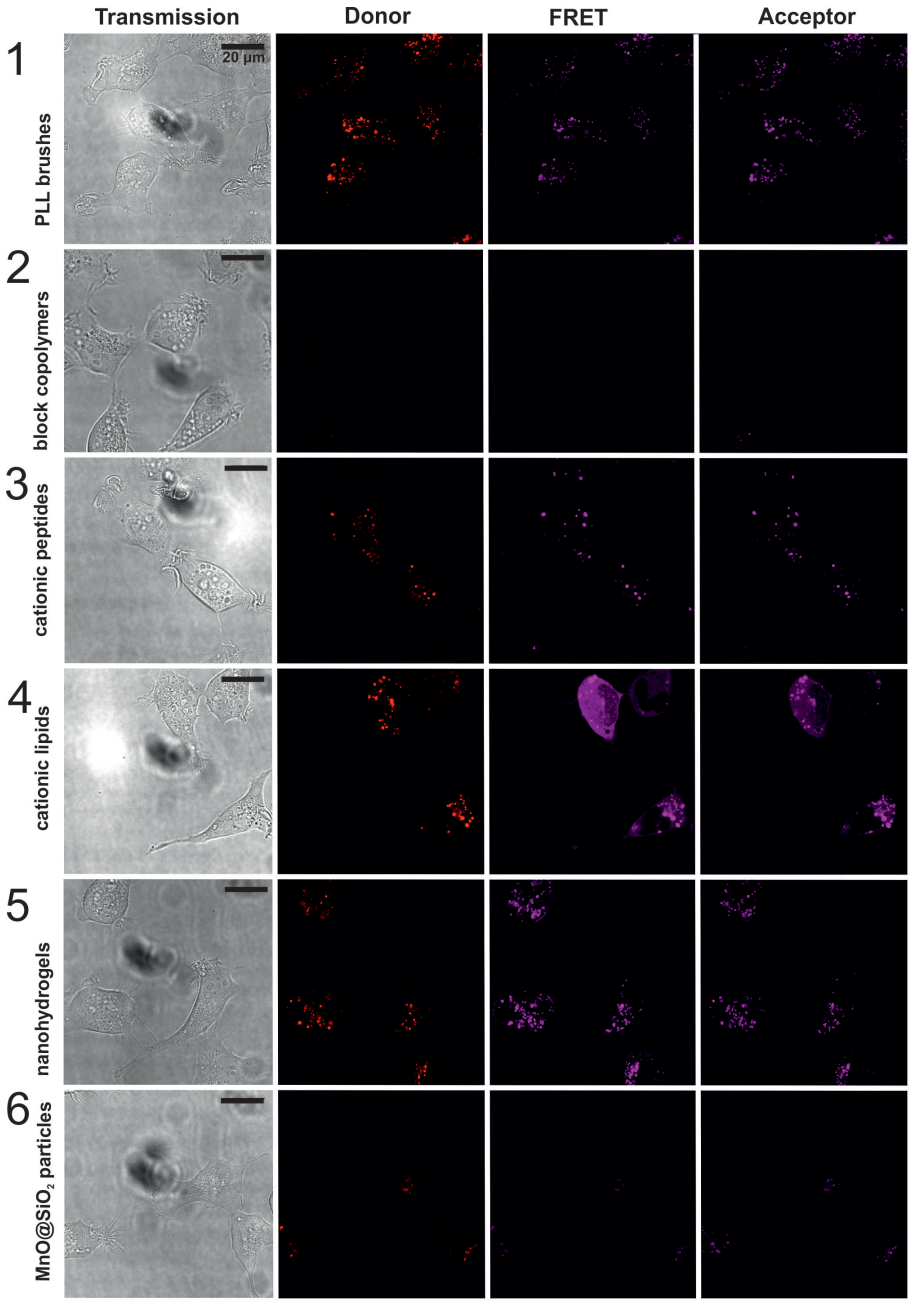

Figure 3.17: Confocal images of polyplexes at cc_1 with Alexa 555/ Atto 647 N labeled siRNA after 4 h incubation, siRNA 40 nM. Transmission, donor, FRET and acceptor channel of (1) poly-L-lysine brushes, (2) block copolymers, (3) cationic peptides, (4) cationic lipids, (5) nanohydrogels, (6) MnO@SiO_2 particles.

The four polyplexes with distinct uptake showed intensities in their FRET channels that largely correspond to those of their donor and acceptor channels. Obtaining exact conclusions about integrity levels would have to include an extensive bioinformatic evaluation [131], and would still be complicated by a certain degree of bleedthrough.

3.3.2 Quantitative assessment of in vitro uptake

Confocal microscopy enabled a rather qualitative judgement on cellular uptake as well as a visual assessment of intracellular release.

As a quantitative evaluation was supposed to possess a higher distinctiveness between the polyplexes, absolute values for siRNA uptake were obtained via two different approaches and their outcomes compared. In parallel, siRNA integrity was assessed based on an intracellular determination of the R/G ratio.

To avoid the bias resulting from measuring whole cells via flow cytometry (see section 1.4.4), uptake was quantified by determining fluorescence in cell lysate [172]. This protocol included cell lysis in TritonX (TrX) and sodium dodecyl sulfate (SDS), the former to lyse the cells and the latter to release siRNA from polyplexes. Prior to the lysis, cells were thoroughly washed with PBS and heparin to release siRNA from those polyplexes that may stick on cell surfaces. A gel showing SDS/TrX release and fluorimetric measurements of regained fluorescence intensities after SDS/TrX treatment is shown in the appendix, figure A7. Cell lysate was analyzed on a plate reader. As the acceptor signal is not influenced by fluorescence changes due to FRET, it was employed for quantifying the siRNA, followed by normalization to protein content (see appendix, figure A8 for calibration curves of siRNA fluorescence and the protein assay).

HeLa cells were incubated with the polyplexes at cc_1 containing an Atto 488/ Atto 590 labeled siRNA at a final concentration of 125 nM. To obtain time profiles of siRNA uptake, timepoints of 4 h, 12 h and 24 h after transfection were assessed. As can be seen in figure 3.18 A, the extent of siRNA uptake differed widely among the polyplexes. Nanohydrogels showed by far the highest uptake. Compared to their level, uptake for PLL brushes and cationic peptides was reduced to 50%. Cationic lipids, block copolymers and $MnO@SiO_2$ particles followed with descending values, with $MnO@SiO_2$ uptake being close to zero. Remarkable was the pronounced drop of siRNA levels for nanohydrogels, cationic lipids and cationic peptides already after 12 h.

Having obtained absolute values, the above mentioned drawbacks of flow cytometry

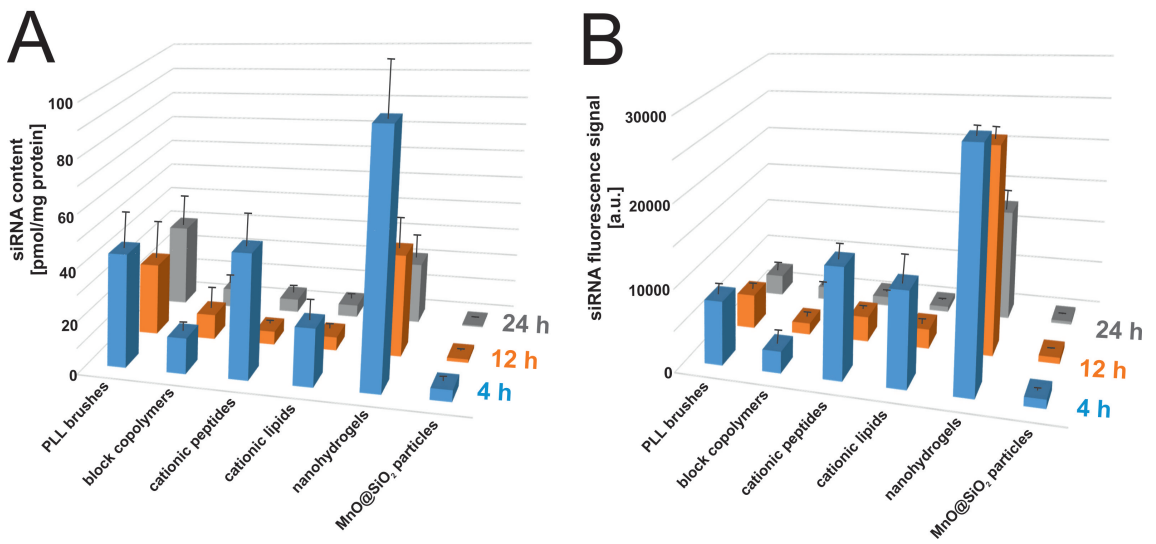

Figure 3.18: Quantification of siRNA uptake for polyplexes 4 h (blue bars), 12 h (orange bars) and 24 h (grey bars) after transfection (A) via fluorescence in cell lysate and (B) via flow cytometry.

were now viewed from another perspective. So the same protocol was repeated, this time with flow cytometric readout and uptake quantified by the median fluorescence intensity of the acceptor channel (see figure 3.18 B). Representative histograms of the acceptor channel are compiled in the appendix, figure A9. A direct comparison between the two methods is of course out of question. It was however assumed that enhanced levels in the flow cytometric time profiles could give evidence about intracellular release: As endocytosis has been described as the major route for polyplex uptake [11], an effusion out of vesicles was expected to be accompanied by an increase in cellular fluorescence. The same would be true for the release from the polyplex.

Differences in the time profiles between the two methods, however, were less pronounced than expected. Only for the nanohydrogels, the siRNA level dropped significantly less in the flow cytometric data after 12 h, which is hard to interpret as intracellular release has not been observed in microscopy over this time period [125].

Cationic lipids, which showed a lesser uptake after 4 h than PLL brushes and cationic peptides via quantification in cell lysate, showed a higher and a comparable level, respectively, in flow cytometry. These observations hint towards a more favourable release profile of the lipids.

Still the most dominant feature of both datasets was the difference between cationic peptides and cationic lipids with their fast decrease in siRNA levels from 4 to 12 h, and PLL brushes and block copolymers that showed a less pronounced reduction of

siRNA levels during 24 h.

The visual impression of the CLSM evaluation correlated in general with the flow cytometric data after 4 h, the cationic peptides with their weak signal in CLSM being the only exception. The general congruence underlines the concept that both methods rather depict intracellular distribution than enable an absolute quantification.

3.3.3 In vitro integrity

Additional acquisition of donor and FRET channel in the same experiment offered the determination of intracellular siRNA integrity. The flow cytometric readout was chosen, as living cells are most appropriate to reflect the integrity status inside cells and the R/G ratio as a relative value is stable against biased fluorescence intensities. By dividing the fluorescence intensity of the FRET channel by that of the donor channel, the R/G ratio was derived as a new parameter for each cell. The median of this parameter across all cells represented the R/G ratio for the whole cell population.

Figure 3.19 displays the time profiles of R/G values (representative histograms of the R/G are compiled in the appendix, figure A10). Again, cationic peptides and cationic lipids showed a distinct time course with high initial values and a strong decrease after 12 h. Nanohydrogels displayed an almost constant R/G during 24 h, while PLL brushes and block copolymers had an R/G close to zero already after 4 h. R/G values for $MnO@SiO_2$ particles could not be obtained as their weak uptake led to fluorescence levels that were too low for meaningful analysis.

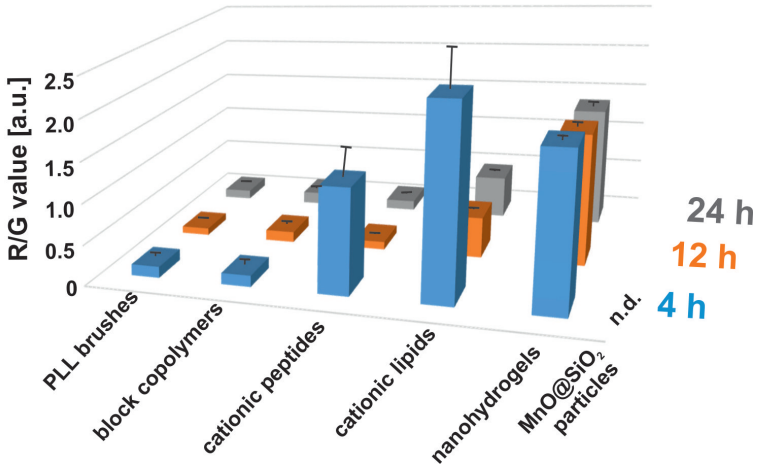

Figure 3.19: Intracellular integrity (R/G value) of siRNA determined via flow cytometry after 4 h (blue bars), 12 h (orange bars) and 24 h (grey bars), n.d.: not determinable.

This data showed a different picture than the nuclease challenge in the cuvette (see section 3.2.2). This could partly be attributed to differing observation times (2 h and from 4 h onwards, respectively). Still this does not explain the low integrity levels for PLL brushes and block copolymers that have previously been classified as strong binders. So this outcome rather highlights the difficulties that lie in approaches to simulate *in vitro* behaviour. The cuvette test only considers one single feature, in this case stability against nuclease. This factor becomes one of many in an *in vitro* setting, where, among others, release by polyanions, reactions to pH changes or dissociation due to intracellular triggers also play a role. The extent of the impact of only one of these factors is therefore hard to predict. Nevertheless, stability against nucleases does not seem to be the major factor influencing intracellular integrity of PLL brushes and block copolymers.

The discussion of intracellular siRNA levels and integrity is continued in section 3.5, where it is viewed in the context of knockdown capability.

3.4 In vitro assays for assessing knockdown capability

In a next step, the polyplexes were tested for their actual assignment, namely mediating the knockdown of a specific gene. To be able to address this question, efforts have been invested in optimizing suitable *in vitro* systems. This section presents two systems, both based on the enhanced green fluorescent protein (eGFP) as target and readout.

The two systems available comprise the incubation of cells with siRNA directed against eGFP for 24 h and the subsequent readout of green fluorescence via flow cytometry.

3.4.1 Knockdown in HEK cells with exogenous eGFP

This test was established in the lab by xxxxx xxxxx and employs HEK cells as well as eGFP plasmid [174]. Plasmid expression led to distinct fluorescence intensities compared to untreated cells, as can be seen from the GFP channel histograms (see figure 3.20 B and A). Administration of siRNA caused a considerable reduction of the fraction of positive cells as well as their fluorescence intensity (see figure 3.20 C).

To include these two changing parameters in the evaluation, knockdown was quantified by multiplying the fraction of positive cells with their mean fluorescence intensity, yielding a product of arbitrary units.

This product was normalized to that of a positive control, cells only transfected with the eGFP plasmid. For the standard transfection agent Lipofectamine^{TM}, a knockdown of more than 95% was achieved for concentrations of unlabeled siRNA above 1 nM (see figure 3.22). Also, a dose response relationship could be established (see figure 3.21).

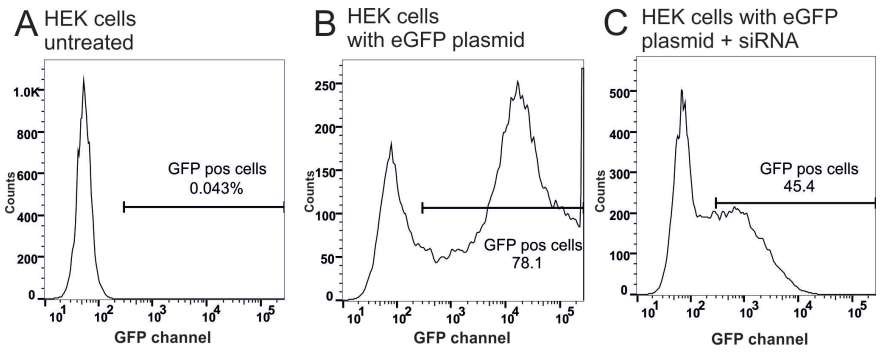

Figure 3.20: Flow cytometric GFP fluorescence histograms for HEK cells. (A) untreated HEKs, (B) HEKs with eGFP plasmid, (C) HEKs with eGFP plasmid and siRNA.

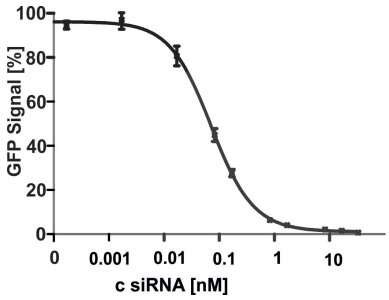

Figure 3.21: Dose-response curve for HEK one step setup with Lipofectamine^{TM}.

This data was acquired with a setup where plasmid and siRNA were administered in the same transfection step, the so-called one step setup. This setup obviously cannot be employed when testing transfection agents, as the plasmid always has to be administered with a reproducible efficiency.

The two step setup separates plasmid and siRNA application. Thereby it is essential that the siRNA is administered before the plasmid. With an eGFP half life of more than 24 h [223], siRNA has to act from the initial moment of eGFP translation, as already translated eGFP would bias the signal at the readout timepoint of 24 h. The standard procedure allows for a time lag of four hours between the two steps. In this setup, however, knockdown could only reach about 60-70% with Lipofectamine^{TM} (see figure 3.22).

This can be reasoned because cationic lipids are not able to transfect the whole cell population (see the remaining peak for negative cells after plasmid administration in figure 3.20 B). In the one step case, transfected cells receive plasmid and siRNA simultaneously, while the two steps provide the possibility that a fraction of the cells receives only plasmid but no siRNA.

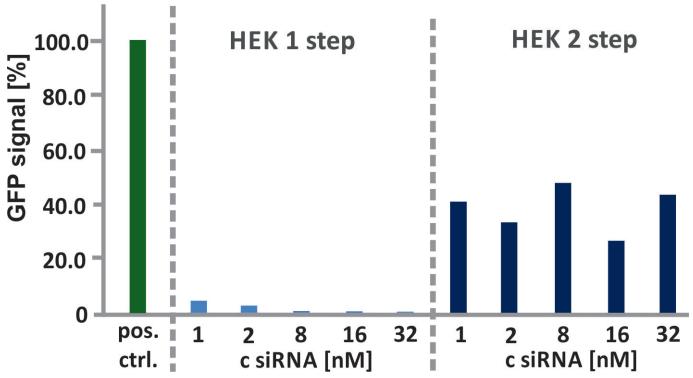

Figure 3.22: Comparison of knockdown capacity for HEK one step and two step setup with Lipofectamine^{TM} and concentrations of unlabeled siRNA from 1 nM to 32 nM.

The two step setup would enable the testing of different agents for siRNA delivery. However one can imagine that in the second (plasmid transfection) step which has to be carried out with standard reagents, siRNA still remaining on the cells from the first step could be coadministered. Though cells are washed thoroughly between the two steps and preliminary testings did not prove evidence for this, this possibility cannot be completely ruled out. For this reason, the two step setup was not further employed for the testing of siRNA carriers.

The HEK system, however, proved to be effective in a one step setup that focused on comparing knockdown efficiencies of differently labeled siRNA (see section 3.6).

3.4.2 Knockdown in HeLa MAZ S06 cells

A way to prevent this drawback would be the adaptation of this test to a cell line that encodes eGFP intrinsically. Thanks to the kind donation from xxxxx xxxxx, a HeLa cell line with an episomal vector encoding a destabilized eGFP was obtained. This vector contains two destabilization signals. Firstly, AU-rich motifs in the 3' untranslated region (UTR) promote rapid mRNA decay. Secondly, the insertion of a sequence encoding for a fragment of mouse ornithin decarboxylase targets the eGFP to the proteasome [224]. The enhanced turnover results in an eGFP half life of approximately 30 min, which meets the requirements for an application in knockdown experiments.

As can be seen in figure 3.23 B, HeLa MAZ cells show enhanced fluorescence compared to HeLa cells that do not contain the vector (A), but the destabilization diminishes fluorecence markedly compared to the plasmid transfected HEK cells (see figure 3.20 B).

As a proof of principle for the fast turnover, fluorescence decreased to almost the level of regular HeLa cells after 4 h treatment with cycloheximide (CHX), an inhibitor of protein synthesis (see figure 3.23 D).

The weak fluorescence of HeLa MAZ cells was sufficient to indicate knockdown (see figure 3.23 E) in a dose dependent manner, as can be seen from the titration with Lipofectamine^{TM} (see figure 3.24 A red curve). The setup could be further improved by incubating the cells with the proteasome inhibitor MG115 after the siRNA transfection period. This treatment slows down eGFP degradation, resulting in a fluorescence boost proportional to the amount of eGFP that has not been knocked down in the previous step. As signals became more distinct (see figure 3.23 C and F) and dose response curves without and with MG115 correlated (see figure 3.24 A red and blue curve), the MG115 treatment was included in the standard protocol. Maximal knockdown was

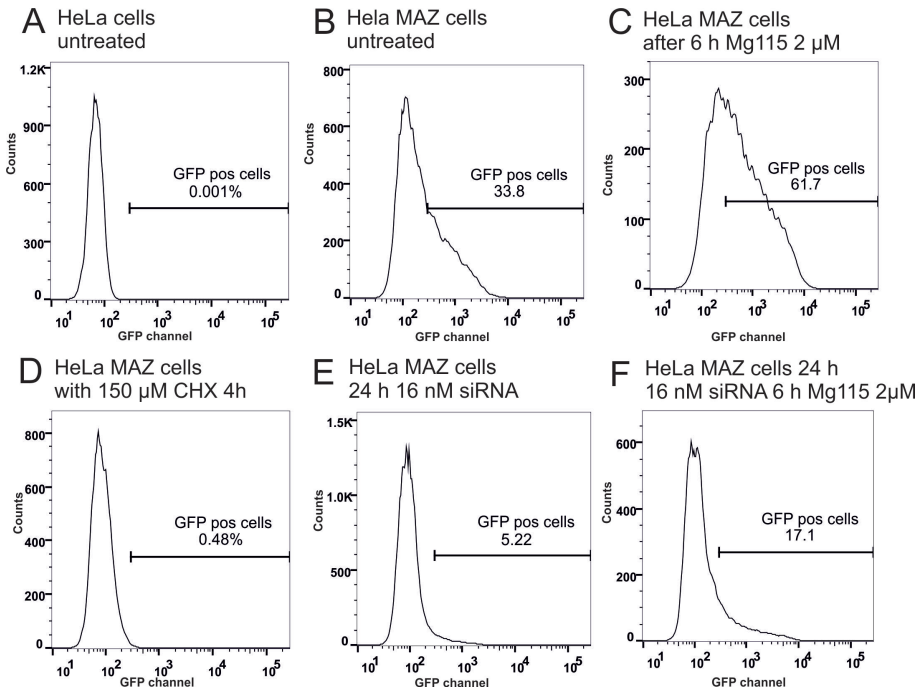

Figure 3.23: Flow cytometric GFP fluorescence histograms for HeLa MAZ cells. (A) HeLa cells untreated, (B) HeLa MAZ cells untreated, (C) HeLa MAZ cells after 6 h 2 µM MG115, (D) HeLa MAZ cells after 4 h 100 µM CHX, (E) HeLa MAZ cells after 24 h 16 nM siRNA, (F) HeLa MAZ cells after 24 h 16 nM siRNA and 6 h 2 µM MG115.

slightly reduced to 80-90% compared to the 95% for the HEK cells. This also could be explained by the fact that siRNA transfection is not quantitative.

Knockdown was calculated with the same approach as for the HEK cell assay. Evaluation was refined by choosing the median instead of the mean for determining fluorescence intensity, as this parameter is less sensitive to outliers and more appropriate for non gaussian distributed populations, like in cytometric data [225].

Both factors included in the quantification, namely fraction of positive cells and fluorescence intensity, were distinctively reduced after siRNA administration for the HEK cells. The knockdown quantification for the HeLa cells, however, was mostly based on the reduction of positive cells. Their fluorescence intensity changed less distinctively, which was due to the low initial fluorescence of these cells (see above).

Further basic testing of the HeLa MAZ system included a comparison of IC_{50} values of Lipofectamine^{TM} and Oligofectamine^{TM}. IC_{50} values of the two agents were in the same range and in accordance with the HEK system (see table 3.8). Oligofectamine^{TM} showed an unexpectedly high maximal knockdown of 98%. Dose response curves indicate that the fluorescence signal for Oligofectamine^{TM} does not return to 100% for the lowest siRNA concentrations, as it is the case for Lipofectamine^{TM} (compare

Table 3.8: IC_{50} values for HEK and HeLa MAZ systems with unlabeled siRNA

	HEK system		HeLa MAZ system		
	Lipofectamine™		Lipofectamine™		Oligofectamine™
	1 step	2 step	without MG115	with MG115	with MG115
IC_{50}[a]	72 pM	n.a.	127 pM	110 pM	157 pM
max KD[b]	95%	65%	88%	85%	98%

[a]determined with the asymmetric 5 parameter fit (GraphPadPrism™)
[b]maximal knockdown achieved in this system

figure 3.24 A and B). So there is a general reduction of the signal for Oligofectamine™ that may be ascribed to an unspecific negative effect of this agent on protein synthesis.

A further test with double labeled siRNA showed an about sevenfold increase in IC_{50} compared to unlabeled siRNA (compare 3.24 B grey and pink curve), which is also in accordance with findings from the HEK system that are discussed in detail in section 3.6.

Despite reduced fluorescence intensities, the HeLa MAZ system indicated knockdown distinctively. In basic testings, features from the established HEK system could be reproduced. With the major advantage that eGFP does not have to be administered separately, this system was from then on favoured over the established one.

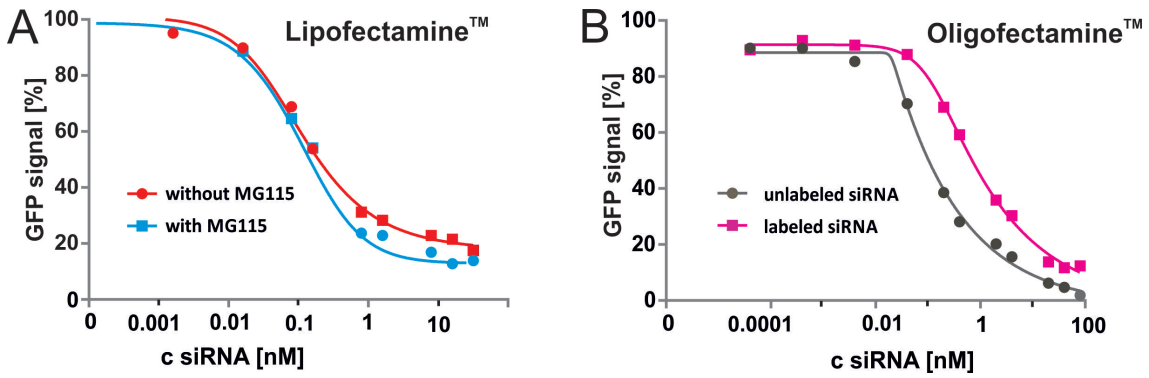

Figure 3.24: Dose-response curves for the HeLa MAZ system. (A) (red) without MG115, (blue) with MG115 for unlabeled siRNA with Lipofectamine™, (B) with MG115 for (grey) unlabeled and (pink) Alexa 555/ Atto 647N labeled siRNA with Oligofectamine™.

3.5 In vitro knockdown capability and toxicity of polyplexes

Having suitable *in vitro* systems at hand, polyplexes were subjected to knockdown and, in addition, toxicity studies.

3.5.1 Toxicity

Toxicity can be conveniently assessed via flow cytometry by adding 4',6–diamidino–2–phenylindole (DAPI) stain to the cell suspension directly before analysis. DAPI negative cells constitute the fraction of viable cells, as DAPI can only cross the membrane of dead cells. HeLa MAZ cells were incubated with the polyplexes at cc_1 and an siRNA concentration of 125 nM. As can be seen in figure 3.25, no toxic effects were noticed for any of the carriers.

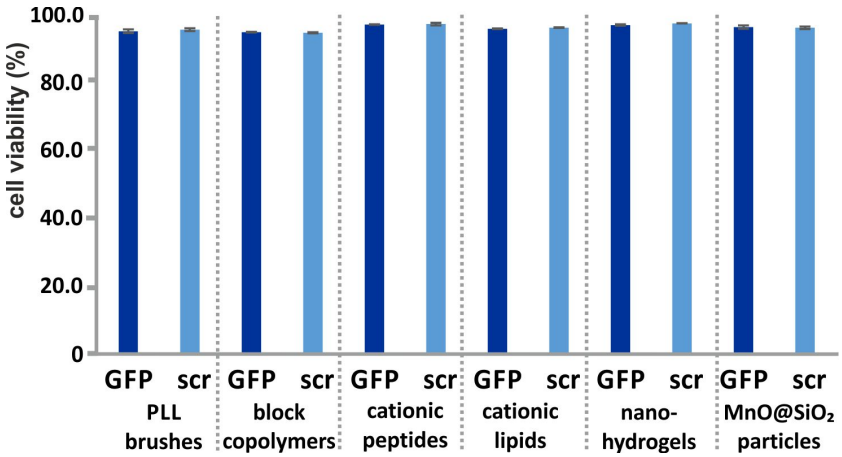

Figure 3.25: Cell viability after 24 h incubation with the polyplexes. Cells were treated with the polyplexes at cc_1 and an siRNA concentration of 125 nM of anti GFP and control siRNA, respectively. 1 µg/ mL DAPI was added to the cell suspensions which were analyzed by flow cytometry.

3.5.2 Knockdown studies

As the HeLa MAZ system had proven to be advantageous (see section 3.4), these cells were incubated with the polyplexes at cc_1. Anti eGFP siRNA and siRNA with a control sequence were both tested at a concentration of 62.5 nM. After 24 h incubation and 5 h of proteasome inhibitor treatment, green fluorescence was read out via flow cytometry.

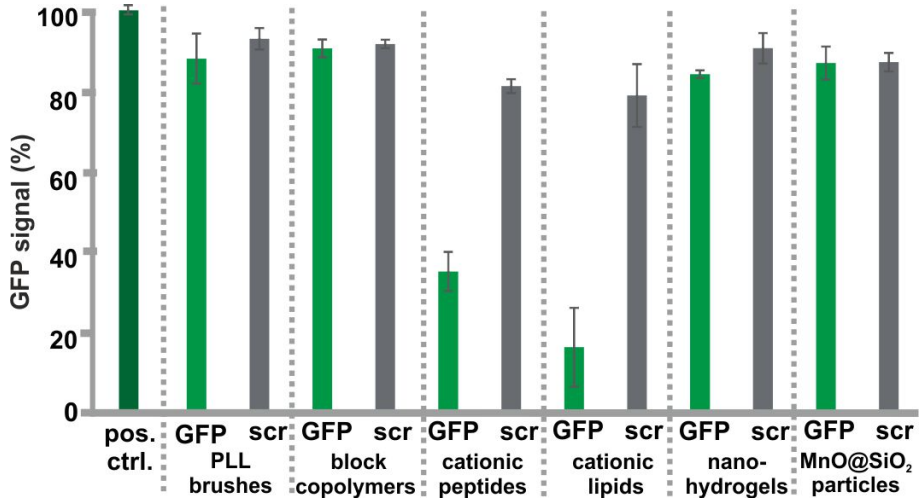

Figure 3.26: HeLa MAZ knockdown for polyplexes at cc_1, c siRNA 62.5 µM.

The outcome is easily summarized, as only cationic lipids and cationic peptides were able to mediate a significant knockdown of 85% and 65%, respectively. Although cells were still viable (see section 3.5.1), a certain unspecific influence on protein synthesis was observed, as none of the polyplexes reached a GFP signal of 100% for the transfection with control siRNA. This effect was most pronounced for cationic lipids and cationic peptides.

This test confirmed a previous HeLa MAZ assay, that also found knockdown only for cationic lipids and cationic peptides (while, however, not assessing block copolymers and MnO@SiO_2 particles). An additional information could be gained from the former assay, as cationic peptides showed a more pronounced knockdown with an increasing m/m (see appendix, figure A11).

The large gap between distinct knockdown effects for two and no effect for the other four carriers raises the question if the features assessed so far offer an explanation. As the uptake experiments (see section 3.3.2) rather illustrated tendencies than significant effects for the intracellular distribution of siRNA, only hypotheses can be formulated. A clearer picture should be obtained by pathway probing and investigations in the mechanism of endosomal release for each polyplex.

In an attempt to relate knockdown capability to cellular uptake (see section 3.3.2) as well as intracellular siRNA integrity (see section 3.3.3) profiles, high initial values for siRNA content as well as integrity followed by a strong decrease seems to be beneficial. This pattern may be ascribed to a fast escape of intact siRNA from e.g. endosomes and its availability in the cytosol, where siRNA is prone to both, RISC incorporation,

as well as degradation by cytosolic RNases. Cytosolic availability has been observed for cationic lipids [131], and is also given for the cationic peptides as they can mediate their endosomal release [41].

Though having been classified as polyplexes that efficiently protect siRNA when challenged with RNase V1 in the cuvette (see section 3.2.2), low initial integrity levels for PLL brushes and block copolymers after cellular uptake prohibited any knockdown effect. Inside of cells, PLL brushes and block copolymers may be prone to other degradation factors than RNase V1 or not be able to escape from endosomes where they are quickly degraded by lytic enzymes present in this compartment. A lack of endosomal release has been described for the material poly-L-lysine [90] and can also be assumed for the block copolymers as they do not possess a feature that facilitates endosomal release.

The sustained level of siRNA integrity for nanohydrogels speaks against their presence in both endosomes and cytosol. These polyplexes seem to reside in a different compartment where they are neither degraded nor available for the RISC complex. Such a behaviour has also been postulated for the special kind of nanohydrogel tested in the *in vitro* experiments [125].

3.6 Influence of siRNA labeling on knockdown efficiency

Covalent modifications of nucleotides in an siRNA are known to impact stability and biological activity [34]. Such modifications, in the form of a covalent attachment of fluorescent labels onto siRNA, are almost indispensible when investigating siRNA delivery (see section 1.4.1). Thus a separate study aimed at comparing knockdown efficiencies of differently labeled siRNAs.

Apart from effects deriving from changes in thermal stability (see 1.4.1), it has also been reported that methylation of the 5'-OH on the antisense strand ablates RNAi activity [226, 227]. As this demonstrates the sensitivity of the 5'-antisense end, it stands to reason if other labeling strategies may be better suited than the attachment on the 5'-phosphate that is conducted by commercial suppliers (see figure 3.27 A). To address this question, xxxx xxxxx xxxxx xxxxx synthesized a guanosine building block with a terminal alkyne attached to the exocyclic *N2* (termed NPI), that was incorporated at the 5'-end into an anti eGFP antisense strand and functionalized with Atto 590 via CuAAC (see figure 3.27 B). This strand was hybridized to a sense strand. This duplex did not show a difference in melting temperature compared to a duplex with the commercially labeled strand [174]. Having ruled out changes in thermal stability, effects of the labeling position on knockdown efficiency were investigated.

A HEK cell reporter gene assay in a one step setup (siRNA and eGFP plasmid were transfected in one transfection step, see 3.4) was employed to establish dose response curves. Different combinations of sense and antisense strands were tested in order to

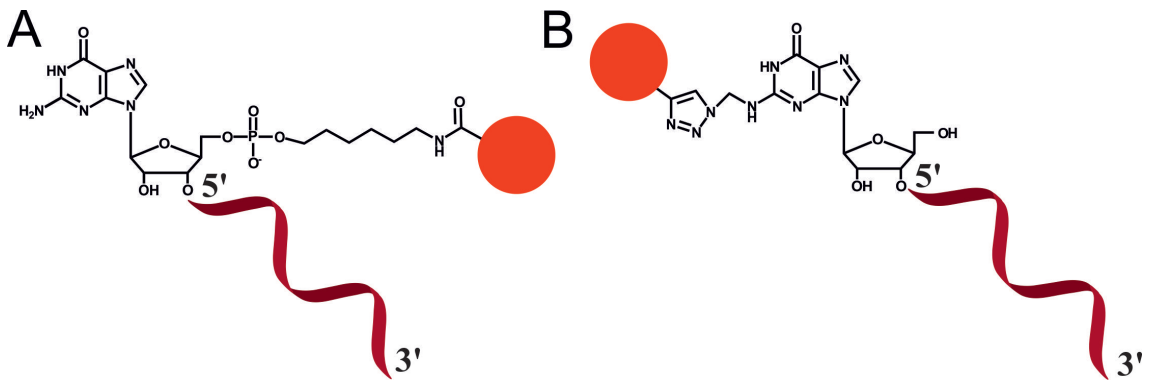

Figure 3.27: Structures of oligonucleotides labeled on the 5'-terminal guanosine. (A) Conventional labeling via the terminal phosphate, (B) labeling on the exocyclic *N2* of the modified guanosine (NPI) via CuAAC.

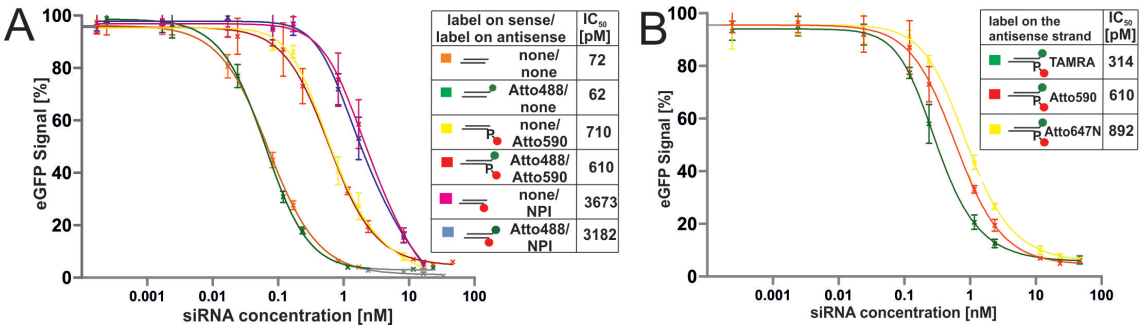

Figure 3.28: IC_{50} curves of differently labeled siRNAs, (A) (orange) unlabeled, (green) single labeled on the sense strand, (yellow and red) antisense labeling via the 5' phosphate, sense strand labeled and unlabeled, respectively, (pink and blue) antisense labeling via the NPI, sense strand labeled and unlabeled, respectively, (B) labeled sense strand and antisense strand labeled with (green) TAMRA, (red) Atto 590 and (yellow) Atto 647N.

attribute changes in efficiency to the different labeling positions.

Figure 3.28 A shows that a label on the 3' end of the sense strand left knockdown efficiency unchanged (compare e.g. the orange and the green curve), in contrast to the labels on the antisense strand: The most efficient knockdown was achieved with an unlabeled antisense strand (orange and green curves) resulting in an IC_{50} value between 60 - 70 pM. A 10x less efficient knockdown, which, however, still displays distinct dose response curves at siRNA concentrations adequate for biologic activitity testings, was obtained from duplexes containing the commercially available antisense strand (yellow and red curves). The duplexes with the antisense strand labeled at the 5'-terminal guanosine (NPI), however, showed a 5x weaker knockdown than the commercially labeled one (blue and pink curves). This outcome indicates that labeling directly on the 5'-terminal nucleobase attenuates knockdown efficiency to a greater extent than the labeling on the 5'-terminal phosphate.

To further investigate the 5' phosphate position, IC_{50} curves for siRNAs with different dyes attached at this position were compared (see figure 3.28 B). IC_{50} values rose from TAMRA (green curve) over Atto 590 (red curve) to Atto 647N (yellow curve), roughly corresponding to the size of the dye (432 g/mol, 691 g/mol and 746 g/mol, respectively), implying sterical hindrance at this position as one possible reason for reduced efficiency.

To summarize, a fluorescent label on the 3' of the sense strand left siRNA activity unchanged. 5'-antisense labeling via the terminal phosphate showed a reduced knockdown effect, which is still completely sufficient for any kind of biologic application. A label on the 5'-nucleobase was not advantageous over the phosphate labeling.

3.7 Evaluation of particles with siRNA entrapping capability

This section briefly turns to particles that are able to entrap siRNA. These particles differ widely from polyplexes in structure as well as in binding and release concepts and therefore constitute a second class of polymeric carriers. They were mainly screened for siRNA cargo encapsulation and integrity with first approaches towards testing *in vitro* knockdown effects. The current status of ongoing studies is summarized for nanocapsules [181], dextran particles [42] and liposomes [129], which are described in detail in the introduction (see section 1.5).

3.7.1 Nanocapsules

Three batches of nanocapsules, two with FRET labeled siRNA and one with single labeled siRNA, were obtained, accompanied by PBS containing control batches. The nanocapsules were synthesized by xxxxx from the Landfester group (MPIP Mainz). These batches are specified in the appendix (see table A1).

An R/G value in the cuvette was determined for the two batches with FRET labeled siRNA. R/G values of 3 (for unpurified siRNA content) and 17 (for SEC purified siRNA), respectively, were obtained (see figure 3.29 A and B). They proved that encapsulated siRNA in both batches endured the capsule manufacturing process.

EMSA for the siRNA containing batches showed one band of free siRNA for each of the three batches, indicating that siRNA was not encapsulated (see figure 3.30 A-C). On the contrary, an RNase digest assay with FRET labeled siRNA containing capsules showed constant R/G values over a period of 75 min (see figure 3.30 D), which suggests that siRNA was protected from degradation. One explanation for this contradiction

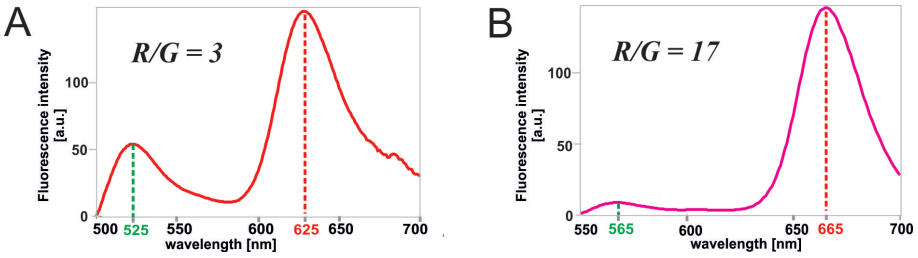

Figure 3.29: Integrity of siRNA in nanocapsules by R/G determination. (A) capsules containing Atto 488/ Atto 590 labeled siRNA, Ex 488 nm. (B) capsules containing Alexa 555/ Atto 647N labeled siRNA (SEC purified), Ex 543 nm. Spectra were corrected by subtracting that of empty capsules.

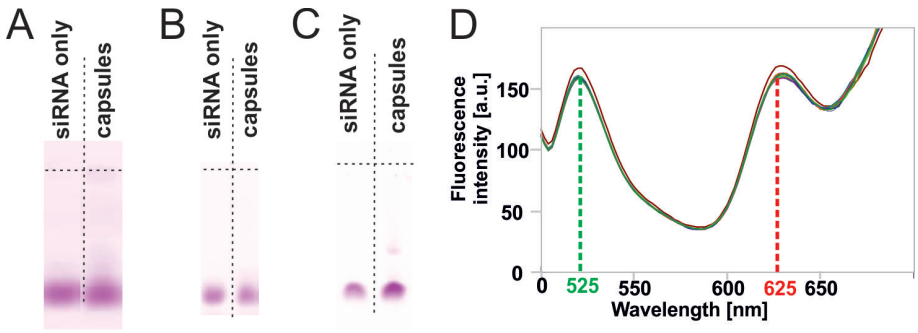

Figure 3.30: Encapsulation of siRNA in nanocapsules. EMSA for (A) Atto 488/ Atto 590 labeled siRNA containing capsules, (B) Alexa 555 labeled siRNA containing capsules, (C) Alexa 555/ Atto 647N labeled siRNA containing capsules. (D) RNase digest of Atto 488/ Atto 590 labeled siRNA containing capsules from 0 s until 75 min, Ex 488 nm.

could be that conditions during electrophoresis were detrimental to capsule integrity or a potential leakage out of capsules might have been intensified due to the electrical field.

A study carried out in the Landfester group showed cellular uptake for PBCA capsules containing Cy5 labeled oligonucleotides [228]. For the siRNA capsules, however, no reproducible knockdown effect could be observed (see appendix, figure A12). New capsule materials, which display a better controlled uptake and release behaviour like the recently developed functionalized hydroxyethyl starch capsules [180], may serve as improved siRNA carriers.

3.7.2 Dextran particles

Two batches of dextran particles were synthesized by xxxxx xxxxx xxxxx xxxxx xxxxx xxxxx [42], one batch containing Alexa 555 single labeled, the other Alexa 555/ Atto 647N FRET labeled siRNA.

The particles with FRET labeled siRNA showed siRNA retention in an EMSA (see figure 3.31 A) and an R/G of 11 (B), which signified that dextran particles enclosed intact siRNA.

CLSM with the single labeled batch showed intensively stained cell membranes, which was supposed to be due to particles sticking on the cells (see figure 3.32) and complicated an evaluation of cellular uptake. A few intracellular spots, however, could be detected.

A knockdown experiment conducted with the FRET labeled batch was also hampered presumably by the particles sticking on the cells. The fluorescence from the

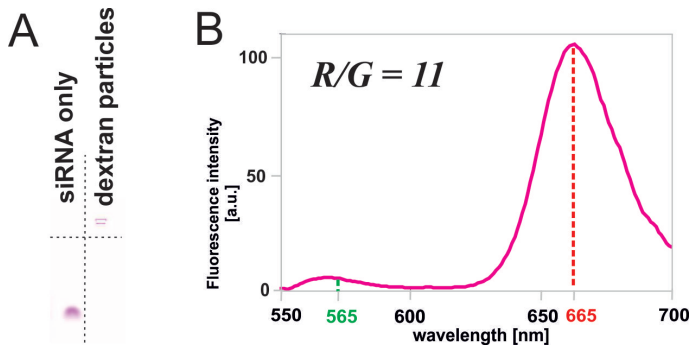

Figure 3.31: (A) EMSA, (B) R/G determination of dextran particles containing Alexa 555/ Atto 647N labeled siRNA (SEC purified), Ex 543 nm. The spectrum was corrected by subtracting that of empty particles.

siRNA was so strong that it bled into the GFP channel, which had previously proven to be nearly unaffected in control measurements with Oligofectamine^{TM} (see appendix, figure A13 A and B). This led to an overestimation of the GFP signal. A compensation of the GFP channel may not be advantageous, as this would even lower the already quite weak fluorescence signals in the HeLa MAZ system (see section 3.4). Another complication was a rise in GFP positive cells at increasing particle concentrations. This was presumably due to the carbohydrates supplied by the dextran resulting in an overall boosted protein synthesis. The effect was addressed by normalizing the GFP signal of the siRNA containing particles to that of empty particles at the same concentration. Despite these difficulties, at 20 nM siRNA concentration, a reduction in the apparent GFP signal was observed that signified an (underestimated, see above) knockdown of about 25%. For higher siRNA concentrations (40 nM), however, the GFP signal was again increasing, as the rise in positive cells was probably too pronounced and could not be balanced by the normalization any more (see appendix, figure A13 C).

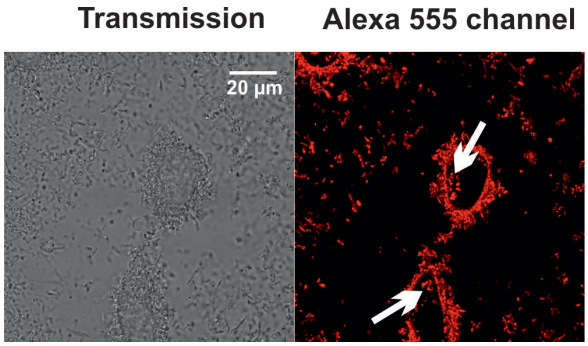

Figure 3.32: Confocal images of HeLa cells after 4 h incubation with dextran particles containing Alexa 555 labeled siRNA, siRNA 40 nM, arrows: intracellular signals.

For future knockdown experiments, the use of unlabeled siRNA would leave the GFP channel unaffected. In addition, a change to a HeLa luc system, that has also been applied in the initial experiments with these particles [42], would be advantageous. As this system normalizes fluorescence to protein content, the potential rise in protein expression would be directly taken into account.

3.7.3 Liposomes

Sterically stabilized liposomes made of 57 mol% egg phosphatidyl choline (EPC), 38 mol% cholesterol (Chol) and 5 mol% DSPE-mPEG(2000) [129], containing Alexa 555/ Atto 647N labeled siRNA, which showed only a small fraction of free siRNA after purification (see figure 3.33 A) and an R/G of about 13 (B), were prepared by xxxxx xxxxx xxxxx.

In vitro testings with these liposomes showed neither cellular uptake in CLSM (see appendix, figure A14 A) nor knockdown in a HeLa MAZ assay (B), which requires their further modification by e.g. reducing their stealth effect (see section 1.5.3) or enhancing cell specific uptake by attaching targeting ligands (see section 1.2.8 and 3.8).

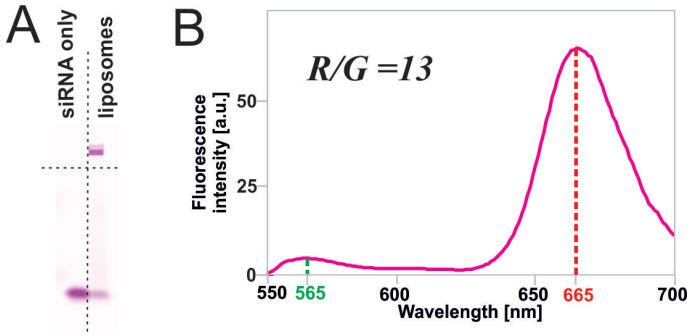

Figure 3.33: (A) EMSA, (B) R/G determination of liposomes containing Alexa 555/ Atto 647N labeled siRNA (SEC purified), Ex 532 nm. The spectrum was corrected by subtracting that of empty liposomes.

3.8 Preparation of targeted carriers

Polymeric carriers should be amenable for functionalization, as the attachment of targeting moieties is a versatile tool to improve cargo delivery to the desired site of action (see section 1.2.8). A first approach towards the formulation of functionalized carriers was undertaken with liposomes, as their preparation was already established in the lab [101, 129, 229]. Mitochondria were chosen as the target site, because RNA delivery to this organelle would be a strategy for treating certain mitochondrial diseases (see section 1.6).

3.8.1 Starting points

The initial concept for the preparation of targeted liposomes included the incorporation of a cholesterol derivative amenable for functionalization into the liposomal membrane and the covalent attachment of a mitochondriotropic moiety to this derivative.

A liposome functionalization protocol, that had previously been established with dyes as model ligands by xxxxx xxxxx [101, 229], was applied. This protocol comprised in a first step liposome preparation with the incorporation of the hydrophilic dye Sulforhodamin B (SB) as model cargo by Dual Centrifugation (DC, see figure 3.34 and section 1.5.3). In a second step, the liposomal suspension was reacted with azide carrying dyes via the copper catalyzed azide alkyne cycloaddition (CuAAC).

Dye molecules (both unincorporated SB and unreacted dye azides) were subsequently removed from the liposomal suspension, which was carried out by SEC in PBS with a custom made Sephadex^{TM} G-100 column followed by analysis of the fractions via fluorescence on a microplate reader (see figure 3.35). The fractions containing the purified liposomes were united and the concentration of the incorporated SB was de-

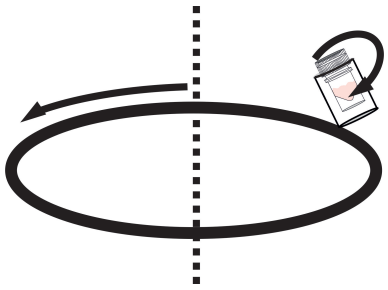

Figure 3.34: Liposome preparation by Dual Centrifugation. Scheme of the centrifugation procedure with the second, counter clockwise rotation of the sample tube around its own axis.

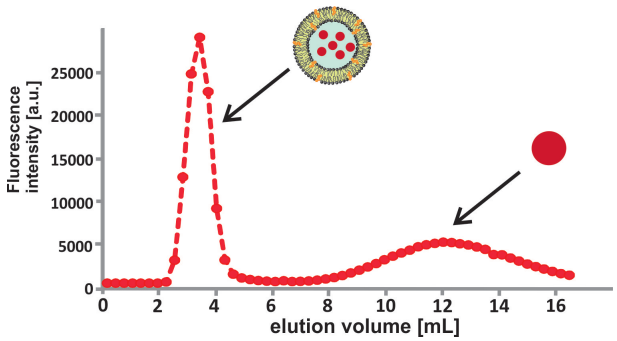

Figure 3.35: Chromatogram of the purification of liposomes from unincorporated Sulforhodamin B by SEC with a Sephadex^{TM} G100 column (Ex 560 nm, Em 590 nm).

termined after cracking the liposomes in 0.5% TritonX. The calibration curve applied in this procedure is shown in the appendix, figure A15.

During the course of the experiments, two different functionalizable cholesterol derivatives were employed: AH231, synthesized by xxxxx xxxxx, containing hyperbranched PEG chains with terminal alkynes (see figure 3.36 A), and SM264, synthesized by xxxxx xxxxx, endowed with a single linear PEG chain with one terminal alkyne (see figure 3.36 B).

Cyanine 5 (Cy5) and Triphenylphosphonium (TPP) (their azides are shown in figure 3.36 C and D), two mitochondriotropic compounds known from the literature [182, 214, 215, 217], were chosen to serve as targeting moieties. While Cy5 azide was commercially available, (4-azidobutyl)triphenylphosphonium (TPP azide) was synthesized as described in the materials and methods section.

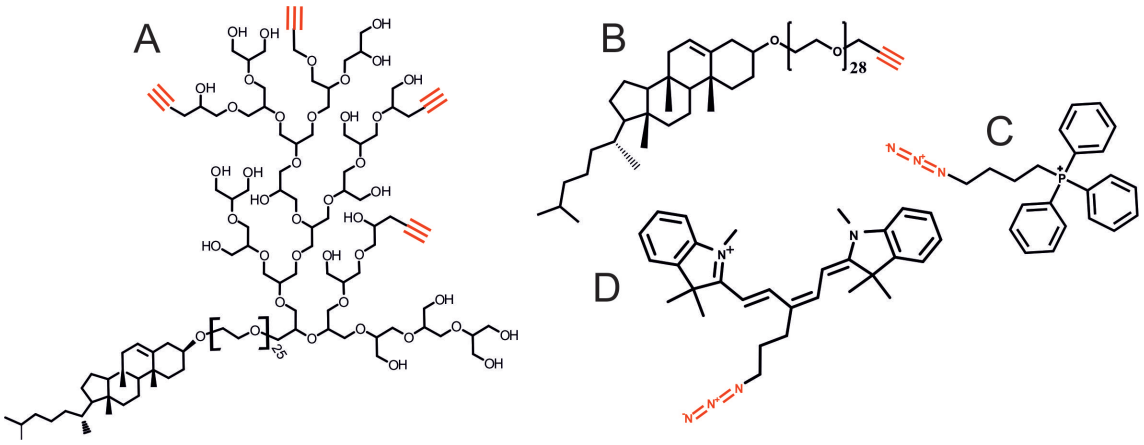

Figure 3.36: Structures of cholesterol derivatives and targeting moieties. (A) AH231, cholesterol with hyperbranched PEG containing terminal alkynes, (B) SM264, cholesterol with a linear PEG chain containing one terminal alkyne, (C) TPP azide, (D) Cyanine 5 azide.

3.8.2 Preliminary experiments

In an initial experiment, liposomes were prepared from a lipid mixture including 80 mol% DOPE, 15 mol% cholesterol (Chol) and 5 mol% AH231. The formation of liposomes with a homogenous size distribution was proven via determination of a hydrodynamic diameter of 212 nm and a polydispersity index (PDI) of 0.2 by DLS (see figure 3.41 A).

Subsequently, the functionalization with azide carrying dyes proceeded via CuAAC in the liposomal suspension, which was then purified from unreacted dye by SEC with Sephadex^{TM} G100 (see above).

The chromatograms of the purification, however, showed that on the one hand, the unreacted Cy5 did not elute as a second peak. On the other hand, also the liposome fraction of a mock incubation carried out without Cu^{2+} and sodium ascorbate showed fluorescence (see appendix, figure A16 A and B). In contrast, after a reaction employing the hydrophilic Atto 488 azide, two clear peaks appeared for the CuAAC reaction mixture and only one for free dye in the mock incubation (see appendix, figure A16 C and D). The outcome for the Cy5 may therefore be attributed to its lipophilicity. Cy5 may form micelles in aqueous medium preventing the elution as a defined peak, and may also insert into the liposomal membrane. The same behaviour was expected for the TPP, as its characteristics are similar to the Cy5 (see section 1.6).

3.8.3 Functionalization of the cholesterol derivative SM264

These observations made it necessary to carry out the reaction on the cholesterol derivative itself before it was incorporated into liposomes. For this purpose, the cholesterol derivative SM264 (see figure 3.36 B), was employed, as the stoichiometry of the

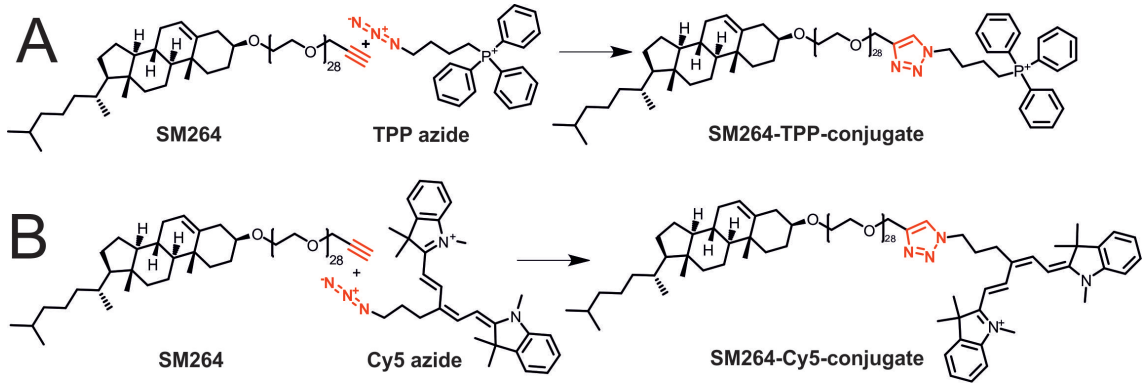

Figure 3.37: CuAAC between SM264 and (A) TPP azide and (B) Cy5 azide.

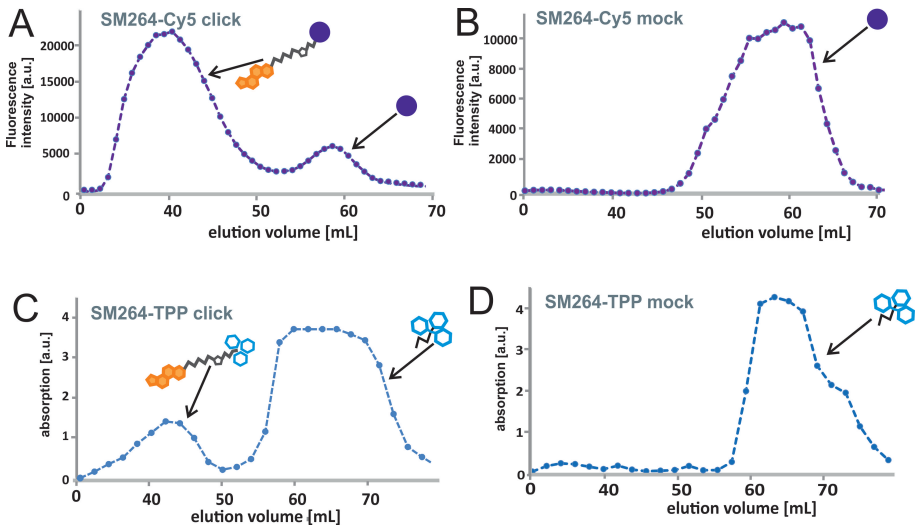

Figure 3.38: Chromatograms of the purification of functionalized SM264 by SEC with Sephadex^{TM} LH20. (A) CuAAC of 1 mg SM264 with Cy5 azide, (B) mock incubation of 0.5 mg SM264 with Cy5 azide (Ex 645 nm, Em 675 nm), (C) CuAAC of 2 mg SM264 with TPP azide (signal saturated above an absorption of 4 a.u.), (D) mock incubation of 1 mg SM264 with TPP azide (absorption at 240 nm).

CuAAC reaction could be better controlled with this molecule compared to the hyperbranched derivative with unknown number of terminal alkynes (see figure 3.36 A). The CuAAC protocol was adapted to functionalize SM264 in a 1-1 mixture of ethanol and water. SM264 at a concentration of 1.5 mM was reacted with 15 mM TPP azide, and 0.15 mM Cy5 azide (as only small amounts of Cy5 azide were available for these initial experiments), respectively (see figure 3.37).

The reaction mixture was purified with column containing Sephadex^{TM} LH20, a matrix that allows elution in organic solvents, in this case ethanol. While the Cy5 was followed via fluorescence, the TPP could be detected via absorption (see the absorption spectrum of TPP azide in the appendix, figure A21). Unreacted Cy5 and TPP, respectively, eluted as a distinct peak separate from that of the SM264-conjugate (see figure 3.38 A and C), indicating that no micelle formation took place. Also, the mock incubations for Cy5 and TPP yielded only one peak for the respective azide (see figure 3.38 B and D). Proportions of the SM264 and azide peak did not correspond for the Cy5 and the TPP reaction because they were carried out at different stoichiometries (see above).

While a lack of material prevented analysis of the SM264-Cy5-conjugate, a MALDI-ToF carried out by xxxxx xxxxx xxxxx confirmed the formation of the SM264-TPP-conjugate. The molecular weight distribution of the SM264 was shifted by an m/z of

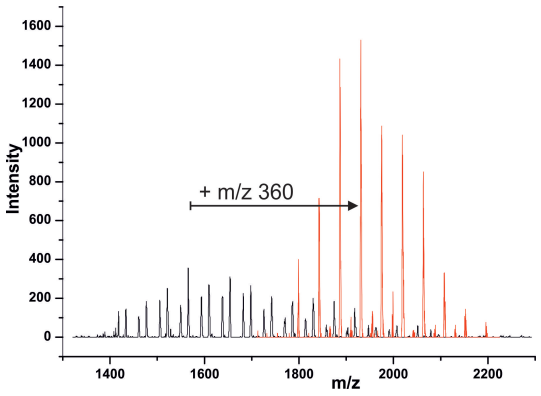

Figure 3.39: Maldi-ToF of (black) SM264 and (red) SM264-TPP-conjugate.

360 after the CuAAC reaction, which corresponded to the M_W of the attached TPP (see figure 3.39).

3.8.4 Incorporation of the SM264-conjugate into liposomes

Two options are available for the incorporation of the SM264-conjugate into liposomes, the so called "post insertion" (see figure 3.40 A) and the "direct incorporation" (B). The post insertion was assessed first, as this technique is more flexible and requires only small amounts of material [230, 231]. Under this method, the conjugate is added to the liposomal suspension, and inserts into the liposomal membrane by itself in a time and temperature dependent manner [232].

The method was envisaged to be applied on DOPE containing (fusogenic) liposomes (see section 1.5.3) in analogy to mitochondriotropic liposomes, called "Mitoporter" described in [185]. In contrast to the 80 mol% DOPE and 20 mol% Chol containing Mitoporter liposomes (that were prepared in a special buffer containing 250 mM sucrose), it was found that the DOPE fraction had to be reduced to 20% (while the liposomes further contained 60 mol% soy phosphatidyl choline (SPC) and 20 mol%

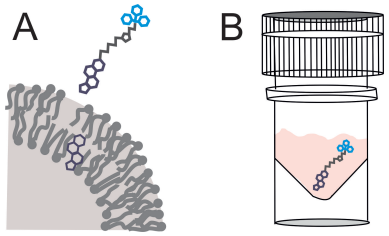

Figure 3.40: Incorporation of a SM264-conjugate into liposomes. Schemes of (A) post insertion, (B) direct incorporation.

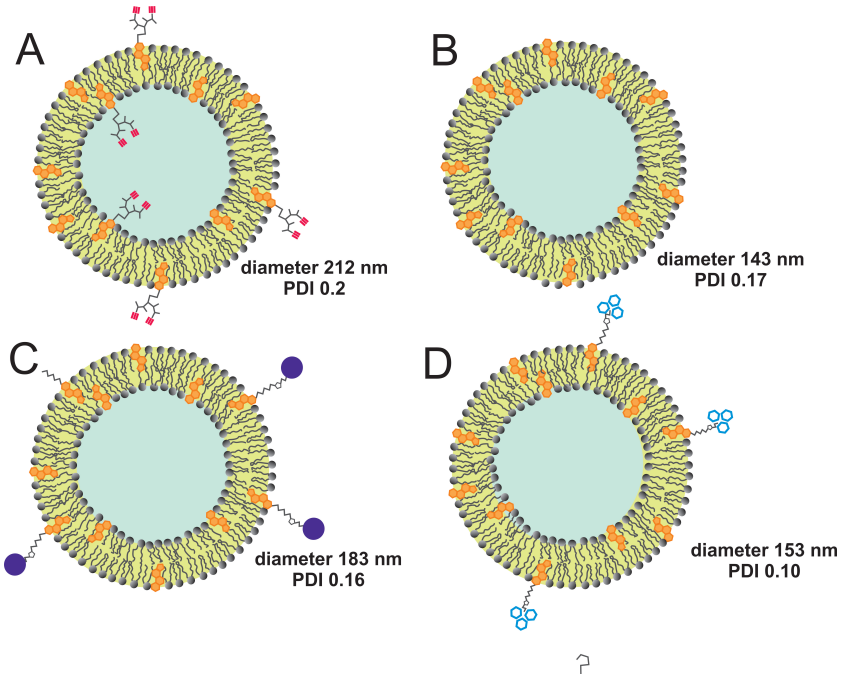

Figure 3.41: Schemes of the prepared liposomes. (A) Liposome with a hyperbranched cholesterol derivative, (B) liposome without cholesterol derivative used for post insertion, (C) liposome with SM264-Cy5-conjugate, (D) liposome with SM264-TPP-conjugate.

Chol) in order to obtain liposomes that are stable in physiologic conditions, like PBS buffer (see figure 3.41 B).

Post insertion of the SM264-Cy5-conjugate

After SEC to remove the unincorporated cargo dye SB, a fraction of the liposomal suspension (200 µL) was incubated with a small volume (5 µL) of SM264-Cy5-conjugate dissolved in ethanol, equalling 5 mol% of lipid content in the liposomal suspension (see figure 3.41 C). This procedure yielded intact liposomes with a slightly enhanced z-average diameter (183 nm compared to the 143 nm of the uninserted liposome) and an unchanged PDI of 0.16.

However, this approach was not successful for the SM264-TPP-conjugate. So the second option, direct incorporation, was assessed for the TPP.

Direct incorporation of the SM264-TPP-conjugate

Direct incorporation signifies the addition of the conjugate to the initial lipid mixture. As a whole liposome batch needs to be functionalized, this approach demands more material. Therefore in a first try, a functionalization with a rather small share of

1 mol% of SM264-TPP-conjugate was carried out and yielded intact liposomes with a z-average diameter of 153 nm and an PDI of 0.10 (see figure 3.41 D).

3.8.5 Colocalization studies

Having a first batch of post inserted Cy5- and directly incorporated TPP-functionalized liposomes, respectively, at hand, a potential colocalization of the cargo dye with mitochondria was assessed via CLSM.

This question was addressed by incubating HeLa cells for 4 h with the following preparations: The cargo dye SB only, the Cy5 azide only as well as the SM264-Cy5-conjugate only, the unfunctionalized liposome, the Cy5- as well as the TPP-functionalized liposome. The SB and Cy5 azide samples were incubated at 100 nM of the respective dye, the SM264-Cy5-conjugate at 13 nM. For the liposomes, concentrations were adjusted to 100 nM SB, which corresponds to a concentration of 13 nM of the SM264-Cy5-conjugate in the respective liposome suspension. Subsequently, cells were stained with Mitotracker^{TM} green and living cells were imaged on a confocal microscope. While the nonfluorescent TPP could not be followed, the Cy5 was traced alongside the cargo dye SB.

It needs, however, to be noted that colocalization with mitochondria is no proof that the molecule has indeed entered this compartment. A colocalization signal could also mean that the molecule is accumulated at the outer mitochondrial membrane. Therefore colocalization is a first hint, which subsequently requires a detailed analysis of the more exact whereabouts of the traced molecule [217].

As can be seen in figure 3.42 (A), the hydrophilic cargo dye SB was not taken up by cells, therefore needing a carrier to mediate its uptake. The lipophilic Cy5 azide (B) was taken up and showed an enrichment at mitochondria, according to the same staining pattern like the Mitotracker^{TM} green. (C) shows the same pattern for the SM264-Cy5-conjugate, proving that also the conjugate was attracted to mitochondria. Fluorescence intensity in the Cy5 channel was lower than that for the Cy5 azide, as the conjugate was incubated at a 9x lower concentration.

The unfunctionalized liposome could mediate uptake of the cargo dye SB, the spot-like signals in the SB channel suggest a localization in endosomes (D). Neither the Cy5 nor the TPP functionalized liposomes, however, changed this pattern for the SB (E and F), while the SM264-Cy5-conjugate itself again showed accumulation at mitochondria (E).

The CLSM images show that the conjugation of Cy5 was able to render the SM264

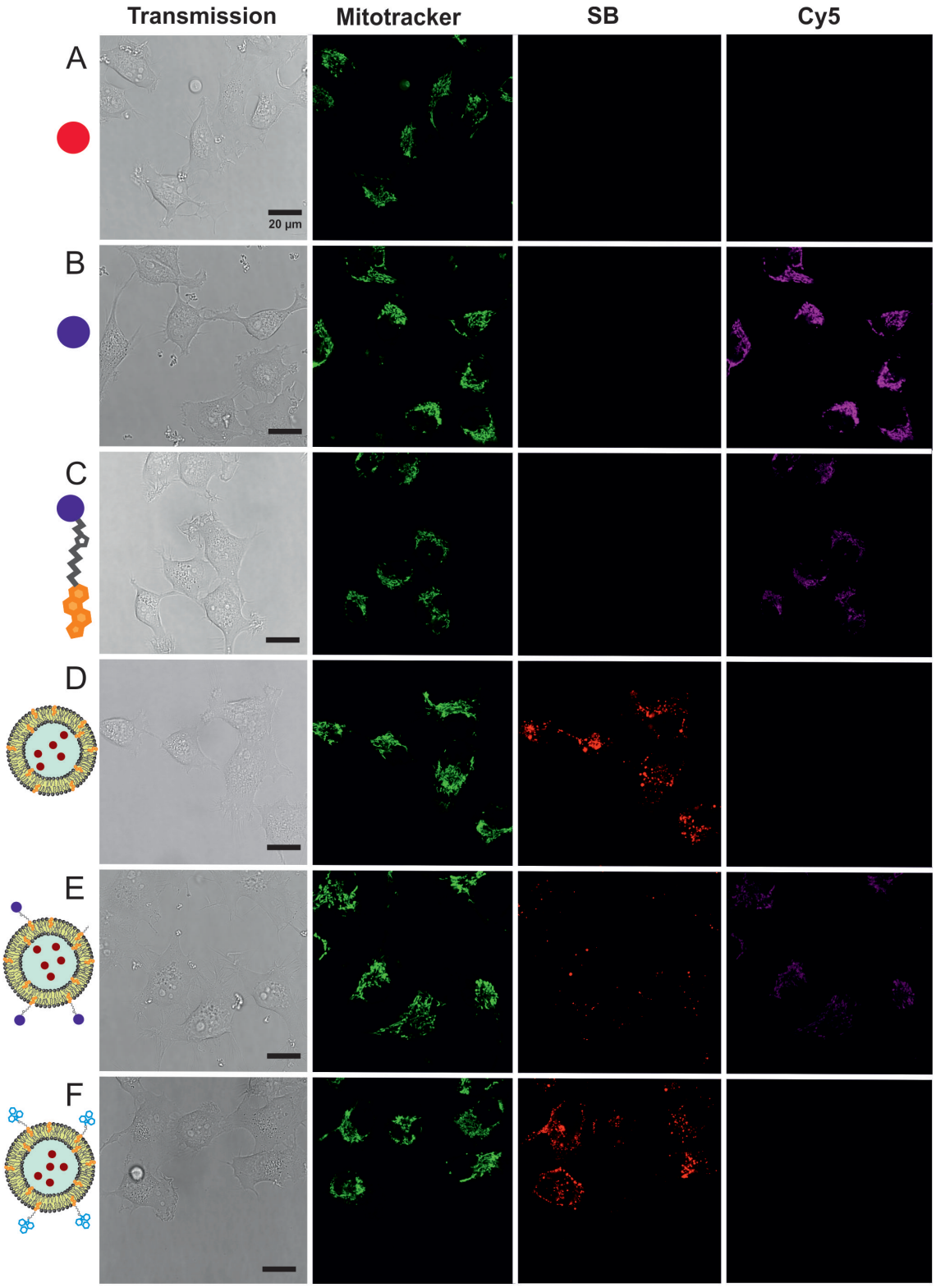

Figure 3.42: Microscopy of functionalized liposomes. (A) SB only 100 nM, (B) Cy5 azide only 100 nM, (C) SM264-Cy5-conjugate only 13 nM, (D) liposome without functionalization, (E) liposome with SM264-Cy5-conjugate, (F) liposome with SM264-TPP-conjugate. For (D-F) c SB 100 nM. Transmission, Mitotracker green^{TM}, Sulforhodamin B (SB) and Cyanine 5 (Cy5) channel shown.

mitochondriotropic. However, the liposomes functionalized with the SM264-Cy5-conjugate could not direct the cargo dye SB towards mitochondria. The same was true for the liposomes that were equipped with the SM264-TPP-conjugate. Possible reasons for this outcome may be that the liposomes did not stay intact during endosomal uptake and/or that the targeting was not efficient enough.

Starting points for optimizing the liposomes are quite obvious, as these initial experiments were not yet carried out under optimal conditions. In the first place, the content of the SM264-conjugate was rather low, for the Cy5 conjugate because the reaction had to be carried out at an excess of SM264 and for the TPP conjugate because its fraction in the liposome was only 1 mol%. Optimization has to comprise an increase in the degree of functionalization.

Further experiments also need to address the stability of liposomes by optimizing the lipid mixture. The use of a fusogenic lipid may be questioned as such lipids destabilize the liposomes. While this is desired for cargo transfer to the cytosol (e.g. in the case of siRNA), more stability may be useful in the case of intracellular targeting, so that targeting moiety and cargo are still joined after intracellular release.

Another approach could address the cellular uptake route. Incorporation of Stearyl-R8 into the liposomal membrane has been shown to steer uptake towards macropinocytosis [233], a pathway that is less prone to lysosomal degradation (see section 1.2.4). The positive charges of the Stearyl-R8 have also been described to engage in electrostatic interactions with the mitochondrial membrane [185].

4 Conclusion & Outlook

In this work, polymeric nanocarriers for RNA delivery as well as methods for their evaluation were investigated from various perspectives.

The main element was a comparative study of six siRNA polyplexes, namely PLL brushes, block copolymers, cationic lipids, cationic peptides, nanohydrogels, and manganese oxide ($MnO@SiO_2$) particles. These carriers were evaluated simultaneously from polyplex formation and stability up to *in vitro* characteristics.

The design of this study allowed a comparison between the different carriers as well as the assessment of one carrier according to a range of features. Thereby, a focus was laid on the development and comparison of alternative methods to assess a specific feature.

The assays regarding polyplex formation showed that all carriers were able to complex siRNA, while the amount of carrier, as well as the N/P ratio needed for complete complexation differed. An electrophoretic mobility shift assay that subjected polyplexes to non-equilibrium conditions was contrasted with thermophoresis, an equilibrium method. Carriers reacted differently towards these two conditions, which already hinted at differences in stability between the polyplexes.

Fluorescence measurements showed quenched or boosted fluorescence intensities of labeled siRNA for the different polyplexes. This underlined the importance of addressing such changes when quantifying siRNA via its fluorescent label e.g. in FCS measurements or after cellular uptake.

An anion competition assay was not able to yield distinct information about polyplex stability. In contrast, a nuclease resistance assay in the cuvette was able to classify the carriers according to their stability. This test monitored the integrity of double labeled siRNA via FRET. A decrease in siRNA integrity showed that siRNA was accessible to nucleases, which was ascribed to unstable binding conditions in the polyplex.

In vitro transfection experiments proved that confocal microscopy was the method of choice for intracellular localization of siRNA. An absolute quantification, however, required a separate method, which was found in the determination of siRNA fluores-

cence in cell lysate. A time profile obtained via this quantification indicated that all polyplexes were taken up 4 h after transfection, while the extent of uptake differed widely. A strong decrease in siRNA content was observed for most carriers between 4 h and 12 h, while levels did not substantially change any more 24 h after transfection.

In addition to the previous determination of siRNA integrity after nuclease challenge in the cuvette, this parameter was also evaluated *in vitro* via flow cytometry. The integrity levels obtained from both tests, however, did not correspond, which proved the difficulty that lies in the simulation of *in vitro* conditions.

Finally, an *in vitro* knockdown assay was conducted, that showed an effect only for the cationic lipids and the cationic peptides. Looking at the features that these two polyplexes displayed during the course of the experiments, they required a comparatively low amount of carrier for complete complexation and showed a moderate stability in the cuvette. A distinct level of cellular uptake after 4 h was observed for them as well as high initial intracellular integrity, while both uptake and integrity substantially decreased after 12 h. Therefore, such a set of characteristics appears to be favourable.

Although this study already assessed a wide spectrum of criteria, it certainly could not cover the whole range of relevant aspects. For example, the role of intracellular release was only briefly addressed by confocal microscopy, and the probing of uptake pathways was not yet considered. It is, however, known, that cationic lipids and cationic peptides, those polyplexes that are able to cause a biological effect, are the only ones in the screen that comprise a strategy for intracellular release: The cationic peptides as they lead to a pH dependent membrane disturbance and the cationic lipids because of their interactions with membranes. It can be assumed that these features also contribute to the ability of these polyplexes to mediate knockdown. Therefore, further experiments should lay additional emphasis on elucidating the intracellular fate of transfected siRNA. To this end, microscopy studies could be expanded to creating a time profile of cellular distribution, the costaining of cellular compartments and the determination of uptake pathways.

Intracellular release may also serve as a starting point for optimizing the carriers that did not yet show a biological effect, like the PLL brushes, the block copolymers and the $MnO@SiO_2$ particles. After endowing them with a mechanism for intracellular release, even further optimization could be envisaged. With intracellular release granted, their stability may be enhanced, as release would not solely depend on a certain degree of instability any more. This may also lead to improved intracellular siRNA integrity.

The additional attachment of targeting ligands would offer a way to improve uptake for carriers like block copolymers or $MnO@SiO_2$ particles, that yet lack efficient uptake.

In conclusion, the screening of different polyplexes revealed for most of the carriers the need for optimization. This was not completely unexpected, as the carriers that were obtained from cooperation partners (the cationic peptides being the only exception) constituted the first generation of these classes of materials. The methods that were set up in this study will thus serve in the forthcoming steps for the testing of "next generation" carriers. These evaluations will take place in the framework of the collaborative research centre "SFB 1066", that investigates targeted delivery of RNA species for the treatment of the malignant melanoma.

The studies on siRNA entrapping particles were conducted under the same premises. Nanocapsules and liposomes are currently optimized for enhanced uptake and intracellular release. The experiments conducted so far with the dextran particles led to conclusions about improved experimental conditions for assessing their knockdown capability.

To address the importance of having reliable methods to determine *in vitro* knockdown capability at hand, a reporter gene assay was established with a cell line that expressed a destabilized eGFP. This assay turned out to be beneficial for the testing of different siRNA carriers, as it could dispense an additional transfection of the eGFP plasmid, which had been mandatory in the assays available so far. Along similar lines, a study considered the question if fluorescently labeled siRNA have an impact on the biological activity. Labeled siRNA showed a reduced, but still efficient knockdown capability compared to unlabeled siRNA, which proved that labeled species can be employed in biological applications.

The last part of this work referred to targeted delivery of RNA. First attempts towards mitochondrial targeting were undertaken with liposomes. A mitochondriotropic moiety was attached to a cholesterol derivative. This conjugate was subsequently incorporated into liposomes, that were loaded with a cargo dye. As confocal microscopy of cells incubated with these liposomes could not yet confirm a colocalization of the cargo dye with mitochondria, these formulations need to be optimized, in the first place by increasing the degree of functionalization. In addition, the attachment of mitochondriotropic tags to block copolymers and dextran particles is currently investigated by our cooperation partners. This will even extend the options to achieve a targeted delivery of RNA to mitochondria.

5 Materials & Methods

5.1 Materials

Chemicals, reagents and ready-to-use buffers

Acetic acid #A2354 (AppliChem, Darmstadt, Germany)
Acetonitrile #34967 (Sigma-Aldrich, St. Louis, USA)
APS #9592.2 (Carl Roth, Karlsruhe, Germany)
Bromphenol Blue #114391 (Sigma-Aldrich)
Cholesterol #8667 (Sigma-Aldrich)
$CuSO_4$ (Sigma Aldrich)
Cy5 azide #CLK-CCA-9295-1 (Jena Biosciences, Jena, Germany)
CHX (gift from xxxxx)
DMEM #61965 (Gibco/ Invitrogen, Karlsruhe, Germany)
DMEM indicator free #21063 (Gibco/Invitrogen)
DMSO #A994.2 (Carl Roth)
DOPE #W0650 (Cordon Pharma, Liestal, Switzerland) and #850725P (Avanti Polar Lipids, Alabaster, USA)
DSPE-mPEG(2000) (Lipoid, Ludwigshafen, Germany)
D-PBS #14190 (Gibco/ Invitrogen)
D-PBS with Ca^{2+} and Mg^{2+} #14040 (Gibco/ Invitrogen)
EPC (Lipoid)
Ethanol, absolute #5054.3 (Carl Roth)
Et_3N #121-44-8 (Acros Organics, Geel, Belgium)
Fetal bovine serum #10500 (Gibco/ Invitrogen)
Formamide #P040.1 (Carl Roth)
GelRed #41001 (Biotium, Hayward, USA)
Glycerol #G5516 (Sigma Aldrich)
Hellmanex^{TM} (Hellma, Müllheim, Germany)
Heparin (5000 U/mL) #L6510 (Biochrom KG, Berlin, Germany)
Hydrogen peroxide (Carl Roth)
KCl (Carl Roth)
KH_2PO_4 (Carl Roth)
Lipofectamine 2000 #11668-019 (Invitrogen)
MG115 #SPC0005 (Sigma Aldrich)

mPEG-2000-DSPE (Lipoid GmbH)
NaAsc (Carl Roth)
Na_2HPO_4 (Carl Roth)
NaCl (Carl Roth)
NaN_3 #S2001 (Sigma Aldrich)
Oligofectamine #1416397 (Invitrogen)
Opti-Mem #31985070 (Gibco/ Invitrogen)
$MgCl_2$ (Merck, Darmstadt, Germany)
Mitotracker^{TM} green FM #M-7514 (Molecular probes/ Invitrogen)
Nanosep^{TM} #ODM45C34 (Pall Life Sciences, Port Washington, USA)
NAP-5 columns (Sephadex^{TM} G-25) #17-0853-02 (GE Healthcare, UK)
NH_4Ac #17836 (Sigma Aldrich)
Penicillin/Streptomycin 10000 Units #15140122 (Invitrogen)
RNase V1, 0.1 U/µL #AM2275 (Invitrogen)
ROTI^{TM} Quant universal assay #0120.1 (Carl Roth)
Rotiphorese DNA sequencing system #A431.1 (Carl Roth)
Rotiphorese 19:1 40 % #3030.1 (Carl Roth)
SDS (Carl Roth)
Sephadex^{TM} G-100 #17-0060-01 (GE Healthcare)
Sephadex^{TM} LH20 #17-0090-10 (GE Healthcare)
SPC # S100 (Lipoid)
Sulforhodamin B #2609-88-3 (Acros)
SybrGold #S-11494 (Invitrogen)
TBE 10x buffer #3061.1 (Carl Roth)
TPPBr #272132 (Sigma Adlrich)
TritonX #T878 (Sigma Aldrich)
TEAA (Acros)
TEMED #2367.1 (Carl Roth)
THPTA (synthesized by xxxxx)
TRIS HCl (Carl Roth)
Trypsin EDTA 0.05 % #25300 (Gibco/ Invitrogen)
Xylene Xyanol #X4126 (Sigma Aldrich)

All other chemicals not included in this list were obtained from the Institute of Pharmacy's in-house chemical store.

Buffers and media

APS solution 10 % m/v Ammoniumpersulfate dissolved in MilliQ water

1x PBS Dilution of 10x PBS in MilliQ water resulting in 137 mM NaCl, 2.7 mM KCl, 1.7 mM KH_2PO_4, 10 mM Na_2HPO_4, pH 7.4

10x PBS 1370 mM NaCl, 27 mM KCl, 17 mM KH_2PO_4, 100 mM Na_2HPO_4 in MilliQ water, pH 6.8

15 % v/v non denaturing PAGE : 10 % 10x TBE, 37.5 % v/v PAGE concentrate (40 %), 52.5 % v/v water

Cuvette cleaning solution 2 % Hellmanex^{TM} in MilliQ water

Degradation buffer 2x 80 mM TrisHCl pH 7.5, 80 mM NaCl, 20 mM $MgCl_2$ in MilliQ water

Non denaturing PAGE loading buffer 50 % v/v Glycerol, 10 % v/v 10x TBE in MilliQ water

10x Phosphate buffer 932 mM Na_2HPO_4, 68 mM M NaH_2PO_4in MilliQ water

Standard medium 89 % v/v DMEM, 10 % v/v FCS, 1 % v/v Pen/Strep

TEAA buffer 2 mol Et_3N and 2 mol acetic acid in 1 L MilliQ water

Transfection medium 90 % v/v DMEM, 10 % v/v FCS

Freezing medium 70 % v/v DMEM, 20 % v/v FCS, 10 % v/v DMSO

Disposables

24 well plates tissue culture treated # 662160 (Greiner Bio-One, Frickenhausen, Germany)

96 well plates black # 655209 (Greiner)

96 well plates UV # 3635 (Corning Life Sciences, Tewksbury, USA)

8 well chamber, µslide # 80826 (Ibidi, Martinsried, Germany)

8 well polystyrene chambered cover glass (Laboratory-Tek, NalgeNunc International, Penfield, USA)

Cell culture flask, 75 cm^2, ventilated cap, tissue culture treated # 83.1813.002 (Sarstedt, Nümbrecht, Germany)

Centrifugation tubes 15 mL # 62.554.502 (Sarstedt)

Centrifugation tubes 50 mL # 62.547.254 (Sarstedt)

Ceramic beads, SiLibeads ZY 0.6 - 0.8 mm (kindly provided by Sigmund Lindner, Warmesteinach, Germany)

Cuvettes (plastic) # 67.741 (Sarstedt)

Disposable sterile serological pipettes, 10 mL # 861.254.001 and 25 mL # 86.1685.001 (Sarstedt)

Dye Ex^{TM} 2.0 Spin Kit #63204 (Qiagen, Hilden, Germany)

FACS tubes, round bottom (Becton Dickinson, Heidelberg, Germany)

Filter top vacuum bottles, PES, 0.2 µm 500 mL # 83.1823.001 (Sarstedt)

GenElute^{TM} HP Endotoxin-Free Plasmid Maxiprep Kit # NA0400S-1KT (Sigma Aldrich)

Nanosep # P/N ODM45C34 (Pall Life Sciences, Crailsheim, Germany)

Nanotemper capillaries standard treated # K002 (Nanotemper, München, Germany)

NAP-5 columns # 17-0853-01 (GE Healthcare)

PCR 8er SoftStrips # 711030 (Biozym, Hessisch Oldendorf, Germany)

Pipet tips sterile with filter, DNase/RNase free 10 µL # 771261, 20 µL # 774288, 200 µL # 739288,

1000 µL # 740288 (Greiner)
Reaction tubes 1.5 mL # 7080.1 (Carl Roth)
Screw cap vials 0.65 mL # T601.1 (Carl Roth)
Suprasil quartz glass cuvette, 15 µL, 1.5 mm light pass (Hellma)
Syringe columns 10 mL #S10149 (MobiTech, Göttingen, Germany)
Syringe filters 0.2 µm # KH54.1 (Carl Roth)
Vivaspins 2 mL 3000 MWCO #Z629405-25EA (Sigma Aldrich)

siRNA and plasmids

eGFP plasmid

The plasmid eEGFP-N1 (GenBank Accession #U55762) was a kind gift from xxxxx xxxxx xxxxx xxxxx xxxxx xxxxx xxxxxx. A plasmid preparation in DH5α cells was carried out with the GenElute^{TM} Maxiprep Kit according to the manufacturer's instructions.

siRNA

siRNA single strands were obtained from IBA GmbH (Göttingen, Germany) and comprise sense and antisense strands for the targeting of eGFP. Control siRNA was obtainded as a double strand from Microsynth (Balgach, Switzerland). Sequences were

eGFP sense strand 5´-GCAAGCUGACCCUGAAGUUCAU-3´

eGFP antisense strand 5´-GAACUUCAGGGUCAGCUUGCCG-3´

control sense strand 5´-AGGUAGUGUAAUCGCCUUGdTdT-3´

control antisense strand 5´-CAAGGCGAUUACACUACCUdTdT-3´

Fluorescent labels were attached via a spacer on the 3´end of the sense and the 5´end of the antisense strand.

Material obtained from cooperation partners

poly-L-lysine brushes [115] obtained from xxxxx xxxxx xxxxx xxxxx xxxxx xxxxx xxxxx xxxxx xxxxx .

HPMA based cationic block copolymers IT1 and IT2 [119] obtained from xxxxx xxxxx xxxxx xxxxx xxxxx xxxxx xxxxx xxxxx xxxxx xxxxx xxxxx xxxxx xxxxx xxxxx, batch IT1 for formation and release studies, batch IT2 for *in vitro* experiments.

Cationic peptides LAH4-L1 [41] obtained from xxxxx xxxxx xxxxx xxxxx xxxxx xxxxx xxxxx.

Nanohydrogels LN247 and LN494 [123, 124] obtained from xxxxx xxxxx xxxxx xxxxx xxxxx xxxxx xxxxx xxxxx xxxxx xxxxx xxxxx xxxxx xxxxx xxxxx xxxxx xxxxx xxxxx xxxxx, batch LN247 for formation and release studies, batch LN494 for *in vitro* experiments.

Manganese oxide (MnO@SiO$_2$) particles SH130 and SH131 [126] obtained from xxxxx xxxxx , who supervised the synthesis conducted by the bachelor student xxxxx, batch SH130 for formation and release studies, batch SH131 for *in vitro* experiments.

Cholesterol derivative with hyperbranched PEG and terminal alkynes AH231 [187] obtained from xxxxx xxxxx xxxxx xxxxx xxxxx xxxxx xxxxx xxxxx xxxxx xxxxx xxxxx xxxxx.

Cholesterol-PEG derivative with a terminal alkyne SM264 obtained from xxxxx xxxxx xxxxx xxxxx xxxxx xxxxx xxxxx xxxxx xxxxx xxxxx xxxxx xxxxx xxxxx xxxxx xxxxxx.

Nanocapsules GB-BK 001 - 006 [181] obtained from xxxxx xxxxx xxxxx xxxxx xxxxx xxxxx xxxxx xxxxx xxxxx xxxxx xxxxx xxxxx xxxxx xxxxx xxxxx xxxxx xxxxx xxxxx.

Dextran particles [42] obtained from xxxxx xxxxx xxxxx xxxxx xxxxx xxxxx xxxxx xxxxx xxxxx xxxxx xxxxx xxxxx xxxxx xxxxx xxxxx xxxxx xxxxx xxxxxx xxxxxx.

Cell lines

HeLa cells An epitheloid cervix carcinoma cell line (DSMZ #ACC57), established from a cervical cancer tissue sample of Henrietta Lacks in 1951. Cells were a kind gift from the group of xxxxx xxxxx xxxxx xxxxx xxxxx xxxxx xxxxx xxxxx xxxxx.

HeLa MAZ cells HeLa cells containing the episomal vector pMARS-mODC-AZ (gene bank accession #EU421131), which encodes for a destabilized eGFP [224]. Cells were a kind gift from xxxxx xxxxx xxxxx xxxxx xxxxx xxxxx xxxxx xxxxx xxxxx xxxxx.

HEK 293 T cells A human embryonal kidney cell line (DSMZ #ACC635). Cells were a kind gift from xxxxx xxxxx xxxxx xxxxx xxxxx xxxxx xxxxx xxxxx xxxxx xxxxx xxxxx xxxxx.

5.2 Instruments

Standard laboratory equipment

Analytical balances Mettler Toledo PM460 and Mettler Toledo Excellence Plus (Gießen, Germany)

Centrifuges 1-15 PK Sigma (Osterode am Harz, Germany), Eppendorf Centrifuge 5810R (Hamburg, Germany)

Pipetting Variable micropipettes Discovery Comfort, 10 µL, 20 µL, 200 µL, 1000 µL, Abimed (Langenfeld, Germany)

Rotary evaporator RV 06-ML

pH measurements FiveEasy^{TM} FE20 pH meter, Mettler Toledo

Sample incubation and shaking Thermoshaker Plus, Eppendorf and BIOER ThermoCell, BIOER (Hangzhou, China)

Sample concentration Concentrator Plus, Eppendorf and Lyophilizer Alpha 2-4 LO, Christ (Osterode, Germany)

Ultrapure water purification system Milli-Q, Millipore (Schwalbach, Germany)

UV Spectrophotometry NanoDrop ND-2000, PeqLab (Erlangen, Germany)

Equipment for special techniques

Gel electrophoresis For PAGE electrophoresis: CBS LSG-400-20 NA vertical electrophoresis chamber (G.B.S. Scientific, San Diego, USA) attached to a Consort EV232 (Consort, Turnhout, Belgium) power supply. For agarose gel electrophoresis: PerfectBlue Gelsystem (PeqLab, Erlangen, Germany) attached to a Model 250/2.5 Power supply (BioRad, München, Germany).

Gel detection Typhoon 9600 with an external blue laser unit (GE Healthcare, Buckinghamshire, UK) equipped with 457 nm, 488 nm, 532 nm, 633 nm laser lines, 560 nm, 580 nm, 630 nm beam splitter and a set of emission filters.

HPLC C18 Reversed phase column LiChroCART 250-10 (Merck) connected to an Agilent 1100 Serie (Merck-Hitachi, Darmstadt, Germany).

Size exclusion chromatography Superdex^{TM} 200 (GE Healthcare) connected to an Agilent 1100 Series (Merck-Hitachi).

Thermophoresis Monolith^{TM} NT.115 (Nanotemper, München, Germany). Data fitting with the NT Analysis software.

Fluorimetry FP-6500 Fluorimeter (JASCO, Tokyo, Japan) equipped with an ETC-273T temperature controller and a HAAKE WKL26 cooling unit (ThermoFisher Scientific, Schwerte, Germany).

Fluorescence correlation spectroscopy FCS setup (Zeiss, Germany) consisting of the module ConfoCor2 and an inverted microscope model Axiovert 200 with a Zeiss C-Apochromat 40x/1.2 W water immersion objective at the group of xxxxx xxxxx xxxxx xxxxx xxxxx xxxxx.

Microscopy Leica TCS SP5 equipped with four laser lines (405 nm, 488 nm, 561 nm, 633 nm) and a 63x oil immersion objective (N.A. 1.4), provided by the Microscopy Core Facility, IMB, Mainz. Image acquisition with the Leica Application Suite (LAS AF), image processing with LAS AF lite and ImageJ.

Microplate reading Infinite M200 pro (Tecan, Austria), provided by the group of xxxxx.

Flow cytometry LSR-FortessaSORP (Becton Dickinson, Heidelberg, Germany), provided by the Cytometry Core Facility, IMB, Mainz. Data processing with FlowJo Software (TreeStar Inc, USA).

Dual centrifugation Rotanta 400 centrifuge (customized with a prototype DC-rotor (Hettich, Tuttlingen, Germany).

Size determination Zetasizer Nano ZS (Malvern, Herrenberg, Germany) provided by the group of xxxxx.

5.3 Methods

Hybridisation of siRNA

Double strands were hybridized from 100 µM single strand stock solutions by adding both strands at the desired final concentration in 1x PBS pH 7.4. Samples were thoroughly mixed, incubated for 3 min at 90 °C for complete denaturation followed by 60 min at 37 °C for duplex formation. The hybridisation was checked via non denaturating 15% PAGE.

HPLC for free dye removal from siRNA solutions

200 pmol of a single strand was loaded on a C18 reversed phase column and run at a flow rate of 3 mL/min in acetonitrile/TEAA using the following acetonitrile gradient: 0 min: 5%, 30 min: 80%, 35 min: 80%, 40 min: 5%, 45 min: 5%.

Size exclusion chromatography for free dye removal from siRNA solutions

A Superdex^{TM} 200 SEC column was attached to the HPLC and equilibrated with 1x PBS pH 7.4 at a constant flow rate of 0.5 mL/ min. 40 µM stock solutions of double strands were loaded with a maximal amount of 3000 pmol per run. The peak of the purified double strand eluting at 32 min was collected, fractions of several runs united and centrifuged in 2 mL Vivaspins 3000 MWCO up to the desired final concentration which was determined by UV absorption. The purification was checked via non denaturating 15% PAGE.

Non denaturating polyacrylamide gel electrophoresis

Casting of gels and electrophoresis Gels were cast between glass plates with 1 mm spacers and run in 1x TBE. For a 20 x 30 cm gel, 100 mL of 15% v/v non denaturing PAGE solution was mixed with 1 mL APS and 40 µL TEMED. Gels were run at 11 W for 3 h, with ventilation and a metallic plate to equally distribute the heat resulting from the procedure. Samples with unlabeled siRNAs were stained with GelRed or SybrGold prior to detection using the Typhoon.

Detection of GelRed stained unlabeled siRNA 532 nm excitation and 610BP30 emission filter.

Detection of SybrGold stained unlabeled siRNA 532 nm excitation and 526SP emission filter.

Detection of Atto 488/ Atto 590 labeled siRNA Donor signal: 488 nm excitation and 520BP40 emission filter, FRET signal: 488 nm excitation and 670BP30 emission filter, acceptor signal: 532 nm excitation and 670BP30 emission filter.

Detection of Alexa 555/ Atto 647N labeled siRNA Donor signal: 532 nm excitation and 580BP30 emission filter, FRET signal: 532 nm excitation and 670BP30 emission filter, acceptor signal: 633 nm excitation and 670BP30 emission filter.

Gel elution of oligonucleotides

The respective bands were excised, shred and shaken in 0.5 M NH_4Ac over night. After filtration through a Nanosep^{TM} device, ice cold ethanol was added in 2.5 x excess to the filtrate. Samples were stored at - 20 °C for 2 h, followed by centrifugation at 16000 g and - 4 °C for 30 min. After discarding the supernatant, pellets were dried and resuspended in 1x PBS.

Electrophoretic mobility shift assay

0.14 µg of Alexa 555/ Atto 647N labeled siRNA were incubated with the carrier at various mass/mass (m/m) ratios in 1x PBS for 20 min at room temperature. Samples were loaded in the centre of a 1% agarose gel which was run at 120 V for 50 min in 1x TBE running buffer. The gel was analyzed with the Typhoon. For data analysis the fluorescence signal of free siRNA (on the level of the siRNA only sample) of the acceptor signal was quantified and expressed as percentage of the fluorescence signal

of the whole lane. Obtained data was fit via a five parametric dose-response curve (Graph Pad prism^{TM}) resulting in a value for 50% binding (BR_{50}).

Thermophoresis

Complexes were prepared by serial dilution of the carrier in 1x PBS at 16 different m/m ratios ranging from 700 to 0.02 and addition of Alexa 555/ Atto 647N labeled siRNA solution leading to a final siRNA concentration of 50 nM in each sample. Samples were incubated for 20 min and loaded into MonolithTM NT.115 standard treated capillaries. Samples were measured with a Monolith NT.115 using red excitation and emission with 100% LED and 20% MST power. Each measurement was repeated five times with 5 s equilibration, 30 s Laser-On and 5 s decay time. An EC50 value was obtained with the NT Analysis software on a Hot/Cold evaluation employing a Hill fit. EC_{50} values were interpreted as BR_{50} values. For determination of heparin release, 8 aliquots of complex solution at the respective m/m were prepared and incubated for 20 min. Heparin was added to each aliquot at a different z^-_{Hep}/z^-_{RNA} ratio. Final concentration of siRNA was 100 nM. After 30 min incubation, samples were analyzed as mentioned above.

Fluorimetry

Emission profiles were recorded on a FP-6500 Fluorimeter in a 15 µL quartz glass cuvette for 1 µM siRNA complex solutions in 1x PBS at donor and acceptor excitation with spectral correction for PMT (emission) and illumination lamp (excitation) at 1 nm datapitch and a bandwidth of 3 nm for excitation and emission.

For the Alexa 555/ Atto 647N labeled siRNA 543 nm donor excitation, 633 nm acceptor excitation, donor emission maximum at 565 nm and acceptor emission maximum at 665 nm.

For the Atto 488/ Atto 590 labeled siRNA 488 nm donor excitation, 532 nm acceptor excitation, donor emission maximum at 525 nm and acceptor emission maximum at 625 nm.

R/G values were calculated from the donor excitation spectrum by dividing the fluorescence intensity at acceptor emission maximum by the fluorescence intensity at donor emission maximum.

Fluorescence correlation spectroscopy

FCS was performed using an FCS setup (Zeiss, Germany) consisting of the module ConfoCor2 and an inverted microscope model Axiovert 200 with a Zeiss C-Apochromat 40x/1.2 W water immersion objective. The acceptor fluorophore was excited by a Helium Neon laser (633 nm) and the emission was collected after filtering by a LP650 long pass filter. For detection, an avalanche photodiode that enables single-photon counting was used. Samples were prepared analogously to the EMSA assays, further diluted in PBS after 20 min incubation to a final concentration of 50 nM (500 nM for the brushes) and transferred to an eight-well polystyrene chambered cover glass (Laboratory-Tek, NalgeNunc International) for the measurement.

Heparin competition assay

Complexes were preformed at two different m/m ratios in 1x PBS and aliquoted in samples containing 0.07 µg Alexa 555/ Atto 647N labeled siRNA. To each aliquot, heparin at a different z^-_{Hep}/z^-_{RNA} (amount of negative charges of heparin per amount of negative charges of siRNA) ratio was added. The z^-_{Hep}/z^-_{RNA} was calculated under the approximation that 200 g heparin and 340 g siRNA each contain 1 mol negative charges. The mixtures were incubated for 30 min and loaded on a 1% agarose gel. The gel was run at 120 V for 50 min. Quantification was carried out as described for the EMSA analysis.

Nuclease resistance assay

Complexes were preformed in 1x PBS and diluted with degradation buffer to achieve final reaction conditions of 40 mM Tris HCl, 40 mM NaCl and 10 mM $MgCl_2$. 19 µL of the 0.5 µM siRNA complex solution was analyzed by recording emission profiles at donor excitation right before and after the addition of 1 µL of RNase V1 at various timepoints over a period of 2 h. The R/G ratio at each timepoint was calculated from corrected spectral data as a ratio of acceptor emission to donor emission and used to calculate the integrity level on the basis of an calibrated R/G system [131]. Free siRNA was incubated under the same reaction conditions and used for normalization and comparison of data from experiments on different days.

Microscopy

One day prior to transfection, 15 x 10^3 HeLa cells were seeded in 300 µL transfection medium into 8 chamber dishes. Prior to transfection, medium was replaced by 92.5 µL DMEM. Polyplexes were prepared with Alexa 555/ Atto 647N labeled siRNA in 32.5 µL OptiMem, incubated for 20 min and added dropwise to the cells at a final siRNA concentration of 40 nM. After 4 h, cells were washed with PBS, 0.2 mg/mL heparin solution and again PBS. Living cells were imaged in DMEM without indicator on a confocal microscope.

general settings 63x 1.4 oil objective, pinhole 95.6 µm/1 Airy, logical size 1024x1024

Alexa 555/ donor channel laser 561 nm (20% software), PMT 573-603 nm, gain 850.

FRET channel laser 561 nm (software 20%), PMT 651-681 nm, gain 850.

Atto 647N/ acceptor channel laser 633 nm (software 12%) PMT 651 - 681 gain 850.

Uptake quantification in cell lysate

One day prior to transfection, 8 x 10^4 HeLa cells were seeded in transfection medium in 24 well plates. Prior to transfection, medium was replaced by 185 µL DMEM. Polyplexes were prepared with Alexa 555/ Atto 647N labeled siRNA in 65 µL OptiMem, incubated for 20 min and added dropwise to the cells at an siRNA concentration of 125 nM. 4 h after transfection, medium was replaced by 1 mL transfection medium. After 20 h, cells were washed with PBS, 0.2 mg/mL heparin solution and again PBS. For lysis, cells were incubated on ice for 30 min in 150 µL PBS containing 2% SDS and 1% TritonX. Cell debris was removed by centrifugation at 16000 g and 4 °C for 20 min. 50 µL of lysate was transferred to black 96 well plates and acceptor fluorescence measured on a plate reader at 561 nm excitation and 610 nm emission. Calibration was carried out by diluting siRNA at various concentrations in cell lysate of untransfected cells. Fluorescence values were normalized to protein content by submitting another 50 µL of lysate to the ROTI^{TM} Quant universal assay according to the manufacturer's instructions. All data result from biological triplicates each done in technical duplicates.

Uptake quantification via flow cytometry

Cells were transfected and incubated as described above. For workup, cells were after the washing steps trypsinized and resuspended in PBS. Cells were analyzed on a LSR-FortessaSORP in the donor (Ex 488 nm, 530BP30 emission filter), FRET (Ex 488 nm, 670BP30 emission filter) and acceptor (Ex 561 nm, 670BP30 emission filter) channels with the FRET channel compensated for bleedthrough of donor and acceptor fluorophores. Data was evaluated with FlowJo Software. Uptake was quantified by the median fluorescence intensity in the acceptor channel. For R/G calculation, the ratio of FRET to donor fluorescence intensity for each cell was derived as a new parameter and its median dessignated as R/G value. All data result from biological triplicates each done in technical duplicates.

Knockdown assay with HEK cells

One step setup/ protocol employed in section 3.6

One day prior to transfection, 6 x 10^4 HEK cells were seeded in 1 mL transfection medium in 24 well plates. At the time of transfection, medium was replaced with 500 µL fresh transfection medium. A mix consisting of the appriate amount of siRNA, 400 ng eGFP plasmid and 1 µL Lipofectamine^{TM} was prepared in a final volume 100 µL OptiMem, incubated for 20 min and added dropwise to the wells. After 24 h, cells were washed with PBS, trypsinized, resuspended in PBS and the eGFP signal measured on a LSR-FortessaSORP with excitation at 488 nm and a 530BP30 emission filter. Data was evaluated with the FACS DIVA Software. GFP signal was calculated as the product of the percentage of GFP positive cells and their mean fluorescence intensity compared to the value of a control only transfected with eGFP plasmid. All data result from biological triplicates each done in technical triplicate. For the determination of IC_{50} values, data was fit with a five parametric dose-response curve (Graph pad prism^{TM}).

Two step setup

One day prior to transfection, 6 x 10^4 HEK cells were seeded in 1 mL transfection medium in 24 well plates. At the time of transfection, medium was replaced with 500 µL fresh transfection medium. siRNA and 1 µL Lipofectamine^{TM} was mixed in a final volume 100 µL OptiMem, incubated for 20 min and added dropwise to the

wells. After 4 h, cells were washed with PBS and 500 µL fresh transfection medium was added. 400 ng eGFP plasmid plasmid and 1 µL Lipofectamine^{TM} was mixed in a final volume 100 µL OptiMem, incubated for 20 min and added dropwise to the wells. After 24 h, cells were washed with PBS, trypsinized, resuspended in PBS and analyzed as described in the one step setup protocol.

Knockdown assay with HeLa MAZ cells

One day prior to transfection, 4 x 10^4 HeLa MAZ ODC cells [224] were seeded in 1 mL transfection medium in 24 well plates. At the time of transfection, medium was replaced by 185 µL DMEM. Polyplexes were prepared in OptiMem in a final volume of 65 µL and after 20 min added dropwise to the wells at a final siRNA concentration of 62.5 µM. For the titration of IC_{50} curves in section 3.4, siRNA was transfected with Lipofectamine^{TM} or Oligofectamine^{TM} according to the manufacturer's instruction. 4 h after transfection, medium was replaced by 1 mL transfection medium. After 20 h, cells were incubated with fresh transfection medium containing 2 µM MG115 for another 5 h. For analysis, cells were washed with PBS, trypsinized, resuspended in PBS and the GFP signal measured on a LSR-FortessaSORP with excitation at 488 nm and an 530BP30 emission filter. Data was evaluated with FlowJo Software. GFP signal was calculated as the product of the percentage of GFP positive cells and their median fluorescence intensity compared to the value of an only MG115 treated control. All data result from biological triplicates each done in technical duplicates.

For viability staining, DAPI at a c of 1 µg/mL was added to the cell suspension 2 min before analyzation with excitation at 405 nm and an 450BP50 emission filter.

Liposome preparation

Ethanolic lipid stock solutions were pipetted into a screw cap vial. Volumes of each lipid solution corresponded to its desired molar fraction and yielded a total lipid mass of 17.5 mg. Solutions were lyophilized for two days and rehydrated with 32.5 µL PBS (if applicable, with dissolved SB). After addition of 250 mg ceramic beads, vials were closed and centrifuged for 20 min at 2500 rpm in the dual centrifuge. Additional 100 µL of PBS were added before a second centrifugation step for 2 min at 2500 rpm.

The size of the liposomes was determined by DLS on a Malvern ZetaSizer Nano by measuring a dilution of 1 µL liposome suspension in 1 mL freshly filtered PBS in a disposable polystyrene cuvette, resulting in count rates between 100 and 300

kcounts per second. The measurement was performed after equilibrating the sample to 25 °C, with the instrument optimizing the number of runs per measurement. All measurements were performed at a scattering angle of 173°. The measurement yielded a hydrodynamic diameter (obtained as z-average) and a PDI.

Non incorporated cargo dye was removed by SEC in custom made columns in MobiTec syringes with an approximate volume of 12 mL of Sephadex^{TM} G100. 50 µL of liposome solution was eluted in PBS under gravity flow and fractions of approximately 350 µL were collected in 96 well plates and analyzed on a microplate reader (for SB: Ex 560 nm, Em 590 nm).

Quantification of the encapsulated cargo dye SB was carried out on a microplate reader after cracking of the liposomes in 0.5% TrX in PBS.

CuAAC procedures

CuAAC of liposomes with azide functionalized dyes

The reaction was carried out for 5 µL of the initial liposome suspension (before purification by SEC) in a total volume of 40 µL H_2O containing 10 mM phosphate buffer, 0.5 mM THPTA, 0.1 mM Cu_2SO_4, 2.5 mM NaAsc and 0.15 mM of the respective dye azide. The reaction was incubated for 2 h at 25 °C and subsequently purified via size exclusion chromatography as described above for the removal of unincorporated dye (for Cy5: Ex 645, Em 675, for Atto488: Ex 488 nm, Em 520 nm).

CuAAC of the lipid SM264 with TPP azide or Cy5 azide

The reaction was carried out for 1 mg of SM264 (1.5 mM) in 300 µL ethanol/H_20 1-1 containing 100 mM phosphate buffer, 0.5 mM THPTA, 0.1 mM Cu_2SO_4, 2.5 mM NaAsc and 15 mM TPP azide or 0.15mM Cy5 azide, respectively. The reaction was incubated for 12 h at 55 °C at 500 rpm.

Unreacted azide was removed by separation in a custom made SEC column of approximately 30 cm height and 1 cm diameter filled with Sephadex^{TM} LH20. The reaction mixture was eluted with EtOH under gravity flow and fractions of approximately 350 µL were collected in the case of Cy5 in 96 well black chambered plates and read out via fluorescence on a plate reader (Ex 645 nm, Em 675 nm). In the case of TPP, fractions were collected in 96 well transparent UV plates and absorption was measured at 240 nm.

The fractions containing the functionalized lipid of several runs were united and

lyophilized. After weighing the lipid pellet, it was redissolved in EtOH at the desired concentration.

Functionalization of liposomes

Post insertion of the Cy5 functionalized lipid SM264

The concentration of the Cy5 functionalized lipid solution was adjusted so that the addition of 5 µL to 200 µL of the liposome suspension added 5 mol% of functionalized lipid to the liposome. The mixture was incubated for 1 h at 37 °C and used without further purification.

Direct incorporation of the TPP functionalized lipid into liposomes

The initial lipid mixture for liposome preparation included 1 mol% of the TPP functionalized lipid SM264. Liposomes were prepared as described above.

Colocalization studies

One day prior to transfection, 15 x 10^3 HeLa cells were seeded in 300 µL transfection medium into 8 chamber dishes. Prior to transfection, medium was replaced by 92.5 µL DMEM. Liposomes were diluted in 32.5 µL OptiMem and added dropwise to the cells at a final concentration of the incorporated Sulforhodamin B of 100 nM in the liposome samples, 100 nM of Cy5 or 13 nM of the SM264-Cy5-conjugate, which corresponds to its concentration in a 100 nM SB liposome suspension. After 4 h, cells were washed three times with PBS. Cells were then incubated in 100 nM Mitotracker^{TM} green in PBS for 30 min at 37 °C. Living cells were imaged in DMEM without indicator on a confocal microscope.

general settings 63x 1.4 oil objective, pinhole 95.6 µm/1 Airy, logical size 2048x2048

Mitotracker channel laser 488 nm (software 20%, hardware 20 %) PMT 505-535 nM, gain 700.

Sulforhodamine B channel laser 561 nm (software 20%), PMT 575-605 nm, gain 500.

Cy5 channel laser 633 nm (software 20%), PMT 655-685 nm, gain 700.

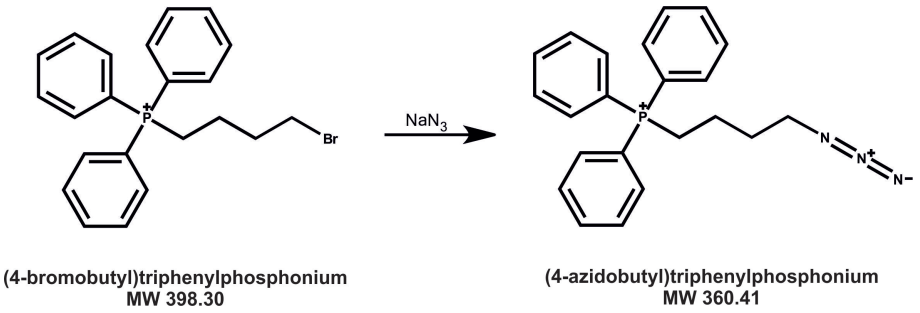

Figure 5.1: Synthesis scheme of TPP azide

Synthesis of TPP azide

5 g TPP bromide and 2.7 g NaN_3 (4 equivalents) were dissolved in a 1-1 mixture of H_2O and EtOH and stirred under reflux for 8 h. The EtOH was removed *in vacuo*. The remaining aqueous liquid was transferred to a seperating funnel, where a 2fold volume of H_2O was added without shaking. An oily phase separated over night, which was redissolved in DCM and dried over $NaSO_4$. The solvent was removed *in vacuo* yielding a white solid. Yield 56%.

^{1}H NMR of the educt (4-bromobutyl)triphenylphosphonium (400 MHz, $CHCl_3$, 25 °C) δ 1.79 (m, CH_2-CH_2-P); 2.25 (m, CH_2-CH_2-Br); 3.50 (t, CH_2-Br, $^3J = 5.8$); 3.86 (m CH_2-Ph); 7.63 (m 6 Phenyl-H), 7.77 (m 9 Phenyl-H) (see appendix, figure A17).

^{1}H NMR of the product (4-azidobutyl)triphenylphosphonium (400 MHz, $CHCl_3$, 25 °C) δ 1.68 (m, CH_2-CH_2-P); 1.93 (m, CH_2-CH_2-N_3); 3.37 (t, CH_2-N_3, $^3J = 6.15$); 3.76 (m CH_2-Ph); 7.65 (m 6 Phenyl-H); 7.77 (m 9 Phenyl-H) (see appendix, figure A18).

FT-IR (cm^{-1}): 2945 (w) and 2872 (w) ν (CH alkane), 2095 (s) ν (azide), 1998 (s), 1585 ν (w) (CC aryl), 1483 (s), 1434 (m), 1344 (m), 1279 (m), 1107 (s), 1058 (m), 1002 (w), 735 (s) γ (CH aryl) (see appendix, figure A19).

HR-ESI-TOF-MS m/z 332.1 (M^+ N_2 eliminated), 361.1 (M^+), 762,3 ($2M^+ + K^+$), 801.3 ($2M^+ + Br^-$ (see appendix, figure A20).

Abbreviations

APMA	N-(3-aminopropyl) methacrylamide
APS	3-amino-propyltriethoxysilane
APS	ammoniumperoxydisulfate
ATP	adenosine triphosphate
BR_{50}	binding $ratio_{50}$ (m/m for half maximal binding)
BSA	bovine serum albumin
C. elegans	Caenorhabditis elegans
Chol	cholesterol
CHX	cycloheximide
CLSM	confocal laser scanning microscopy
CPP	cell penetrating peptide
CuAAC	Cu^+ catalyzed azide alkyne cycloaddition
$CuSO_4$	copper sulfate
Cy5	cyanine 5
Da	Dalton
DAB	diaminobutane-dendrimer-$(NH_2)_{64}$
DAPI	4',6–diamidino–2–phenylindole
DC	dual centrifugation
DLS	dynamic light scattering
DMEM	Dulbecco's modified eagle medium
DMSO	dimethylsulfoxide
DNA	deoxyribonucleic acid
DOPE	1,2-dioleoyl-sn-glycero-3-phosphoethanolamine
DOSPA	2,3-dioleyloxy-N-[2(spermine carboxamido) ethyl] - N,N-dimethyl-1-propanaminium trifluoroacetate
DOTAP	1,2-dioleoyl-3-trimethylammonium-propane
ds	double stranded
DSPE-mPEG(2000)	Distearoyl-phosphatidylethanolamine-methyl-polyethyleneglycol 2000
EC_{50}	half maximal effective concentration
eGFP	enhanced green fluorescent protein
Em	emission
EMSA	electrophoretic mobiity shift assay
EPC	egg phosphatidyl choline
ESI-TOF-MS	electron spray ionization - time of flight - mass spectroscopy

Et_3N	triethylamine
Ex	excitation
FACS	fluorescence activated cell sorting
FCS	fetal bovine serum
FCS	fluorescence correlation spectroscopy
FCCS	fluorescence cross correlation spectroscopy
FI	fluorescence intensity
fL	femtoliter
FRET	Förster resonance energy transfer
h	hour
GPMA	3-guanidinopropyl methacrylamide
HEK 293T	cell line derived from human embryonic kidney cells
HeLa	cell line derived from a tissue sample of Henrietta Lacks
HeLa luc	HeLa cells stably transfected with firefly luciferase
HPLC	high performance liquid chromatography
HPMA	N-(2-hydroxypropyl) methacrylamide
HR	high resolution
KCl	potassium chloride
KH_2PO_4	potassium dihydrogen phosphate
IC_{50}	half maximal inhibitory concentration
IPB	Institute of Pharmacy and Biochemistry
IR	infrared
LHON	Leber hereditary optic neuropathy
$MgCl_2$	magnesium chloride
m/m	$mass_{carrier}$/ $mass_{siRNA}$ ratio
M_W	molecular weight
MEO_3MA	tri- (ethylene glycol)methyl ether methacrylate
MELAS	mitochondrial encephalomyopathy with lactic acidosis and stroke-like episodes
MERRF	myoclonic epilepsy with ragged red fibers
min	minute
miRNA	micro RNA
MnO	manganese oxide
MPIP	Max Planck Institute for Polymer Research, Mainz
mRNA	messenger RNA
MSC	mesenchymal stem cells
MST	microscale thermophoresis
mt	mitochondrial
M_W	molecular weight
NaAsc	Sodium Ascorbate
NaCl	sodium chloride
NADH	nicotinamide adenine dinucleotide
Na_2HPO_4	disodium hydrogen phosphate

NaN_3	sodium azide
NH_4Ac	ammonium acetate
NHS	N-hydroxysuccinimide
NMR	nuclear magnetic resonance
N/P ratio	nitrogen/phosphate ratio
ODN	oligodeoxynucleotide
QNPHOS	poly(3,5-bis(dimethylaminomethylene)- p-hydroxyl styrene)
PAGE	polyacrylamide gel electrophoresis
PAMAM	poly(amido amine)
PBCA	poly(n-butylcyanoacrylate)
PBS	phosphate buffered saline
PDI	polydispersity index
pDMAEMA	poly(2-dimethylamino)ethyl methacrylate
PEG	poly(ethylene)glycol
PEI	poly(ethylene)imine
Pen/Strep	penicillin and streptomycin
PFPMA	pentafluorophenyl methacrylate
piRNA	piwi interacting RNA
PLGA	poly(lactide-co-glycolide)
PLL	poly-L-lysine
PLLA	poly-L-lactide
PVA	polyvinylalcohol
RES	reticuloendothelial system
R/G	ratio of red to green fluorescence
RISC	RNA induced silencing complex
RNA	ribonucleic acid
RNAi	RNA interference
RNase	ribonuclease
ROS	reactive oxygen species
RP	reversed phase
s	second
SB	Sulforhodamine B
SDS	sodium dodecyl sulfate
SEC	size exclusion chromatography
shRNA	small hairpin RNA
SiO_2	silicon dioxide
siRNA	small interfering RNA
SLS	static light scattering
SPC	soy phosphatidyl choline
spermine-Ac-Dex	acetal-modified dextran endowed with spermine moieties
ss	single stranded
STAT3	signal transducer and activator of transcription 3

TBE	tris/borate/EDTA buffer
TEAA	triethylammonium acetate buffer
TEMED	tetramethylethylenediamine
THTPA	tris-(3-hydroxypropyltriazolylmethyl)amine
TPPBr	(4-bromobutyl)triphenylphosphonium bromide
TPP azide	(4-azidobutyl)triphenylphosphonium azide
TRIS HCl	tris(hydroxymethyl)aminomethane HCl
tRNA	transfer RNA
UTR	untranslated region
UV	ultraviolet
VEGF	vascular endothelial growth factor
$v_{antisense}/v_{sense}$	$volume_{antisense}/volume_{sense}$ ratio

Cooperation partners

Bibliography

[1] F. Crick. Central dogma of molecular biology. *Nature*, 227(5258):561–3, August 1970.

[2] P. Svoboda. Renaissance of mammalian endogenous RNAi. *FEBS letters*, 588(15):2550–2556, August 2014.

[3] C. Napoli, C. Lemieux, and R. Jorgensen. Introduction of a Chimeric Chalcone Synthase Gene into Petunia Results in Reversible Co-Suppression of Homologous Genes in trans. *The Plant cell*, 2(4):279–289, April 1990.

[4] A. Fire, S. Xu, M. K. Montgomery, S. A. Kostas, S. E. Driver, and C. C. Mello. Potent and specific genetic interference by double-stranded RNA in Caenorhabditis elegans. *Nature*, 391 (6669):806–11, February 1998.

[5] P. D. Zamore, T. Tuschl, P. a. Sharp, and D. P. Bartel. RNAi: double-stranded RNA directs the ATP-dependent cleavage of mRNA at 21 to 23 nucleotide intervals. *Cell*, 101(1):25–33, March 2000.

[6] S. M. Hammond, E. Bernstein, D. Beach, and G. J. Hannon. An RNA-directed nuclease mediates post-transcriptional gene silencing in Drosophila cells. *Nature*, 404(6775):293–6, March 2000.

[7] S. M. Elbashir, J. Harborth, W. Lendeckel, a. Yalcin, K. Weber, and T. Tuschl. Duplexes of 21-nucleotide RNAs mediate RNA interference in cultured mammalian cells. *Nature*, 411 (6836):494–8, May 2001.

[8] E. Bernstein, A. A. Caudy, S. M. Hammond, and G. J. Hannon. Role for a bidentate ribonuclease in the initiation step of RNA interference. *Nature*, 409(6818):363–6, January 2001.

[9] J. Martinez, A. Patkaniowska, H. Urlaub, R. Lührmann, and T. Tuschl. Single-stranded antisense siRNAs guide target RNA cleavage in RNAi. *Cell*, 110(5):563–74, September 2002.

[10] Y. Tomari, C. Matranga, B. Haley, N. Martinez, and P. D. Zamore. A protein sensor for siRNA asymmetry. *Science (New York, N.Y.)*, 306(5700):1377–80, November 2004.

[11] K. A. Whitehead, R. Langer, and D. G. Anderson. Knocking down barriers: advances in siRNA delivery. *Nature reviews. Drug discovery*, 8(2):129–38, February 2009.

[12] S. Mohr, C. Bakal, and N. Perrimon. Genomic screening with RNAi: results and challenges. *Annual review of biochemistry*, 79:37–64, January 2010.

[13] A. P. McCaffrey, L. Meuse, T.-T. T. Pham, D. S. Conklin, G. J. Hannon, and M. a. Kay. RNA interference in adult mice. *Nature*, 418(6893):38–9, July 2002.

[14] M. E. Davis, J. E. Zuckerman, C. H. J. Choi, D. Seligson, A. Tolcher, C. a. Alabi, Y. Yen, J. D. Heidel, and A. Ribas. Evidence of RNAi in humans from systemically administered siRNA via targeted nanoparticles. *Nature*, 464(7291):1067–70, April 2010.

[15] S. Y. Wu, G. Lopez-Berestein, G. A. Calin, and A. K. Sood. RNAi Therapies: Drugging the Undruggable. *Science translational medicine*, 6(240), June 2014.

[16] J. K. Watts and D. R. Corey. Clinical status of duplex RNA. *Bioorganic and medicinal chemistry letters*, 20(11):3203–7, June 2010.

[17] M. Cavazzana-Calvo, A. Thrasher, and F. Mavilio. The future of gene therapy. *Nature*, 427 (6977):779–81, February 2004.

[18] G. R. Devi. siRNA-based approaches in cancer therapy. *Cancer gene therapy*, 13(9):819–29, September 2006.

[19] E. Zorde Khvalevsky, R. Gabai, I. H. Rachmut, E. Horwitz, Z. Brunschwig, A. Orbach, A. Shemi, T. Golan, A. J. Domb, E. Yavin, H. Giladi, L. Rivkin, A. Simerzin, R. Eliakim, A. Khalaileh, A. Hubert, M. Lahav, Y. Kopelman, E. Goldin, A. Dancour, Y. Hants, S. Arbel-Alon, R. Abramovitch, A. Shemi, and E. Galun. Mutant KRAS is a druggable target for pancreatic cancer. *Proceedings of the National Academy of Sciences of the United States of America*, 110(51):20723–8, December 2013.

[20] A. Reynolds, D. Leake, Q. Boese, S. Scaringe, W. S. Marshall, and A. Khvorova. Rational siRNA design for RNA interference. *Nature biotechnology*, 22(3):326–30, March 2004.

[21] Y. Pei and T. Tuschl. On the art of identifying effective and specific siRNAs. *Nature methods*, 3(9):670–6, September 2006.

[22] M. Diken, S. Kreiter, a. Selmi, C. M. Britten, C. Huber, O. Türeci, and U. Sahin. Selective uptake of naked vaccine RNA by dendritic cells is driven by macropinocytosis and abrogated upon DC maturation. *Gene therapy*, 18(7):702–8, July 2011.

[23] K. E. Broderick, A. Chan, F. Lin, X. Shen, G. Kichaev, A. S. Khan, J. Aubin, T. S. Zimmermann, and N. Y. Sardesai. Optimized in vivo transfer of small interfering RNA targeting dermal tissue using in vivo surface electroporation. *Molecular therapy. Nucleic acids*, 1(January), January 2012.

[24] K. Raemdonck, K. Remaut, B. Lucas, N. N. Sanders, J. Demeester, and S. C. De Smedt. In situ analysis of single-stranded and duplex siRNA integrity in living cells. *Biochemistry*, 45 (35):10614–23, September 2006.

[25] K. Jensen, J. A. Anderson, and E. J. Glass. Comparison of small interfering RNA (siRNA) delivery into bovine monocyte-derived macrophages by transfection and electroporation. *Veterinary immunology and immunopathology*, 158(3-4):224–32, April 2014.

[26] M. Gooding, L. P. Browne, F. M. Quinteiro, and D. L. Selwood. siRNA delivery: from lipids to cell-penetrating peptides and their mimics. *Chemical biology and drug design*, 80(6):787–809, December 2012.

[27] H. Lv, S. Zhang, B. Wang, S. Cui, and J. Yan. Toxicity of cationic lipids and cationic polymers in gene delivery. *Journal of controlled release: official journal of the Controlled Release Society*, 114(1):100–9, August 2006.

[28] N. S. Yew and R. K. Scheule. Toxicity of cationic lipid-DNA complexes. *Advances in genetics*, 53:189–214, January 2005.

[29] H. Xia, Q. Mao, H. L. Paulson, and B. L. Davidson. siRNA-mediated gene silencing in vitro and in vivo. *Nature biotechnology*, 20(10):1006–10, October 2002.

[30] D. a. Rubinson, C. P. Dillon, A. V. Kwiatkowski, C. Sievers, L. Yang, J. Kopinja, D. L. Rooney, M. Zhang, M. M. Ihrig, M. T. McManus, F. B. Gertler, M. L. Scott, and L. Van Parijs. A lentivirus-based system to functionally silence genes in primary mammalian cells, stem cells

and transgenic mice by RNA interference. *Nature genetics*, 33(3):401–6, March 2003.

[31] C. E. Thomas, A. Ehrhardt, and M. a. Kay. Progress and problems with the use of viral vectors for gene therapy. *Nature reviews. Genetics*, 4(5):346–58, May 2003.

[32] S. Choung, Y. J. Kim, S. Kim, H.-O. Park, and Y.-C. Choi. Chemical modification of siRNAs to improve serum stability without loss of efficacy. *Biochemical and Biophysical Research Communications*, 342(3):919–927, April 2006.

[33] M. Robbins, A. Judge, L. Liang, K. McClintock, E. Yaworski, and I. MacLachlan. 2'-O-methyl-modified RNAs act as TLR7 antagonists. *Molecular therapy: the journal of the American Society of Gene Therapy*, 15(9):1663–9, September 2007.

[34] J. K. Watts, G. F. Deleavey, and M. J. Damha. Chemically modified siRNA: tools and applications. *Drug discovery today*, 13(19-20):842–55, October 2008.

[35] J. Soutschek, A. Akinc, B. Bramlage, K. Charisse, R. Constien, M. Donoghue, S. Elbashir, A. Geick, P. Hadwiger, J. Harborth, M. John, V. Kesavan, G. Lavine, R. K. Pandey, T. Racie, K. G. Rajeev, I. Röhl, I. Toudjarska, G. Wang, S. Wuschko, D. Bumcrot, V. Koteliansky, S. Limmer, M. Manoharan, and H.-P. Vornlocher. Therapeutic silencing of an endogenous gene by systemic administration of modified siRNAs. *Nature*, 432(7014):173–8, November 2004.

[36] Y.-l. Chiu, A. Ali, C.-y. Chu, H. Cao, and T. M. Rana. Visualizing a Correlation between siRNA Localization , Cellular Uptake , and RNAi in Living Cells. *Chemistry and Biologly*, 11: 1165–1175, 2004.

[37] D. Reischl and A. Zimmer. Drug delivery of siRNA therapeutics: potentials and limits of nanosystems. *Nanomedicine : nanotechnology, biology, and medicine*, 5(1):8–20, March 2009.

[38] K. A. Howard. Delivery of RNA interference therapeutics using polycation-based nanoparticles. *Advanced drug delivery reviews*, 61(9):710–20, July 2009.

[39] P. Resnier, T. Montier, V. Mathieu, J.-P. Benoit, and C. Passirani. A review of the current status of siRNA nanomedicines in the treatment of cancer. *Biomaterials*, 34(27):6429–43, September 2013.

[40] A. Zintchenko, A. Philipp, A. Dehshahri, and E. Wagner. Simple modifications of branched PEI lead to highly efficient siRNA carriers with low toxicity. *Bioconjugate chemistry*, 19(7): 1448–55, July 2008.

[41] J. K. W. Lam, W. Liang, Y. Lan, P. Chaudhuri, M. Y. T. Chow, K. Witt, L. Kudsiova, and A. J. Mason. Effective endogenous gene silencing mediated by pH responsive peptides proceeds via multiple pathways. *Journal of controlled release: official journal of the Controlled Release Society*, 158(2):293–303, March 2012.

[42] J. L. Cohen, S. Schubert, P. R. Wich, L. Cui, J. A. Cohen, J. L. Mynar, and J. M. J. Fréchet. Acid-degradable cationic dextran particles for the delivery of siRNA therapeutics. *Bioconjugate chemistry*, 22(6):1056–65, June 2011.

[43] T. Suma, K. Miyata, T. Ishii, S. Uchida, H. Uchida, K. Itaka, N. Nishiyama, and K. Kataoka. Enhanced stability and gene silencing ability of siRNA-loaded polyion complexes formulated from polyaspartamide derivatives with a repetitive array of amino groups in the side chain. *Biomaterials*, 33(9):2770–9, March 2012.

[44] S. E. L. Andaloussi, T. Lehto, I. Mäger, K. Rosenthal-Aizman, I. I. Oprea, O. E. Simonson, H. Sork, K. Ezzat, D. M. Copolovici, K. Kurrikoff, J. R. Viola, E. M. Zaghloul, R. Sillard, H. J.

Johansson, F. Said Hassane, P. Guterstam, J. Suhorutšenko, P. M. D. Moreno, N. Oskolkov, J. Hälldin, U. Tedebark, A. Metspalu, B. Lebleu, J. Lehtiö, C. I. E. Smith, and U. Langel. Design of a peptide-based vector, PepFect6, for efficient delivery of siRNA in cell culture and systemically in vivo. *Nucleic acids research*, 39(9):3972–87, May 2011.

[45] D. J. Gary, N. Puri, and Y.-Y. Won. Polymer-based siRNA delivery: perspectives on the fundamental and phenomenological distinctions from polymer-based DNA delivery. *Journal of controlled release: official journal of the Controlled Release Society*, 121(1-2):64–73, August 2007.

[46] C. Scholz and E. Wagner. Therapeutic plasmid DNA versus siRNA delivery: common and different tasks for synthetic carriers. *Journal of controlled release: official journal of the Controlled Release Society*, 161(2):554–65, July 2012.

[47] A. H. van Asbeck, A. Beyerle, H. McNeill, P. H. M. Bovee-Geurts, S. Lindberg, W. P. R. Verdurmen, M. Hällbrink, U. Langel, O. Heidenreich, and R. Brock. Molecular parameters of siRNA–cell penetrating peptide nanocomplexes for efficient cellular delivery. *ACS nano*, 7(5): 3797–807, May 2013.

[48] M. Kim, H. R. Kim, S. Y. Chae, R. G. Larson, H. Lee, and J. C. Park. Effect of arginine-rich peptide length on the structure and binding strength of siRNA-peptide complexes. *The journal of physical chemistry. B*, 117(23):6917–26, June 2013.

[49] D. J. Gary, J. Min, Y. Kim, K. Park, and Y.-Y. Won. The effect of N/P ratio on the in vitro and in vivo interaction properties of PEGylated poly[2-(dimethylamino)ethyl methacrylate]-based siRNA complexes. *Macromolecular bioscience*, 13(8):1059–71, August 2013.

[50] D. Ouyang, H. Zhang, H. S. Parekh, and S. C. Smith. Structure and dynamics of multiple cationic vectors-siRNA complexation by all-atomic molecular dynamics simulations. *The journal of physical chemistry. B*, 114(28):9231–7, July 2010.

[51] M. Zheng, G. M. Pavan, M. Neeb, A. K. Schaper, A. Danani, G. Klebe, O. M. Merkel, and T. Kissel. Targeting the blind spot of polycationic nanocarrier-based siRNA delivery. *ACS nano*, 6(11):9447–54, November 2012.

[52] C. L. Grigsby and K. W. Leong. Balancing protection and release of DNA: tools to address a bottleneck of non-viral gene delivery. *Journal of the Royal Society, Interface / the Royal Society*, 7 Suppl 1(September 2009):S67–82, February 2010.

[53] S. P. Strand, S. Lelu, N. K. Reitan, C. de Lange Davies, P. Artursson, and K. M. Vå rum. Molecular design of chitosan gene delivery systems with an optimized balance between polyplex stability and polyplex unpacking. *Biomaterials*, 31(5):975–87, February 2010.

[54] C. Arigita, N. J. Zuidam, D. J. Crommelin, and W. E. Hennink. Association and dissociation characteristics of polymer/DNA complexes used for gene delivery. *Pharmaceutical research*, 16 (10):1534–41, October 1999.

[55] E. Vuorimaa, A. Urtti, R. Seppänen, H. Lemmetyinen, and M. Yliperttula. Time-resolved fluorescence spectroscopy reveals functional differences of cationic polymer-DNA complexes. *Journal of the American Chemical Society*, 130(35):11695–700, September 2008.

[56] D. Fischer, Y. Li, B. Ahlemeyer, J. Krieglstein, and T. Kissel. In vitro cytotoxicity testing of polycations: influence of polymer structure on cell viability and hemolysis. *Biomaterials*, 24 (7):1121–31, March 2003.

[57] A. K. Varkouhi, G. Mountrichas, R. M. Schiffelers, T. Lammers, G. Storm, S. Pispas, and W. E. Hennink. Polyplexes based on cationic polymers with strong nucleic acid binding properties. *European journal of pharmaceutical sciences*, 45(4):459–66, March 2012.

[58] C. H. Jones, C.-K. Chen, M. Jiang, L. Fang, C. Cheng, and B. Pfeifer. Synthesis of cationic polylactides with tunable charge densities as nanocarriers for effective gene delivery. *Molecular pharmaceutics*, 10(3):1138–45, March 2013.

[59] P. Pereira, A. F. Jorge, R. Martins, A. a. C. C. Pais, F. Sousa, and A. Figueiras. Characterization of polyplexes involving small RNA. *Journal of colloid and interface science*, 387(1):84–94, December 2012.

[60] J. H. Lee, Y. Lim, J. S. Choi, Y. Lee, T. Kim, H. J. Kim, J. K. Yoon, K. Kim, and J. Park. Polyplexes assembled with internally quaternized PAMAM-OH dendrimer and plasmid DNA have a neutral surface and gene delivery potency. *Bioconjugate chemistry*, 14(6):1214–21, 2003.

[61] M. Behlke. Progress towards in vivo use of siRNAs. *Molecular therapy: the journal of the American Society of Gene Therapy*, 13(4):644–70, April 2006.

[62] U. Paderborn. http://chemie.uni-paderborn.de/fachgebiete/tc/cmp/ausstattung/zetasizer-nano-zs/. *ZetaSizer Nano ZS Info2*, (Date accessed 20140817), 2014.

[63] S.-H. Huh, H.-J. Do, H.-Y. Lim, D.-K. Kim, S.-J. Choi, H. Song, N.-H. Kim, J.-K. Park, W.-K. Chang, H.-M. Chung, and J.-H. Kim. Optimization of 25 kDa linear polyethylenimine for efficient gene delivery. *Biologicals journal of the International Association of Biological Standardization*, 35(3):165–71, July 2007.

[64] M. Glodde, S. R. Sirsi, and G. J. Lutz. Physiochemical properties of low and high molecular weight poly(ethylene glycol)-grafted poly(ethylene imine) copolymers and their complexes with oligonucleotides. *Biomacromolecules*, 7(1):347–56, January 2006.

[65] Y. Lee, K. Miyata, M. Oba, T. Ishii, S. Fukushima, M. Han, H. Koyama, N. Nishiyama, and K. Kataoka. Charge Conversion Ternary Polyplex with Endosome Disruption Moiety: A Technique for Efficient and Safe Gene Delivery. *Angewandte Chemie*, 120(28):5241–5244, June 2008.

[66] S.-D. Li and L. Huang. Gene therapy progress and prospects: non-viral gene therapy by systemic delivery. *Gene therapy*, 13(18):1313–9, September 2006.

[67] S. Akhtar and I. F. Benter. Nonviral delivery of synthetic siRNAs in vivo. 117(12):3623–3632, 2007.

[68] D. W. Pack, A. S. Hoffman, S. Pun, and P. S. Stayton. Design and development of polymers for gene delivery. *Nature reviews. Drug discovery*, 4(July):581–593, 2005.

[69] I. A. Khalil, K. Kogure, H. Akita, and H. Harashima. Uptake Pathways and Subsequent Intracellular Trafficking in Nonviral Gene Delivery. 58(1):32–45, 2006.

[70] M. Walsh, M. Tangney, M. J. O'Neill, J. O. Larkin, D. M. Soden, S. L. McKenna, R. Darcy, G. C. O'Sullivan, and C. M. O'Driscoll. Evaluation of cellular uptake and gene transfer efficiency of pegylated poly-L-lysine compacted DNA: implications for cancer gene therapy. *Molecular pharmaceutics*, 3(6):644–53.

[71] L. Crombez, a. Charnet, M. C. Morris, G. Aldrian-Herrada, F. Heitz, and G. Divita. A non-covalent peptide-based strategy for siRNA delivery. *Biochemical Society transactions*, 35(Pt 1):44–6, March 2007.

[72] J. J. Lu, R. Langer, and J. Chen. A novel mechanism is involved in cationic lipid-mediated functional siRNA delivery. *Molecular pharmaceutics*, 6(3):763–71.

[73] M. van der Aa, U. S. Huth, S. Y. Häfele, R. Schubert, R. S. Oosting, E. Mastrobattista, W. E. Hennink, R. Peschka-Süss, G. Koning, and D. J. Crommelin. Cellular uptake of cationic polymer-DNA complexes via caveolae plays a pivotal role in gene transfection in COS-7 cells. *Pharmaceutical research*, 24(8):1590–8, August 2007.

[74] M. Agirre, J. Zarate, E. Ojeda, G. Puras, J. Desbrieres, and J. Pedraz. Low Molecular Weight Chitosan (LMWC)-based Polyplexes for pDNA Delivery: From Bench to Bedside. *Polymers*, 6(6):1727–1755, June 2014.

[75] S. Mayor and R. E. Pagano. Pathways of clathrin-independent endocytosis. *Nature reviews. Molecular cell biology*, 8(8):603–12, August 2007.

[76] K. Takei and V. Haucke. Clathrin-mediated endocytosis: membrane factors pull the trigger. *Trends in cell biology*, 11(9):385–91, October 2001.

[77] J. Rejman, V. Oberle, I. S. Zuhorn, and D. Hoekstra. Size-dependent internalization of particles via the pathways of clathrin- and caveolae-mediated endocytosis. *The Biochemical journal*, 377: 159–69, January 2004.

[78] J. Harris, D. Werling, J. C. Hope, G. Taylor, and C. J. Howard. Caveolae and caveolin in immune cells: distribution and functions. *Trends in immunology*, 23(3):158–64, March 2002.

[79] J. S. Wadia, R. V. Stan, and S. F. Dowdy. Transducible TAT-HA fusogenic peptide enhances escape of TAT-fusion proteins after lipid raft macropinocytosis. *Nature medicine*, 10(3):310–5, March 2004.

[80] N. P. Gabrielson and D. W. Pack. Efficient polyethylenimine-mediated gene delivery proceeds via a caveolar pathway in HeLa cells. *Journal of controlled release: official journal of the Controlled Release Society*, 136(1):54–61, May 2009.

[81] T.-I. Kim, J.-U. Baek, J. K. Yoon, J. S. Choi, K. Kim, and J.-S. Park. Synthesis and characterization of a novel arginine-grafted dendritic block copolymer for gene delivery and study of its cellular uptake pathway leading to transfection. *Bioconjugate chemistry*, 18(2):309–17, 2007.

[82] S. Oliveira, I. van Rooy, O. Kranenburg, G. Storm, and R. M. Schiffelers. Fusogenic peptides enhance endosomal escape improving siRNA-induced silencing of oncogenes. *International journal of pharmaceutics*, 331(2):211–4, March 2007.

[83] M. Matzke and J. Birchler. RNAi-mediated pathways in the nucleus. *Nature reviews. Genetics*, 6(1):24–35, January 2005.

[84] M. Meyer, A. Philipp, R. Oskuee, C. Schmidt, and E. Wagner. Breathing life into polycations: functionalization with pH-responsive endosomolytic peptides and polyethylene glycol enables siRNA delivery. *Journal of the American Chemical Society*, 130(11):3272–3, March 2008.

[85] D. Peer and J. Lieberman. Special delivery: targeted therapy with small RNAs. *Gene therapy*, 18(12):1127–33, December 2011.

[86] M. Dominska and D. M. Dykxhoorn. Breaking down the barriers: siRNA delivery and endosome escape. *Journal of cell science*, 123(Pt 8):1183–9, April 2010.

[87] L. Wasungu and D. Hoekstra. Cationic lipids, lipoplexes and intracellular delivery of genes. *Journal of controlled release: official journal of the Controlled Release Society*, 116(2):255–64,

November 2006.

[88] O. Zelphati and F. C. Szoka. Mechanism of oligonucleotide release from cationic liposomes. *Proceedings of the National Academy of Sciences of the United States of America*, 93(21): 11493–8, October 1996.

[89] A. Akinc, M. Thomas, A. M. Klibanov, and R. Langer. Exploring polyethylenimine-mediated DNA transfection and the proton sponge hypothesis. *The journal of gene medicine*, 7(5): 657–63, May 2005.

[90] G. X. Zhao, H. Tanaka, C. W. Kim, K. Li, D. Funamoto, T. Nobori, Y. Nakamura, T. Niidome, A. Kishimura, T. Mori, and Y. Katayama. Histidinylated poly-L-lysine-based vectors for cancer-specific gene expression via enhancing the endosomal escape. *Journal of biomaterials science. Polymer edition*, 25(5):519–34, January 2014.

[91] D. T. Auguste, K. Furman, A. Wong, J. Fuller, S. P. Armes, T. J. Deming, and R. Langer. Triggered release of siRNA from poly(ethylene glycol)-protected, pH-dependent liposomes. *Journal of controlled release: official journal of the Controlled Release Society*, 130(3):266–74, September 2008.

[92] P. Vader, L. J. van der Aa, J. F. J. Engbersen, G. Storm, and R. M. Schiffelers. Physicochemical and biological evaluation of siRNA polyplexes based on PEGylated Poly(amido amine)s. *Pharmaceutical research*, 29(2):352–61, February 2012.

[93] A. Masotti, G. Mossa, C. Cametti, G. Ortaggi, A. Bianco, N. D. Grosso, D. Malizia, and C. Esposito. Comparison of different commercially available cationic liposome-DNA lipoplexes: Parameters influencing toxicity and transfection efficiency. *Colloids and surfaces. B, Biointerfaces*, 68(2):136–44, March 2009.

[94] W. T. Godbey, K. K. Wu, and A. G. Mikos. Size matters: molecular weight affects the efficiency of poly(ethylenimine) as a gene delivery vehicle. *Journal of biomedical materials research*, 45 (3):268–75, June 1999.

[95] G. Sonavane, K. Tomoda, and K. Makino. Biodistribution of colloidal gold nanoparticles after intravenous administration: effect of particle size. *Colloids and surfaces. B, Biointerfaces*, 66 (2):274–80, October 2008.

[96] M. Kapoor, D. J. Burgess, and S. D. Patil. Physicochemical characterization techniques for lipid based delivery systems for siRNA. *International journal of pharmaceutics*, 427(1):35–57, May 2012.

[97] D. Schaffert and E. Wagner. Gene therapy progress and prospects: synthetic polymer-based systems. *Gene therapy*, 15(16):1131–8, August 2008.

[98] C. Tros de Ilarduya, Y. Sun, and N. Düzgünes. Gene delivery by lipoplexes and polyplexes. *European journal of pharmaceutical sciences*, 40(3):159–70, June 2010.

[99] P. Kesharwani, V. Gajbhiye, and N. K. Jain. A review of nanocarriers for the delivery of small interfering RNA. *Biomaterials*, 33(29):7138–50, October 2012.

[100] J. E. Zuckerman, C. H. J. Choi, H. Han, and M. E. Davis. Polycation-siRNA nanoparticles can disassemble at the kidney glomerular basement membrane. *Proceedings of the National Academy of Sciences of the United States of America*, 109(8):3137–42, February 2012.

[101] T. Fritz, M. Hirsch, F. C. Richter, S. S. Müller, A. M. Hofmann, K. A. K. Rusitzka, J. Markl, U. Massing, H. Frey, and M. Helm. Click Modification of Multifunctional Liposomes Bearing

Hyperbranched Polyether Chains. *Biomacromolecules*, 15:2440–2448, 2014.

[102] B. Urban-Klein, S. Werth, S. Abuharbeid, F. Czubayko, and A. Aigner. RNAi-mediated gene-targeting through systemic application of polyethylenimine (PEI)-complexed siRNA in vivo. *Gene therapy*, 12(5):461–6, March 2005.

[103] M. Wagner, A. C. Rinkenauer, A. Schallon, and U. S. Schubert. Opposites attract: influence of the molar mass of branched poly(ethylene imine) on biophysical characteristics of siRNA-based polyplexese. *RSC Advances*, 3(31):12774, July 2013.

[104] C. Brus, H. Petersen, A. Aigner, F. Czubayko, and T. Kissel. Physicochemical and Biological Characterization of Polyethylenimine-graft-Poly (ethylene glycol) Block Copolymers as a Delivery System for Oligonucleotides and Ribozymes. (18):677–684, 2004.

[105] A. Malek, O. Merkel, L. Fink, F. Czubayko, T. Kissel, and A. Aigner. In vivo pharmacokinetics, tissue distribution and underlying mechanisms of various PEI(-PEG)/siRNA complexes. *Toxicology and applied pharmacology*, 236(1):97–108, April 2009.

[106] E. Bertrand, C. Gonçalves, L. Billiet, J. P. Gomez, C. Pichon, H. Cheradame, P. Midoux, and P. Guégan. Histidinylated linear PEI: a new efficient non-toxic polymer for gene transfer. *Chemical communications (Cambridge, England)*, 47(46):12547–9, December 2011.

[107] R. Kircheis, S. Schüller, S. Brunner, M. Ogris, K. H. Heider, W. Zauner, and E. Wagner. Polycation-based DNA complexes for tumor-targeted gene delivery in vivo. *The journal of gene medicine*, 1(2):111–20.

[108] Y. Inoue, R. Kurihara, A. Tsuchida, M. Hasegawa, T. Nagashima, T. Mori, T. Niidome, Y. Katayama, and O. Okitsu. Efficient delivery of siRNA using dendritic poly(L-lysine) for loss-of-function analysis. *Journal of controlled release: official journal of the Controlled Release Society*, 126(1):59–66, February 2008.

[109] A. Sato, S. W. Choi, M. Hirai, A. Yamayoshi, R. Moriyama, T. Yamano, M. Takagi, A. Kano, A. Shimamoto, and A. Maruyama. Polymer brush-stabilized polyplex for a siRNA carrier with long circulatory half-life. *Journal of controlled release: official journal of the Controlled Release Society*, 122(3):209–16, October 2007.

[110] J. Nguyen, R. Reul, S. Roesler, E. Dayyoub, T. Schmehl, T. Gessler, W. Seeger, and T. H. Kissel. Amine-modified poly(vinyl alcohol)s as non-viral vectors for siRNA delivery: effects of the degree of amine substitution on physicochemical properties and knockdown efficiency. *Pharmaceutical research*, 27(12):2670–82, December 2010.

[111] E. Van Rompaey, Y. Engelborghs, N. Sanders, S. C. De Smedt, and J. Demeester. Interactions between oligonucleotides and cationic polymers investigated by fluorescence correlation spectroscopy. *Pharmaceutical research*, 18(7):928–36, July 2001.

[112] H. Ragelle, R. Riva, G. Vandermeulen, B. Naeye, V. Pourcelle, C. S. Le Duff, C. D'Haese, B. Nysten, K. Braeckmans, S. C. De Smedt, C. Jérôme, and V. Préat. Chitosan nanoparticles for siRNA delivery: optimizing formulation to increase stability and efficiency. *Journal of controlled release: official journal of the Controlled Release Society*, 176:54–63, February 2014.

[113] M. Ruponen, S. Ylä-Herttuala, and a. Urtti. Interactions of polymeric and liposomal gene delivery systems with extracellular glycosaminoglycans: physicochemical and transfection studies. *Biochimica et biophysica acta*, 1415(2):331–41, January 1999.

[114] X.-Q. Liu, J.-Z. Du, C.-P. Zhang, F. Zhao, X.-Z. Yang, and J. Wang. Brush-shaped polycation

with poly(ethylenimine)-b-poly(ethylene glycol) side chains as highly efficient gene delivery vector. *International journal of pharmaceutics*, 392(1-2):118–26, June 2010.

[115] M. Sahl, S. Muth, R. Branscheid, K. Fischer, and M. Schmidt. Helix−Coil Transition in Cylindrical Brush Polymers with Poly-L-Lysine Side Chains. *Macromolecules*, 45:5167–5175, 2012.

[116] J. Hedrich, Y. Wu, S. Kuan, F. Kühn, E. Pietrowski, M. Sahl, S. Muth, K. Müllen, H. Luhmann, T. Weil, and M. Schmidt. Polymer complexes in biological applications. In T. Basché, K. Müllen, and M. Schmidt, editors, *From single molecules to nanoscopically structured materials*, pages 211–235. Springer, Berlin, Heidelberg, 2014.

[117] P. A. Wender, D. J. Mitchell, K. Pattabiraman, E. T. Pelkey, L. Steinman, and J. B. Rothbard. The design, synthesis, and evaluation of molecules that enable or enhance cellular uptake: peptoid molecular transporters. *Proceedings of the National Academy of Sciences of the United States of America*, 97(24):13003–8, November 2000.

[118] N. J. Treat, D. Smith, C. Teng, J. D. Flores, B. A. Abel, A. W. York, F. Huang, and C. L. McCormick. Guanidine-Containing Methacrylamide (Co)polymers via aRAFT: Toward a Cell Penetrating Peptide Mimic. *ACS macro letters*, 1(1):100–104, January 2012.

[119] I. Tabujew, C. Freidel, B. Krieg, M. Helm, K. Koynov, K. Müllen, and K. Peneva. The Guanidinium Group as a Key Part of Water-Soluble Polymer Carriers for siRNA Complexation and Protection against Degradation. *Macromolecular rapid communications*, 35(13):1191–7, April 2014.

[120] A. J. Mason, C. Leborgne, G. Moulay, A. Martinez, O. Danos, B. Bechinger, and A. Kichler. Optimising histidine rich peptides for efficient DNA delivery in the presence of serum. *Journal of controlled release: official journal of the Controlled Release Society*, 118(1):95–104, March 2007.

[121] B. Langlet-Bertin, C. Leborgne, D. Scherman, B. Bechinger, A. J. Mason, and A. Kichler. Design and evaluation of histidine-rich amphipathic peptides for siRNA delivery. *Pharmaceutical research*, 27(7):1426–36, July 2010.

[122] E. Uchida, H. Mizuguchi, A. Ishii-Watabe, and T. Hayakawa. Comparison of the efficiency and safety of non-viral vector-mediated gene transfer into a wide range of human cells. *Biological and pharmaceutical bulletin*, 25(7):891–7, July 2002.

[123] L. Nuhn, M. Hirsch, B. Krieg, K. Koynov, K. Fischer, M. Schmidt, M. Helm, and R. Zentel. Cationic nanohydrogel particles as potential siRNA carriers for cellular delivery. *ACS nano*, 6 (3):2198–214, March 2012.

[124] L. Nuhn, S. Gietzen, K. Mohr, K. Fischer, K. Toh, K. Miyata, Y. Matsumoto, K. Kataoka, M. Schmidt, and R. Zentel. Aggregation behavior of cationic nanohydrogel particles in human blood serum. *Biomacromolecules*, 15(4):1526–33, April 2014.

[125] L. Nuhn. *Multifunctional Carriers for Peptide and Oligonucleotide Delivery by Reactive Precursor Polymers*. PhD thesis, Johannes Gutenberg-Universität Mainz, 2014.

[126] T. D. Schladt, K. Koll, S. Prüfer, H. Bauer, F. Natalio, O. Dumele, R. Raidoo, S. Weber, U. Wolfrum, L. M. Schreiber, M. P. Radsak, H. Schild, and W. Tremel. Multifunctional superparamagnetic MnO@SiO2 core/shell nanoparticles and their application for optical and magnetic resonance imaging. *Journal of Materials Chemistry*, 22(18):9253, 2012.

[127] S. Duhr and D. Braun. Why molecules move along a temperature gradient. *Proceedings of the National Academy of Sciences of the United States of America*, 103(52):19678–82, December 2006.

[128] J. Ries and P. Schwille. Fluorescence correlation spectroscopy. *BioEssays: news and reviews in molecular, cellular and developmental biology*, 34(5):361–8, May 2012.

[129] M. Hirsch, V. Ziroli, M. Helm, and U. Massing. Preparation of small amounts of sterile siRNA-liposomes with high entrapping efficiency by dual asymmetric centrifugation (DAC). *Journal of controlled release: official journal of the Controlled Release Society*, 135(1):80–8, April 2009.

[130] A. Järve, J. Müller, I.-H. Kim, K. Rohr, C. MacLean, G. Fricker, U. Massing, F. Eberle, A. Dalpke, R. Fischer, M. F. Trendelenburg, and M. Helm. Surveillance of siRNA integrity by FRET imaging. *Nucleic acids research*, 35(18):e124, January 2007.

[131] M. Hirsch. *Dynamics of small interfering RNA*. PhD thesis, Johannes Gutenberg-Universität Mainz, 2013.

[132] LifeTechnologies. http://www.lifetechnologies.com/de/de/home/references/molecular-probes-the-handbook/technical-notes-and-product-highlights/fluorescence-resonance-energy-transfer-fret.html. *The molecular probes handbook*, (date accessed 20140824), 2010.

[133] R. M. Clegg. Fluorescence resonance energy transfer. *Current opinion in biotechnology*, 6(1): 103–10, February 1995.

[134] Lambert Instruments. http://www.lambert-instruments.com/index.php/applications/fret/fret-efficiency. (Date accessed 20140826), 2014.

[135] Nikon. http://www.nikoninstruments.com/Information-Center/Crosstalk. *Nikon Information center*, (Date accessed 20140807), 2014.

[136] K. Kurokawa, A. Takaya, K. Terai, A. Fujioka, and M. Matsuda. Review Visualizing the Signal Transduction Pathways in Living Cells with GFP-Based FRET. *Acta Histochem. Cytochem*, 37(6):347–355, 2004.

[137] I. D. Rupenthal, C. R. Green, and R. G. Alany. Evaluation of Fluorescence Resonance Energy Transfer Approaches as a Tool to Quantify the Stability of Antisense Oligodeoxynucleotides. *Current Pharmaceutical Analysis*, 8(1):20–27, February 2012.

[138] S. Schneider, D. Lenz, M. Holzer, K. Palme, and R. Süss. Intracellular FRET analysis of lipid/DNA complexes using flow cytometry and fluorescence imaging techniques. *Journal of controlled release: official journal of the Controlled Release Society*, 145(3):289–96, August 2010.

[139] K. Remaut, B. Lucas, K. Braeckmans, N. N. Sanders, S. C. De Smedt, and J. Demeester. FRET-FCS as a tool to evaluate the stability of oligonucleotide drugs after intracellular delivery. *Journal of controlled release: official journal of the Controlled Release Society*, 103(1):259–71, March 2005.

[140] A. M. Portis, G. Carballo, G. L. Baker, C. Chan, and S. P. Walton. Confocal microscopy for the analysis of siRNA delivery by polymeric nanoparticles. *Microscopy research and technique*, 73(9):878–85, September 2010.

[141] R. M. Schiffelers, A. Ansari, J. Xu, Q. Zhou, Q. Tang, G. Storm, G. Molema, P. Y. Lu, P. V. Scaria, and M. C. Woodle. Cancer siRNA therapy by tumor selective delivery with ligand-targeted sterically stabilized nanoparticle. *Nucleic acids research*, 32(19):e149, January 2004.

[142] Z. Medarova, W. Pham, C. Farrar, V. Petkova, and A. Moore. In vivo imaging of siRNA delivery and silencing in tumors. *Nature medicine*, 13(3):372–7, March 2007.

[143] C. Alabi, K. T. Love, G. Sahay, T. Stutzman, W. T. Young, R. Langer, and D. G. Anderson. FRET-labeled siRNA probes for tracking assembly and disassembly of siRNA nanocomplexes. *ACS nano*, 6(7):6133–41, July 2012.

[144] D. S. Schwarz, G. Hutvágner, T. Du, Z. Xu, N. Aronin, and P. D. Zamore. Asymmetry in the assembly of the RNAi enzyme complex. *Cell*, 115(2):199–208, October 2003.

[145] J. Bramsen, M. Laursen, A. Nielsen, T. Hansen, C. Bus, N. Langkjaer, R. Babu, T. Hø jland, M. Abramov, A. Van Aerschot, D. Odadzic, R. Smicius, J. Haas, C. Andree, J. Barman, M. Wenska, P. Srivastava, C. Zhou, D. Honcharenko, S. Hess, E. Müller, G. V. Bobkov, S. Mikhailov, E. Fava, T. F. Meyer, J. Chattopadhyaya, M. Zerial, J. W. Engels, P. Herdewijn, J. Wengel, and J. r. Kjems. A large-scale chemical modification screen identifies design rules to generate siRNAs with high activity, high stability and low toxicity. *Nucleic acids research*, 37(9):2867–81, May 2009.

[146] O. Domingo. *Investigations into the effect of nucleoside modifications on the physicochemical and biological function of DNA and RNA*. PhD thesis, Johannes Gutenberg-Universität Mainz, 2013.

[147] S.-D. Li, S. Chono, and L. Huang. Efficient gene silencing in metastatic tumor by siRNA formulated in surface-modified nanoparticles. *Journal of controlled release: official journal of the Controlled Release Society*, 126(1):77–84, February 2008.

[148] M. Jafari, W. Xu, S. Naahidi, B. Chen, and P. Chen. A new amphipathic, amino-acid-pairing (AAP) peptide as siRNA delivery carrier: physicochemical characterization and in vitro uptake. *The journal of physical chemistry. B*, 116(44):13183–91, November 2012.

[149] O. M. Merkel, A. Beyerle, D. Librizzi, A. Pfestroff, T. M. Behr, B. Sproat, P. J. Barth, and T. Kissel. Nonviral siRNA Delivery to the Lung: Investigation of PEG-PEI Polyplexes and Their In Vivo Performance. *Molecular pharmaceutics*, 6(4):1246–1260, 2009.

[150] E. Van Rompaey, N. Sanders, S. C. De Smedt, J. Demeester, E. Van Craenenbroeck, and Y. Engelborghs. Complex Formation between Cationic Polymethacrylates and Oligonucleotides. *Macromolecules*, 33(22):8280–8288, October 2000.

[151] V. S. Trubetskoy, P. M. Slattum, J. E. Hagstrom, J. Wolff, and V. G. Budker. Quantitative assessment of DNA condensation. *Analytical biochemistry*, 267(2):309–13, March 1999.

[152] A. Adenier and J. J. Aaron. A spectroscopic study of the fluorescence quenching interactions between biomedically important salts and the fluorescent probe merocyanine 540. *Spectrochimica acta. Part A, Molecular and biomolecular spectroscopy*, 58(3):543–51, February 2002.

[153] L. Sikurova, B. Cunderlikova, J. Turisova, and I. Waczulikova. Interaction of merocyanine 540 with cations of physiological solutions. *Analytica Chimica Acta*, 303:79–83, 1995.

[154] J. M. Pagano, C. C. Clingman, and S. P. Ryder. Quantitative approaches to monitor protein-nucleic acid interactions using fluorescent probes. *RNA (New York, N.Y.)*, 17(1):14–20, January 2011.

[155] M. Jerabek-Willemsen, C. J. Wienken, D. Braun, P. Baaske, and S. Duhr. Molecular interaction studies using microscale thermophoresis. *Assay and drug development technologies*, 9(4):342–53, August 2011.

[156] C. J. Wienken, P. Baaske, S. Duhr, and D. Braun. Thermophoretic melting curves quantify the conformation and stability of RNA and DNA. *Nucleic acids research*, 39(8), April 2011.

[157] Y. T. Maeda, T. Tlusty, and A. Libchaber. Effects of long DNA folding and small RNA stem-loop in thermophoresis. *Proceedings of the National Academy of Sciences of the United States of America*, 109(44):17972–7, October 2012.

[158] K. Buyens, B. Lucas, K. Raemdonck, K. Braeckmans, J. Vercammen, J. Hendrix, Y. Engelborghs, S. C. De Smedt, and N. N. Sanders. A fast and sensitive method for measuring the integrity of siRNA-carrier complexes in full human serum. *Journal of controlled release: official journal of the Controlled Release Society*, 126(1):67–76, February 2008.

[159] B. Lucas, K. Remaut, N. N. Sanders, K. Braeckmans, S. C. De Smedt, and J. Demeester. Studying the intracellular dissociation of polymer-oligonucleotide complexes by dual color fluorescence fluctuation spectroscopy and confocal imaging. *Biochemistry*, 44(29):9905–12, July 2005.

[160] M. Wang, H. V. Adikane, J. Duhamel, and P. Chen. Protection of oligodeoxynucleotides against nuclease degradation through association with self-assembling peptides. *Biomaterials*, 29(8): 1099–108, March 2008.

[161] B. a. Lobo, G. S. Koe, J. G. Koe, and C. R. Middaugh. Thermodynamic analysis of binding and protonation in DOTAP/DOPE (1:1): DNA complexes using isothermal titration calorimetry. *Biophysical chemistry*, 104(1):67–78, May 2003.

[162] P. Holzerny, B. Ajdini, W. Heusermann, K. Bruno, M. Schuleit, L. Meinel, and M. Keller. Biophysical properties of chitosan/siRNA polyplexes: profiling the polymer/siRNA interactions and bioactivity. *Journal of controlled release: official journal of the Controlled Release Society*, 157(2):297–304, January 2012.

[163] Y. Zhao, Y. Qin, Y. Liang, H. Zou, X. Peng, H. Huang, M. Lu, and M. Feng. Salt-induced stability and serum-resistance of polyglutamate polyelectrolyte brushes/nuclear factor-κB p65 siRNA Polyplex enhance the apoptosis and efficacy of doxorubicin. *Biomacromolecules*, 14(6): 1777–86, June 2013.

[164] H. H. Chen, Y.-P. Ho, X. Jiang, H.-Q. Mao, T.-H. Wang, and K. W. Leong. Quantitative comparison of intracellular unpacking kinetics of polyplexes by a model constructed from quantum dot-FRET. *Molecular therapy: the journal of the American Society of Gene Therapy*, 16(2): 324–32, February 2008.

[165] C. Troiber, D. Edinger, P. Kos, L. Schreiner, R. Kläger, A. Herrmann, and E. Wagner. Stabilizing effect of tyrosine trimers on pDNA and siRNA polyplexes. *Biomaterials*, 34(5):1624–33, February 2013.

[166] Y. Xu and F. C. Szoka. Mechanism of DNA release from cationic liposome/DNA complexes used in cell transfection. *Biochemistry*, 35(18):5616–23, May 1996.

[167] H. Uchiyama, K. Hirano, M. Kashiwasake-Jibu, and K. Taira. Detection of undegraded oligonucleotides in vivo by fluorescence resonance energy transfer. Nuclease activities in living sea urchin eggs. *The Journal of biological chemistry*, 271(1):380–4, January 1996.

[168] M. Hirsch, D. Strand, and M. Helm. Dye selection for live cell imaging of intact siRNA. *Biological chemistry*, 393(1-2):23–35, January 2012.

[169] K. von Gersdorff, N. N. Sanders, R. Vandenbroucke, S. C. De Smedt, E. Wagner, and M. Ogris.

The internalization route resulting in successful gene expression depends on both cell line and polyethylenimine polyplex type. *Molecular therapy: the journal of the American Society of Gene Therapy*, 14(5):745–53, November 2006.

[170] K. Itaka, A. Harada, Y. Yamasaki, K. Nakamura, H. Kawaguchi, and K. Kataoka. In situ single cell observation by fluorescence resonance energy transfer reveals fast intra-cytoplasmic delivery and easy release of plasmid DNA complexed with linear polyethylenimine. *The journal of gene medicine*, 6(1):76–84, January 2004.

[171] M. Breunig, U. Lungwitz, R. Liebl, and A. Goepferich. Breaking up the correlation between efficacy and toxicity for nonviral gene delivery. *Proceedings of the National Academy of Sciences of the United States of America*, 104(36):14454–14459, 2007.

[172] P. Vader, L. J. van der Aa, J. F. J. Engbersen, G. Storm, and R. M. Schiffelers. A method for quantifying cellular uptake of fluorescently labeled siRNA. *Journal of controlled release: official journal of the Controlled Release Society*, 148(1):106–9, November 2010.

[173] R. H. Mo, J. L. Zaro, and W.-C. Shen. Comparison of cationic and amphipathic cell penetrating peptides for siRNA delivery and efficacy. *Molecular pharmaceutics*, 9(2):299–309, February 2012.

[174] S. Seidu-Larry, B. Krieg, M. Hirsch, M. Helm, and O. Domingo. A modified guanosine phosphoramidite for click functionalization of RNA on the sugar edge. *Chemical communications (Cambridge, England)*, 48(89):11014–6, November 2012.

[175] E. V. B. van Gaal, R. van Eijk, R. S. Oosting, R. J. Kok, W. E. Hennink, D. J. a. Crommelin, and E. Mastrobattista. How to screen non-viral gene delivery systems in vitro? *Journal of controlled release: official journal of the Controlled Release Society*, 154(3):218–32, September 2011.

[176] D. Ouyang, H. Zhang, D.-P. Herten, H. S. Parekh, and S. C. Smith. Structure, dynamics, and energetics of siRNA-cationic vector complexation: a molecular dynamics study. *The journal of physical chemistry. B*, 114(28):9220–30, July 2010.

[177] L. B. Jensen, J. Griger, B. Naeye, A. K. Varkouhi, K. Raemdonck, R. Schiffelers, T. Lammers, G. Storm, S. C. de Smedt, B. S. Sproat, H. M. Nielsen, and C. Foged. Comparison of polymeric siRNA nanocarriers in a murine LPS-activated macrophage cell line: gene silencing, toxicity and off-target gene expression. *Pharmaceutical research*, 29(3):669–82, March 2012.

[178] A. Musyanovych, J. Schmitz-Wienke, V. Mailänder, P. Walther, and K. Landfester. Preparation of biodegradable polymer nanoparticles by miniemulsion technique and their cell interactions. *Macromolecular bioscience*, 8(2):127–39, February 2008.

[179] C. Bouclier, L. Moine, H. Hillaireau, V. Marsaud, E. Connault, P. Opolon, P. Couvreur, E. Fattal, and J.-M. Renoir. Physicochemical characteristics and preliminary in vivo biological evaluation of nanocapsules loaded with siRNA targeting estrogen receptor alpha. *Biomacromolecules*, 9(10):2881–90, October 2008.

[180] G. Baier, D. Baumann, J. M. Siebert, A. Musyanovych, V. Mailänder, and K. Landfester. Suppressing unspecific cell uptake for targeted delivery using hydroxyethyl starch nanocapsules. *Biomacromolecules*, 13(9):2704–15, September 2012.

[181] G. Baier, A. Musyanovych, K. Landfester, A. Best, S. Lorenz, and V. Mailänder. DNA amplification via polymerase chain reaction inside miniemulsion droplets with subsequent poly(n-

butylcyanoacrylate) shell formation and delivery of polymeric capsules into mammalian cells. *Macromolecular bioscience*, 11(8):1099–109, August 2011.

[182] S. Lorenz, S. Tomcin, and V. Mailänder. Staining of mitochondria with Cy5-labeled oligonucleotides for long-term microscopy studies. *Microscopy and microanalysis: the official journal of Microscopy Society of America, Microbeam Analysis Society, Microscopical Society of Canada*, 17(3):440–5, June 2011.

[183] S. Lee, S. C. Yang, C.-Y. Kao, R. H. Pierce, and N. Murthy. Solid polymeric microparticles enhance the delivery of siRNA to macrophages in vivo. *Nucleic acids research*, 37(22):e145, December 2009.

[184] D. E. Lopes de Menezes, M. J. Kirchmeier, J.-F. Gagne, L. M. Pilarski, and T. M. Allen. Cellular Trafficking and Cytotoxicity of Anti-Cd19-Targeted Liposomal Doxorubicin in B Lymphoma Cells. *Journal of Liposome Research*, 9(2):199–228, January 1999.

[185] Y. Yamada, H. Akita, H. Kamiya, K. Kogure, T. Yamamoto, Y. Shinohara, K. Yamashita, H. Kobayashi, H. Kikuchi, and H. Harashima. MITO-Porter: A liposome-based carrier system for delivery of macromolecules into mitochondria via membrane fusion. *Biochimica et biophysica acta*, 1778(2):423–32, February 2008.

[186] V. Rhoden and S. M. Goldin. Formation of unilamellar lipid vesicles of controllable dimensions by detergent dialysis. *Biochemistry*, 18(19):4173–6, September 1979.

[187] A. M. Hofmann, F. Wurm, E. Hühn, T. Nawroth, P. Langguth, and H. Frey. Hyperbranched polyglycerol-based lipids via oxyanionic polymerization: toward multifunctional stealth liposomes. *Biomacromolecules*, 11(3):568–74, March 2010.

[188] S. Fletcher, A. Ahmad, W. S. Price, M. R. Jorgensen, and A. D. Miller. Biophysical properties of CDAN/DOPE-analogue lipoplexes account for enhanced gene delivery. *Chembiochem: a European journal of chemical biology*, 9(3):455–63, February 2008.

[189] S. Biswas, N. S. Dodwadkar, P. P. Deshpande, S. Parab, and V. P. Torchilin. Surface functionalization of doxorubicin-loaded liposomes with octa-arginine for enhanced anticancer activity. *European journal of pharmaceutics and biopharmaceutics: official journal of Arbeitsgemeinschaft für Pharmazeutische Verfahrenstechnik e.V*, 84(3):517–25, August 2013.

[190] T. M. Allen, P. Sapra, and E. Moase. Use of the post-insertion method for the formation of ligand-coupled liposomes. *Cellular and molecular biology letters*, 7(3):889–94, January 2002.

[191] Y. Zhang, H. Li, J. Sun, J. Gao, W. Liu, B. Li, Y. Guo, and J. Chen. DC-Chol/DOPE cationic liposomes: a comparative study of the influence factors on plasmid pDNA and siRNA gene delivery. *International journal of pharmaceutics*, 390(2):198–207, May 2010.

[192] M. S. Shim and Y. J. Kwon. Efficient and targeted delivery of siRNA in vivo. *The FEBS journal*, 277(23):4814–27, December 2010.

[193] G. G. M. D'Souza and V. Weissig. Subcellular targeting: a new frontier for drug-loaded pharmaceutical nanocarriers and the concept of the magic bullet. *Expert opinion on drug delivery*, 6(11):1135–48, November 2009.

[194] A. R. Fernie, F. Carrari, and L. J. Sweetlove. Respiratory metabolism: glycolysis, the TCA cycle and mitochondrial electron transport. *Current opinion in plant biology*, 7(3):254–61, June 2004.

[195] C. Desler, A. Lykke, and L. J. Rasmussen. The effect of mitochondrial dysfunction on cytosolic

nucleotide metabolism. *Journal of nucleic acids*, 2010, January 2010.

[196] M. T. Lin and M. F. Beal. Mitochondrial dysfunction and oxidative stress in neurodegenerative diseases. *Nature*, 443(7113):787–95, October 2006.

[197] A. Chacinska, C. M. Koehler, D. Milenkovic, T. Lithgow, and N. Pfanner. Importing mitochondrial proteins: machineries and mechanisms. *Cell*, 138(4):628–44, August 2009.

[198] C. Desler and L. J. Rasmussen. Mitochondria in biology and medicine. *Mitochondrion*, 12(4): 472–6, July 2012.

[199] G. G. M. D'Souza, S. V. Boddapati, and V. Weissig. Gene therapy of the other genome: the challenges of treating mitochondrial DNA defects. *Pharmaceutical research*, 24(2):228–38, February 2007.

[200] A. Schneider. Mitochondrial tRNA import and its consequences for mitochondrial translation. *Annual review of biochemistry*, 80:1033–53, January 2011.

[201] F. Sieber, A.-M. Duchêne, and L. Maréchal-Drouard. Mitochondrial RNA import: from diversity of natural mechanisms to potential applications. *International review of cell and molecular biology*, 287:145–90, January 2011.

[202] P. F. Chinnery. http://www.ncbi.nlm.nih.gov/books/NBK1224/. *Gene reviews (NCBI online)*, (Date accessed 20140826), August 2008.

[203] T. Pulkes and M. G. Hanna. Human mitochondrial DNA diseases. *Advanced drug delivery reviews*, 49(1-2):27–43, July 2001.

[204] J. Abbott, C. S. Francklyn, and S. M. Robey-Bond. Transfer RNA and human disease. *Frontiers in genetics*, 5(June):158, January 2014.

[205] O. Z. Karicheva, O. A. Kolesnikova, T. Schirtz, M. Y. Vysokikh, A.-M. Mager-Heckel, A. Lombès, A. Boucheham, I. A. Krasheninnikov, R. P. Martin, N. Entelis, and I. Tarassov. Correction of the consequences of mitochondrial 3243A to G mutation in the MT-TL1 gene causing the MELAS syndrome by tRNA import into mitochondria. *Nucleic acids research*, 39 (18):8173–86, October 2011.

[206] C. T. Moraes, E. Ricci, E. Bonilla, S. DiMauro, and E. A. Schon. The mitochondrial tRNA(Leu(UUR)) mutation in mitochondrial encephalomyopathy, lactic acidosis, and stroke-like episodes (MELAS): genetic, biochemical, and morphological correlations in skeletal muscle. *American journal of human genetics*, 50(5):934–49, May 1992.

[207] G. Silvestri, C. T. Moraes, S. Shanske, S. J. Oh, and S. DiMauro. A new mtDNA mutation in the tRNA(Lys) gene associated with myoclonic epilepsy and ragged-red fibers (MERRF). *American journal of human genetics*, 51(6):1213–7, December 1992.

[208] A. Verma, C. T. Moraes, R. T. Shebert, and W. G. Bradley. A MERRF/PEO overlap syndrome associated with the mitochondria1 DNA 3243 mutation. *Neurology*, 46(5):1334–1334, May 1996.

[209] N. Howell, I. Kubacka, R. Smith, F. Frerman, J. K. Parks, and W. D. Parker. Association of the mitochondrial 8344 MERRF mutation with maternally inherited spinocerebellar degeneration and Leigh disease. *Neurology*, 46(1):219–222, January 1996.

[210] P. F. Chinnery, R. W. Taylor, K. Diekert, R. Lill, D. M. Turnbull, and R. N. Lightowlers. Peptide nucleic acid delivery to human mitochondria. *Gene therapy*, 6(12):1919–28, December 1999.

[211] A. Flierl, C. Jackson, B. Cottrell, D. Murdock, P. Seibel, and D. C. Wallace. Targeted delivery

of DNA to the mitochondrial compartment via import sequence-conjugated peptide nucleic acid. *Molecular therapy: the journal of the American Society of Gene Therapy*, 7(4):550–7, April 2003.

[212] V. Geromel, A. Cao, D. Briane, J. Vassy, A. Rotig, P. Rustin, R. Coudert, J. P. Rigaut, A. Munnich, and E. Taillandier. Mitochondria transfection by oligonucleotides containing a signal peptide and vectorized by cationic liposomes. *Antisense and nucleic acid drug development*, 11(3):175–80, June 2001.

[213] R. W. Horobin, S. Trapp, and V. Weissig. Mitochondriotropics: a review of their mode of action, and their applications for drug and DNA delivery to mammalian mitochondria. *Journal of controlled release: official journal of the Controlled Release Society*, 121(3):125–36, August 2007.

[214] S. V. Boddapati, G. G. M. D'Souza, S. Erdogan, V. P. Torchilin, and V. Weissig. Organelle-targeted nanocarriers: specific delivery of liposomal ceramide to mitochondria enhances its cytotoxicity in vitro and in vivo. *Nano letters*, 8(8):2559–63, August 2008.

[215] V. Weissig, S.-M. Cheng, and G. G. M. D'Souza. Mitochondrial pharmaceutics. *Mitochondrion*, 3(4):229–44, March 2004.

[216] L. B. Chen. Mitochondrial membrane potential in living cells. *Annual review of cell biology*, 4: 155–81, January 1988.

[217] W. J. Rhee and G. Bao. Slow non-specific accumulation of 2'-deoxy and 2'-O-methyl oligonucleotide probes at mitochondria in live cells. *Nucleic acids research*, 38(9), May 2010.

[218] G. G. M. D'Souza, R. Rammohan, S.-M. Cheng, V. P. Torchilin, and V. Weissig. DQAsome-mediated delivery of plasmid DNA toward mitochondria in living cells. *Journal of controlled release: official journal of the Controlled Release Society*, 92(1-2):189–97, September 2003.

[219] R. a. J. Smith, R. C. Hartley, H. M. Cochemé, and M. P. Murphy. Mitochondrial pharmacology. *Trends in pharmacological sciences*, 33(6):341–52, June 2012.

[220] L. V. Johnson, M. L. Walsh, B. J. Bockus, and L. B. Chen. Monitoring of relative mitochondrial membrane potential in living cells by fluorescence microscopy. *The Journal of cell biology*, 88 (3):526–35, March 1981.

[221] S. Biswas, N. S. Dodwadkar, R. R. Sawant, A. Koshkaryev, and V. P. Torchilin. Surface modification of liposomes with rhodamine-123-conjugated polymer results in enhanced mitochondrial targeting. *Journal of drug targeting*, 19(7):552–61, August 2011.

[222] C. Troiber, J. C. Kasper, S. Milani, M. Scheible, I. Martin, F. Schaubhut, S. Küchler, J. Rädler, F. C. Simmel, W. Friess, and E. Wagner. Comparison of four different particle sizing methods for siRNA polyplex characterization. *European journal of pharmaceutics and biopharmaceutics*, 84(2):255–64, June 2013.

[223] X. Li, G. Zhang, N. Ngo, X. Zhao, S. R. Kain, J. B. Chem, and C. Huang. Protein chemistry and structure: Deletions of the Aequorea victoria Green Fluorescent Protein Define the Minimal Domain Required for Fluorescence Deletions of the Aequorea victoria Green Fluorescent Protein Define the Minimal Domain Required for Fluoresc. *The Journal of biological chemistry*, 272: 28545–28549, 1997.

[224] N. Kitsera, A. Khobta, and B. Epe. Destabilized green fluorescent protein detects rapid removal of transcription blocks after genotoxic exposure. *BioTechniques*, 43(2):222–7, August 2007.

[225] Sanguine. http://technical.sanguinebio.com/understanding-mfi-in-the-context-of-facs-data/. *Understanding MFI in the context of FACS data — Sanguine Bio Researcher Blog*, (Date accessed 20140826), 2014.

[226] D. S. Schwarz, G. Hutvágner, B. Haley, and P. D. Zamore. Evidence that siRNAs function as guides, not primers, in the Drosophila and human RNAi pathways. *Molecular cell*, 10(3): 537–48, September 2002.

[227] P. Y. Chen, L. Weinmann, D. Gaidatzis, Y. Pei, M. Zavolan, T. Tuschl, and G. Meister. Strand-specific 5'-O-methylation of siRNA duplexes controls guide strand selection and targeting specificity. *RNA (New York, N.Y.)*, 14(2):263–74, February 2008.

[228] S. Tomcin. *Analyse der intrazellulären Freisetzung von Wirkstoffmodellen via konfokaler Laser-Raster-Mikroskopie*. PhD thesis, Max Planck Institute for Polymer Research Mainz, 2014.

[229] T. Fritz. Functionalizable liposomes made by dual asymmetric centrifugation. *Diploma Thesis*, (Johannes Gutenberg-Universität Mainz), 2012.

[230] P. S. Uster, T. M. Allen, B. E. Daniel, C. J. Mendez, M. S. Newman, and G. Z. Zhu. Insertion of poly(ethylene glycol) derivatized phospholipid into pre-formed liposomes results in prolonged in vivo circulation time. *FEBS letters*, 386(2-3):243–6, May 1996.

[231] O. K. Nag, V. R. Yadav, A. Hedrick, and V. Awasthi. Post-modification of preformed liposomes with novel non-phospholipid poly(ethylene glycol)-conjugated hexadecylcarbamoylmethyl hexadecanoic acid for enhanced circulation persistence in vivo. *International journal of pharmaceutics*, 446(1-2):119–29, March 2013.

[232] D. L. Iden and T. M. Allen. In vitro and in vivo comparison of immunoliposomes made by conventional coupling techniques with those made by a new post-insertion approach. *Biochimica et biophysica acta*, 1513(2):207–16, August 2001.

[233] I. Khalil, K. Kogure, S. Futaki, and H. Harashima. High density of octaarginine stimulates macropinocytosis leading to efficient intracellular trafficking for gene expression. *The Journal of biological chemistry*, 281(6):3544–51, February 2006.

Appendix

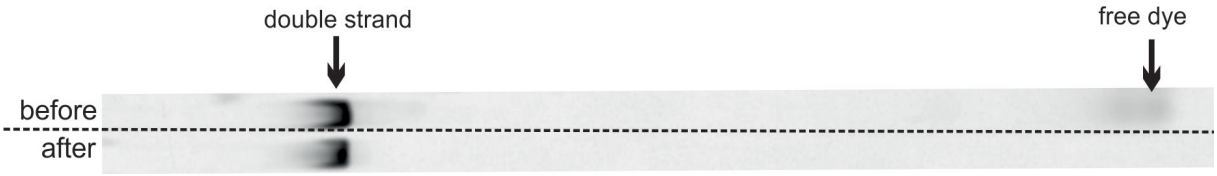

Figure A1: Non denaturating PAGE analysis of gel extraction as a method to remove free dye. Alexa 555 labeled double strand before and after gel extraction. Ex 532 nm, Em 580BP30.

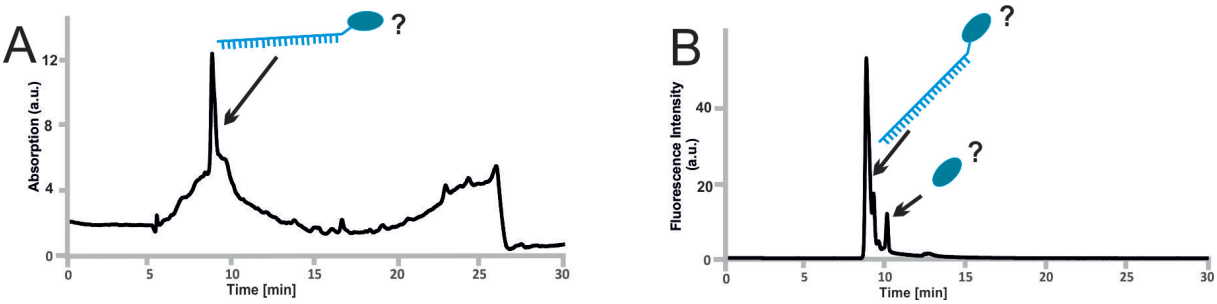

Figure A2: Purification of an Atto 488 labeled ss RNA by RP HPCL. Chromatograms of (A) absorption at 254 nm and (B) fluorescence at Ex 490 nm, Em 520 nm.

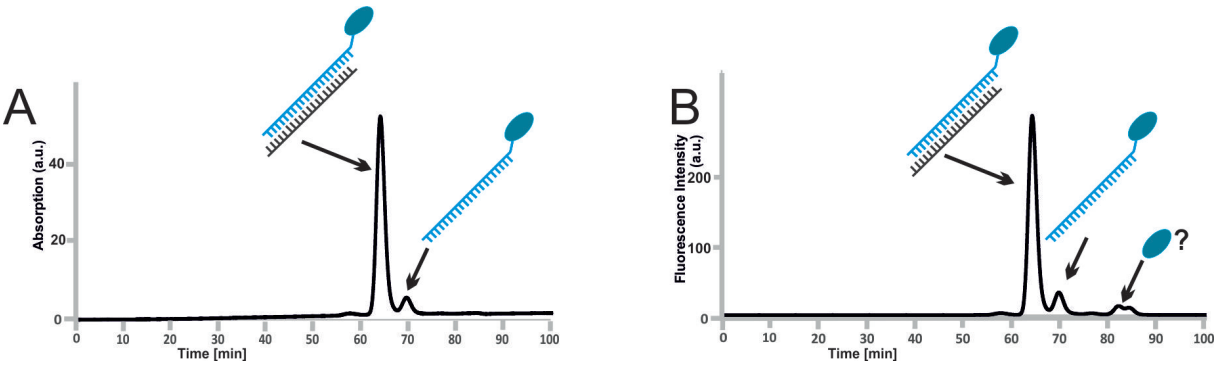

Figure A3: SEC of an Atto 488 labeled ds RNA at a flow rate of 0.25 mL/min. Chromatograms of (A) absorption at 254 nm and (B) fluorescence at Ex 490 nm, Em 520 nm.

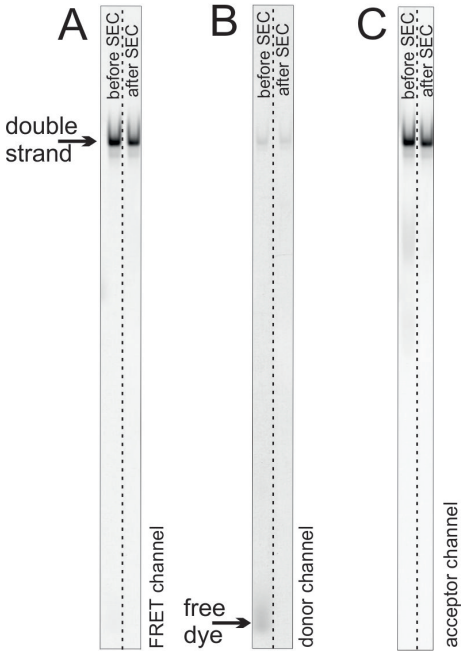

Figure A4: (A-C) Non denaturating PAGE analysis of SEC purified Alexa 555/ Atto 647N labeled ds RNA. (A) FRET channel: Ex 532, Em 670BP30, (B) donor channel: Ex 532, Em 580BP30, (C) acceptor channel: Ex 633 nm, Em 670BP30.

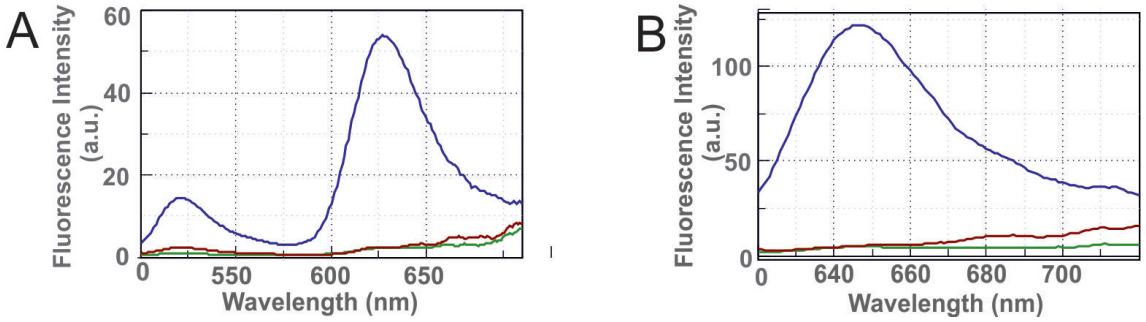

Figure A5: Fluorescence quenching of poly-L-lysine brushes and block copolymers with another FRET labeled siRNA. Emission spectra of 1 µM Atto 488/ Atto 590 labeled siRNA (blue) only, (green) complexed in brushes at cc_1 and (red) in block copolymers at cc_1 at (A) donor excitation (488 nm) and (B) acceptor excitation (532 nm).

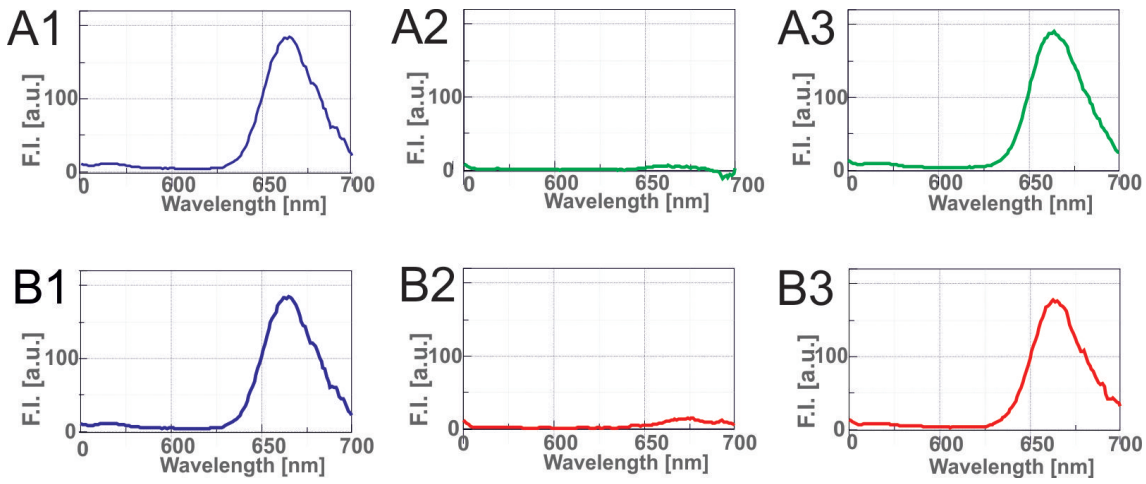

Figure A6: Ruling out that quenching in polyplexes is caused by sedimentation for (A) PLL brushes and (B) block copolymers. Spectra at donor excitation (543 nm) for 0.5 µM Alexa 555/ Atto 647N labeled siRNA (1) only, (2) complexed at cc_1 and (3) after transfer in a second cuvette and release with heparin at z^-_{Hep}/z^-_{RNA} 20.

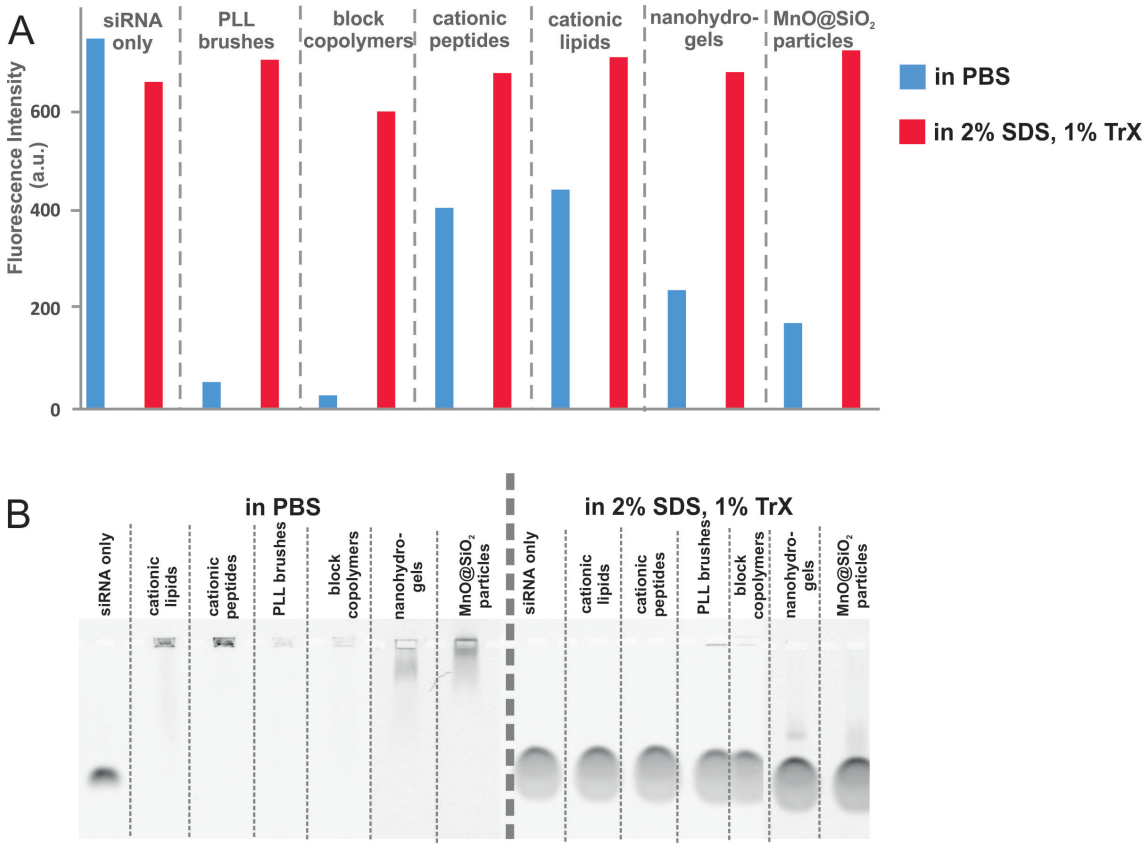

Figure A7: Controls for SDS/TrX release from polyplexes at cc_1. (A) Fluorimetric measurements of polyplexes in PBS and in 2% SDS and 1% TrX at an siRNA concentration of 0.23 µM, acceptor signal: Ex 561 nm, Em 610 nm. (B) EMSA of Atto 488/ Atto 590 labeled siRNA in polyplexes in PBS and in 2% SDS and 1% TrX, acceptor channel: Ex 532, Em 670BP30.

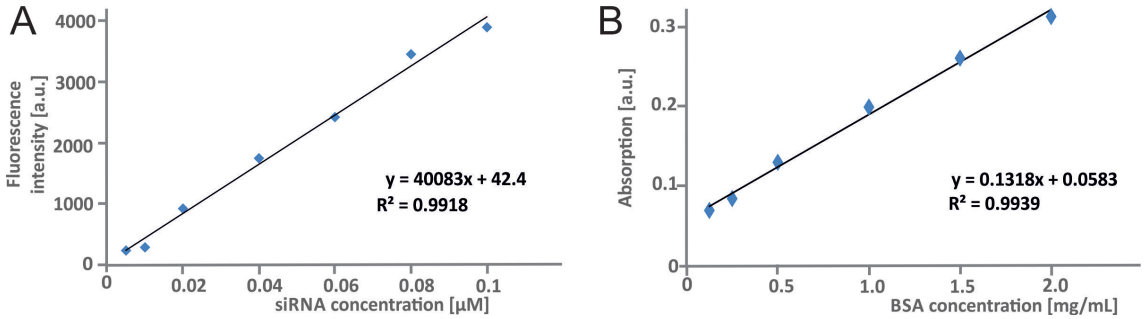

Figure A8: Calibration curves for siRNA quantification in cell lysate. (A) Titration of Atto 488/ Atto 590 labeled siRNA in cell lysate, acceptor signal: Ex 561 nm, Em 610 nm, (B) Calibration of bovine serum albumin (BSA) in 2% SDS and 1% TrX, absorption at 503 nm.

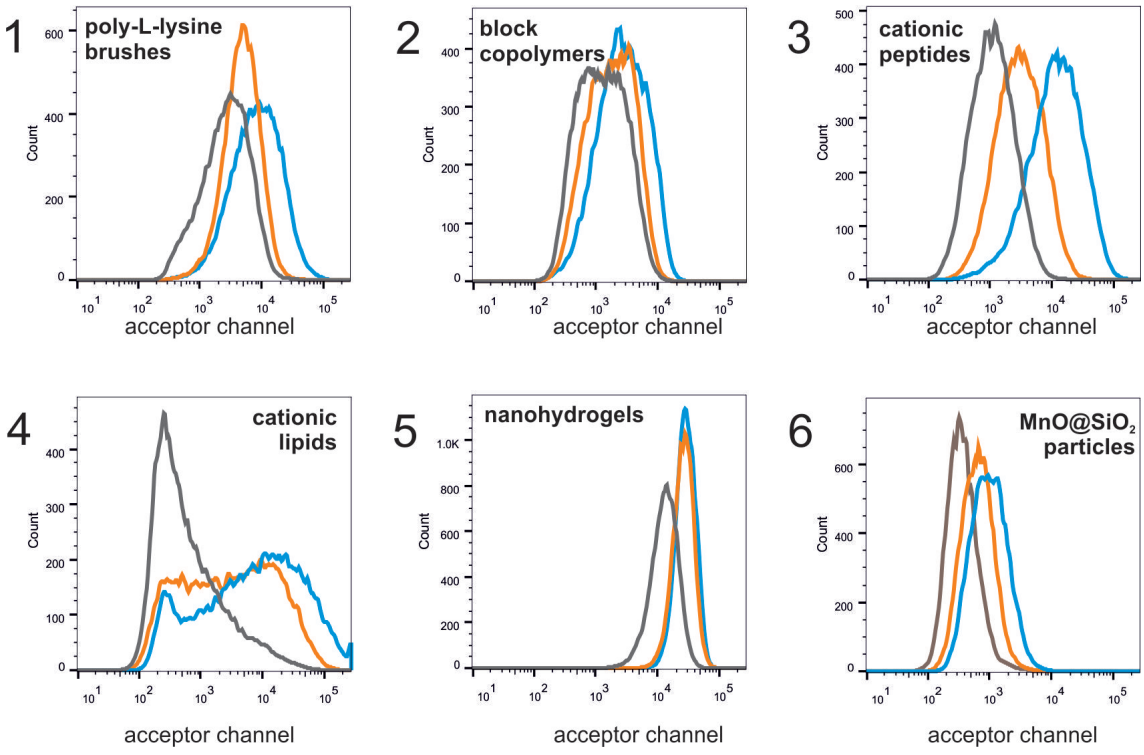

Figure A9: Histograms of the flow cytometric acceptor channel after 4 h (blue curve), 12 h (orange curve) and 24 h (grey curve) for (1) poly-L-lysine brushes, (2) block copolymers, (3) cationic peptides, (4) cationic lipids, (5) nanohydrogels, (6) MnO@SiO_2 particles.

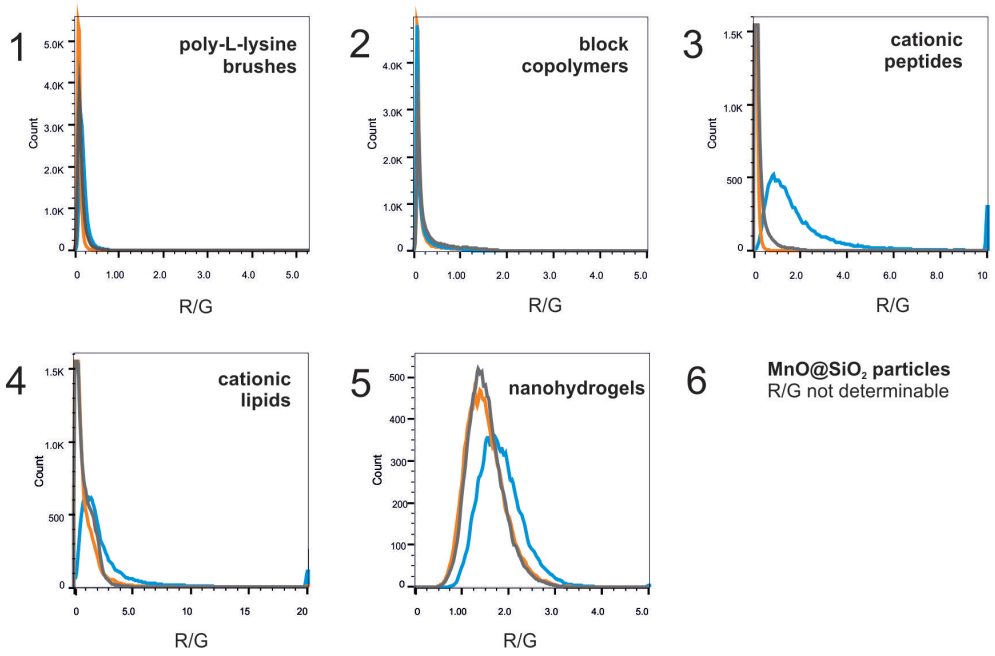

Figure A10: Histograms of the intracellular R/G values after 4 h (blue curve), 12 h (orange curve) and 24 h (grey curve) for (1) poly-L-lysine brushes, (2) block copolymers, (3) cationic peptides, (4) cationic lipids, (5) nanohydrogels, (6) MnO@SiO_2 particles.

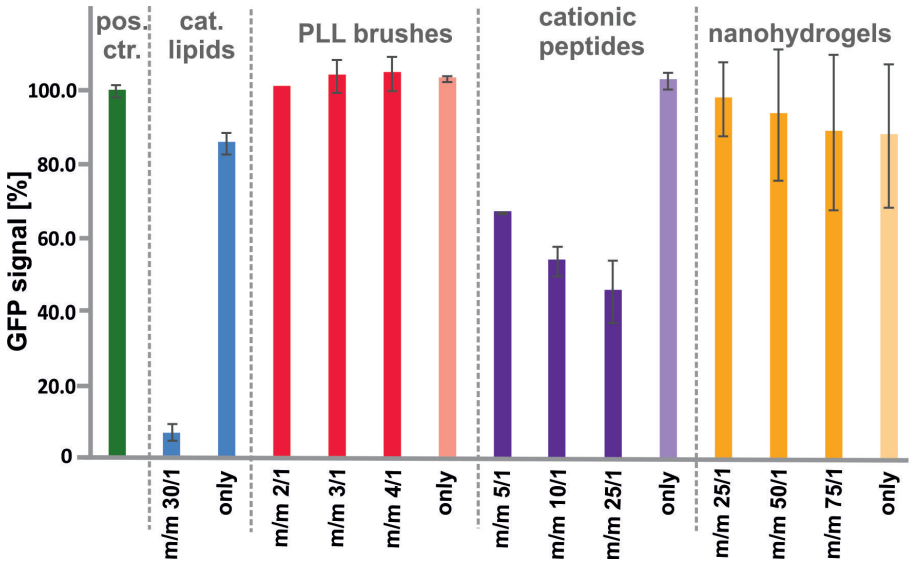

Figure A11: HeLa MAZ knockdown of polyplexes with Alexa 555/ Atto 647N labeled siRNA at 30 nM. Three different m/m ratios starting from cc_1 were tested for cationic lipids, PLL brushes, cationic peptides and nanohydrogels, lipids transfected at m/m 30/1 according to the manufacturer's instructions.

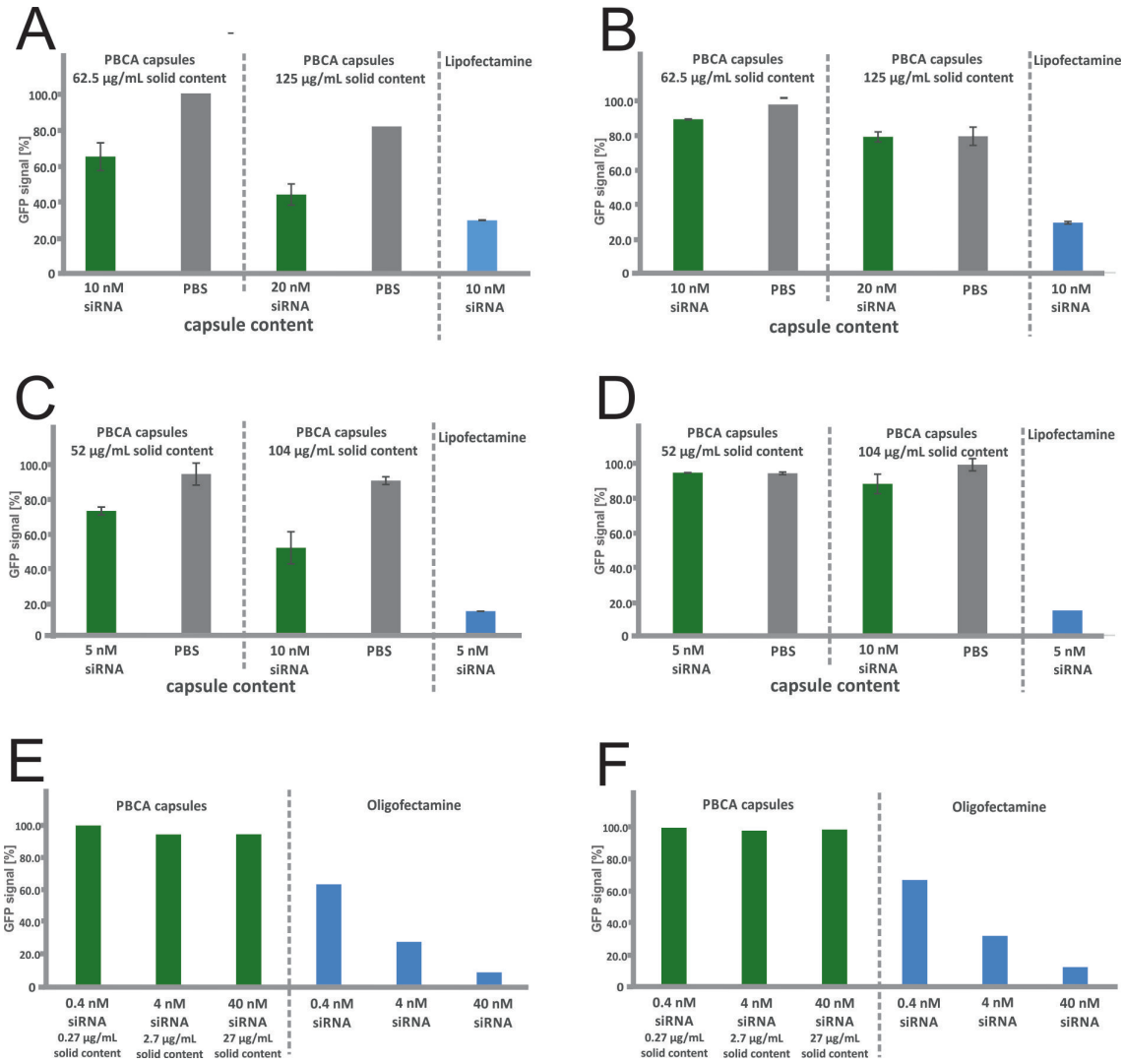

Figure A12: eGFP reporter gene assays for nanocapsules. Each batch was tested in duplicate without obtaining reproducible effects. (A and B) Atto 488/ Atto 590 labeled siRNA containing capsules and control capsules containing PBS only tested in the HEK cell two step setup, (C and D) Alexa 555 labeled siRNA containing capsules and control capsules containing PBS only tested with HeLa MAZ cells, (E and F) Alexa 555/ Atto 647N labeled siRNA containing capsules tested with HeLa MAZ cells, (E) readout after 24 h, (F) readout after 48 h, GFP signal of positive control always 100%.

Table A1: Specifications of PBCA nanocapsule batches obtained from xxxx

batch	Date obtained	content	label on siRNA	c siRNA [µM][a]	solid content mg/mL[b]
GB-BK 001	17.03.2011	siRNA in PBS	Atto 488/ Atto 590	0.8	5
GB-BK 002	17.03.2011	PBS			5
GB-BK 003	20.05.2011	PBS			11.5
GB-BK 004	13.01.2012	siRNA in PBS	Alexa 555	1	10
GB-BK 005	08.08.2013	siRNA in PBS	Alexa 555/ Atto 647N	12	8
GB-BK 006	08.08.2013	PBS			10

[a]theoretical value for 50% inclusion of the amount of siRNA employed in the synthesis

[b]solid content of capsule material (PBCA), *in vitro* toxicity above 75 µg/mL.

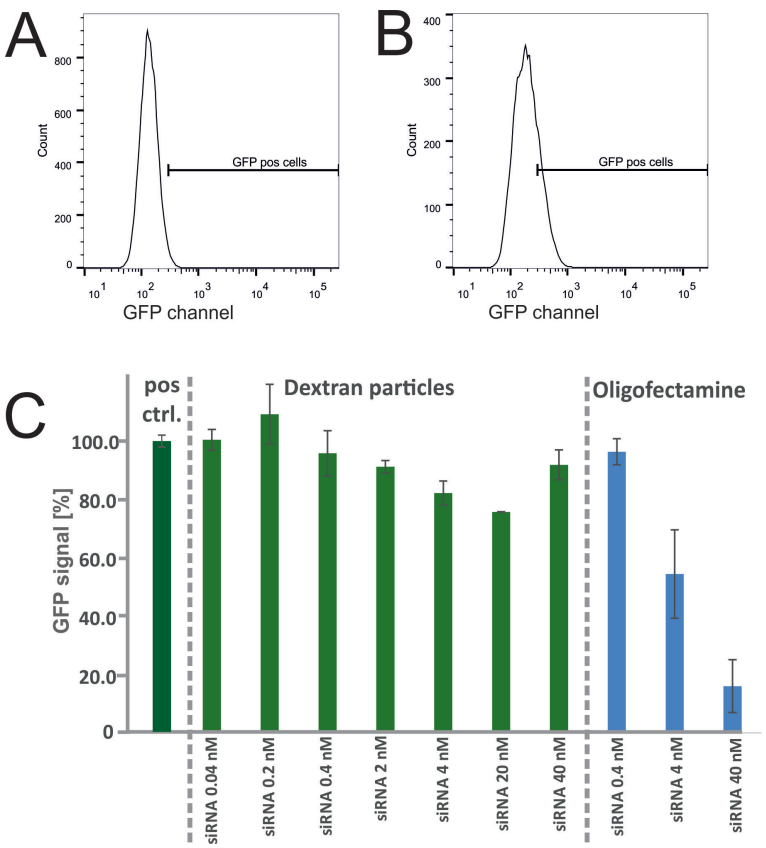

Figure A13: Knockdown of dextran particles. (A) GFP channel for (no eGFP expressing) HeLa cells after transfection of 30 nM Alexa 555/ Atto 647N labeled siRNA with Oligofectamine^{TM}, (B) GFP channel for (no eGFP expressing) HeLa cells after transfection of the same amount of siRNA with dextran particles. (C) Knockdown assay with HeLa MAZ cells. GFP signal of dextran particles normalized to empty particles of the same concentration, GFP signal overestimated due to bleedthrough.

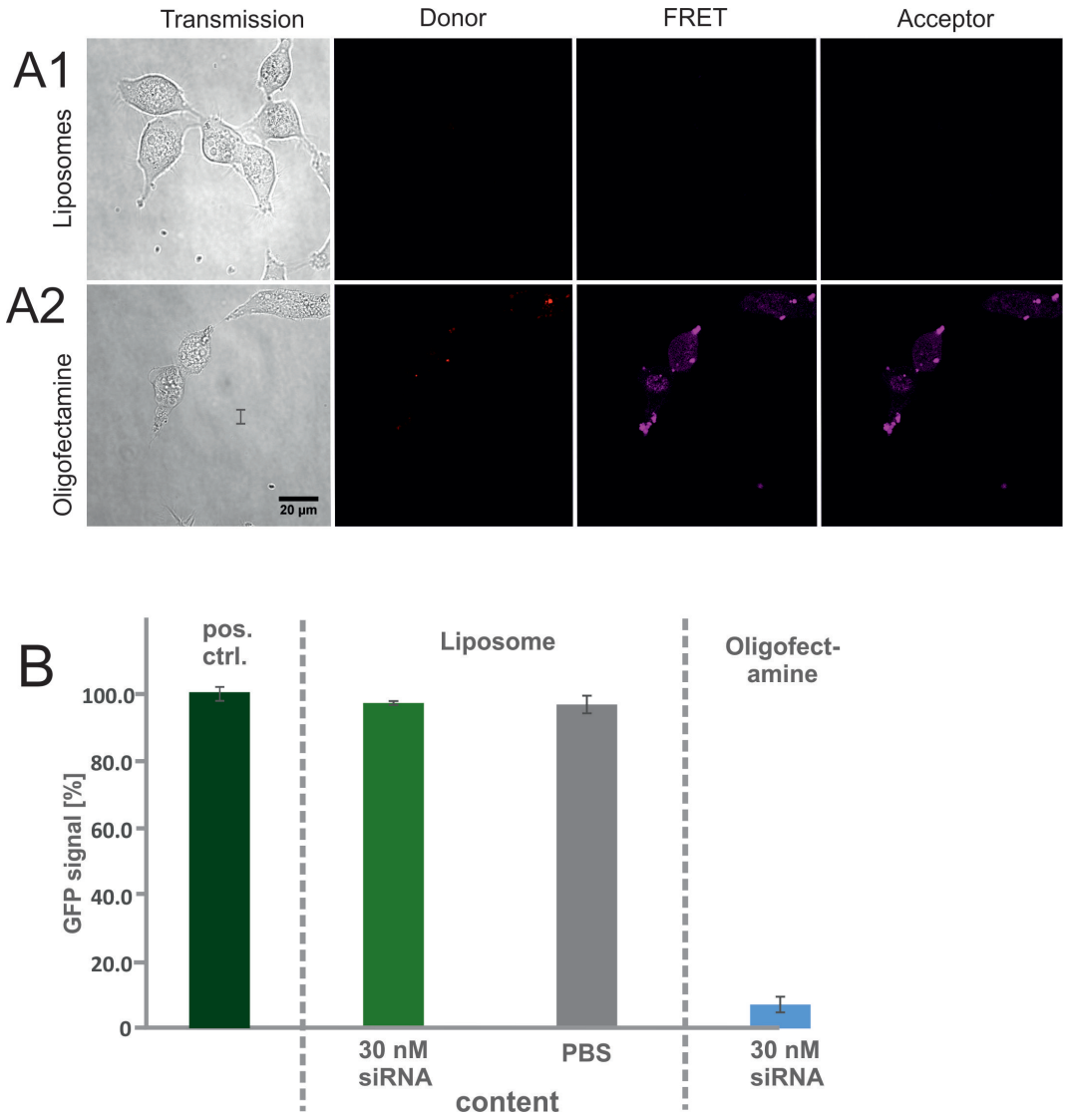

Figure A14: *In vitro* assays with liposomes. (A1) Confocal images after 4 h incubation of liposomes at 80 nM Alexa 555/ Atto 647N labeled siRNA, (A2) transfection under identical conditions with Oligofectamine^{TM}. (B) HeLa MAZ knockdown of liposomes at 30 nM Alexa 555/ Atto 647N labeled siRNA, control liposomes containing PBS and 30 nM siRNA transfected with Oligofectamine.

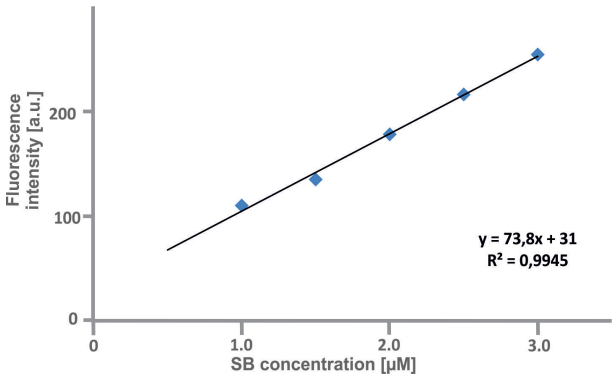

Figure A15: Calibration of Sulforhodamin B in 0.5% TrX, samples analyzed on a microplate reader at Ex 560 nm and Em 590 nm.

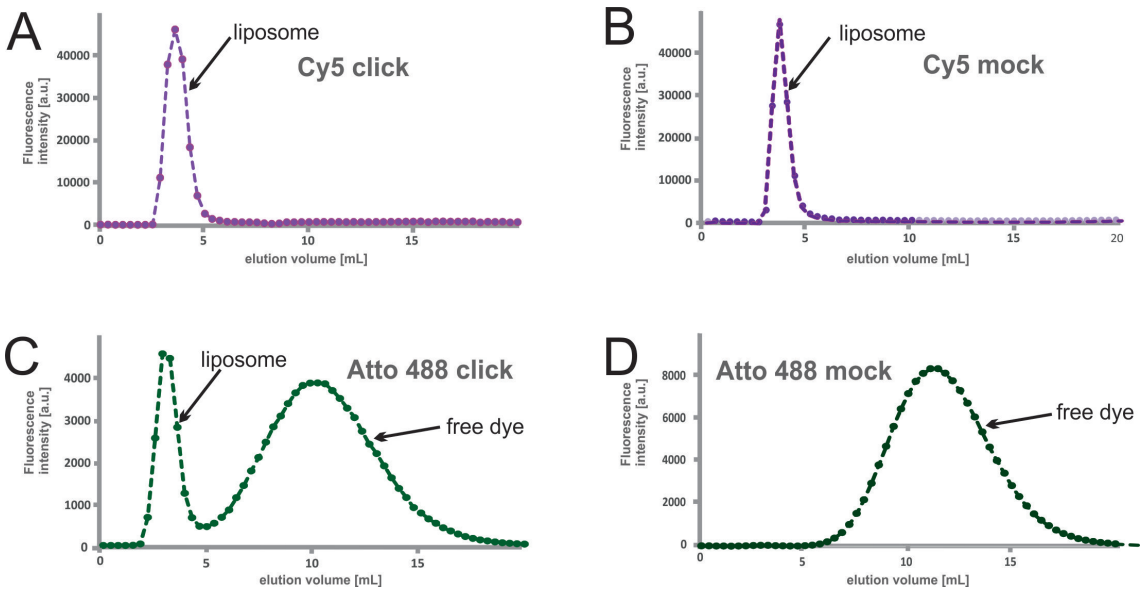

Figure A16: Purification of liposome click. Azide carrying dyes were attached to liposomes containing a cholesterol derivative with terminal alkynes. Chromatograms of the purification with a Sephadex^{TM} G100 column for (A) CuAAC with Cy5 azide, (B) mock incubation with Cy5 azide (Ex 645 nm, Em 675 nm), (C) CuAAC with Atto 488, (D) mock incubation with Atto 488 (Ex 488 nm, Em 520 nm).

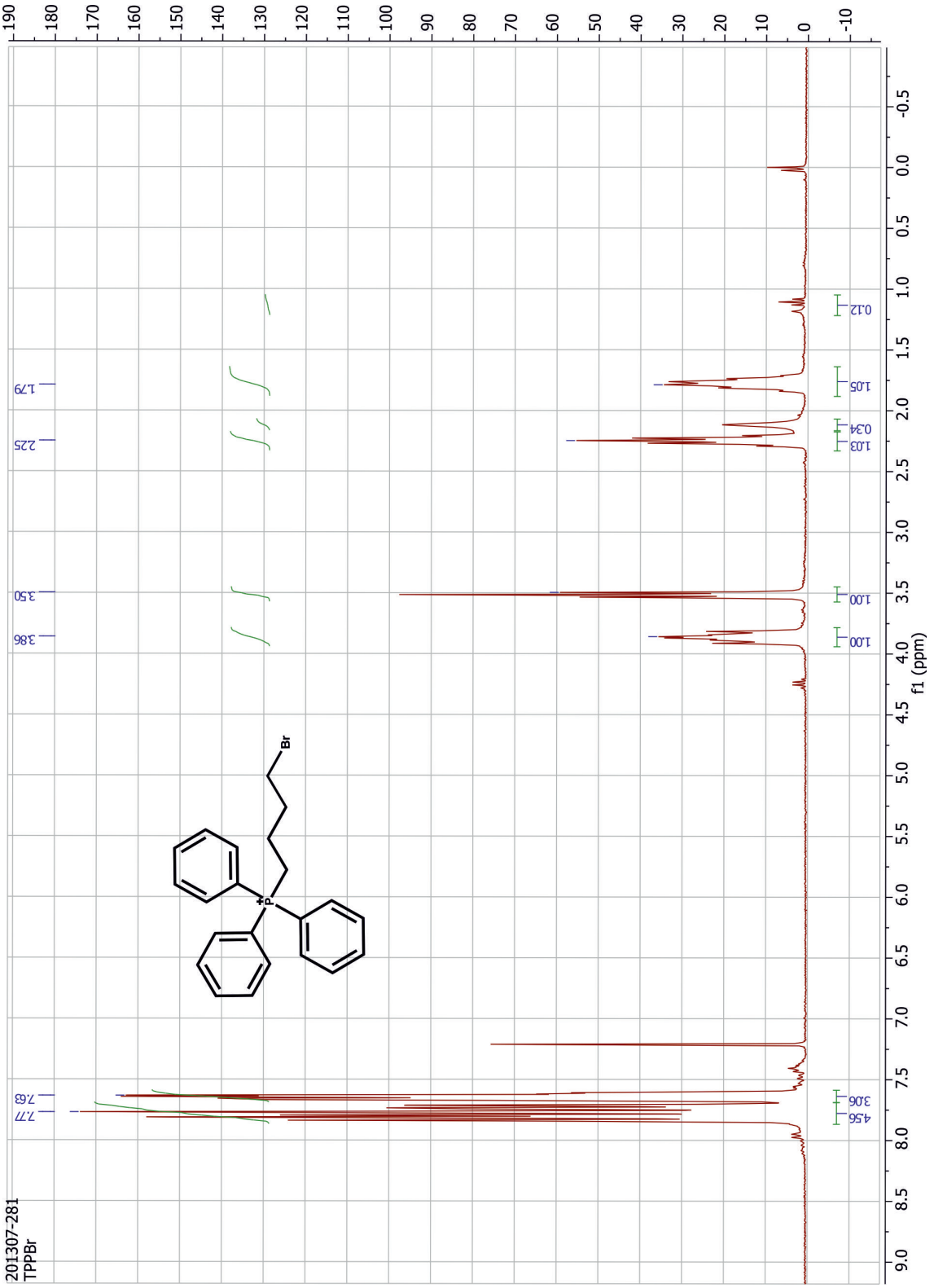

Figure A17: TPP bromide (starting material) NMR spectrum

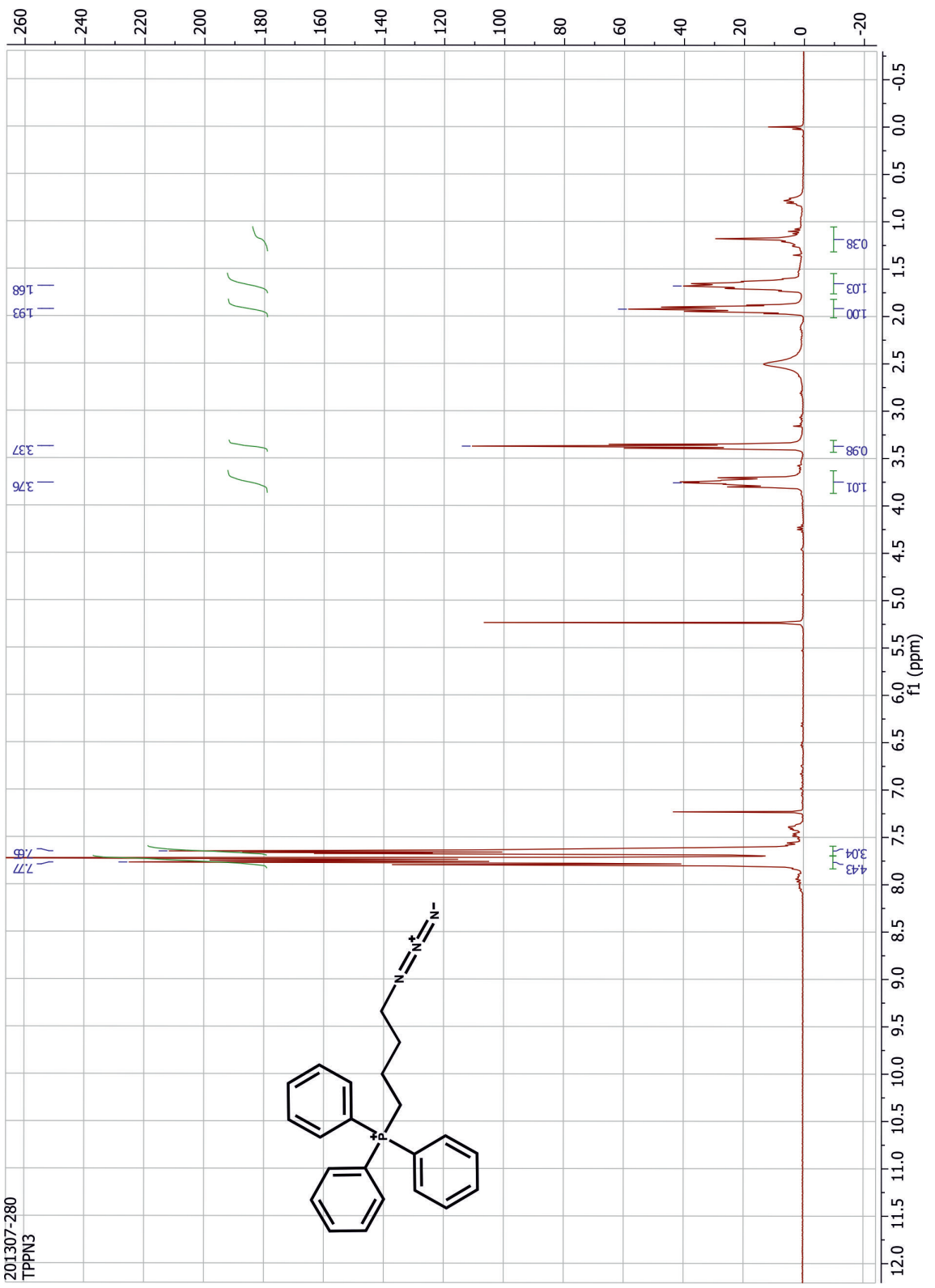

Figure A18: TPP azide (product) NMR spectrum

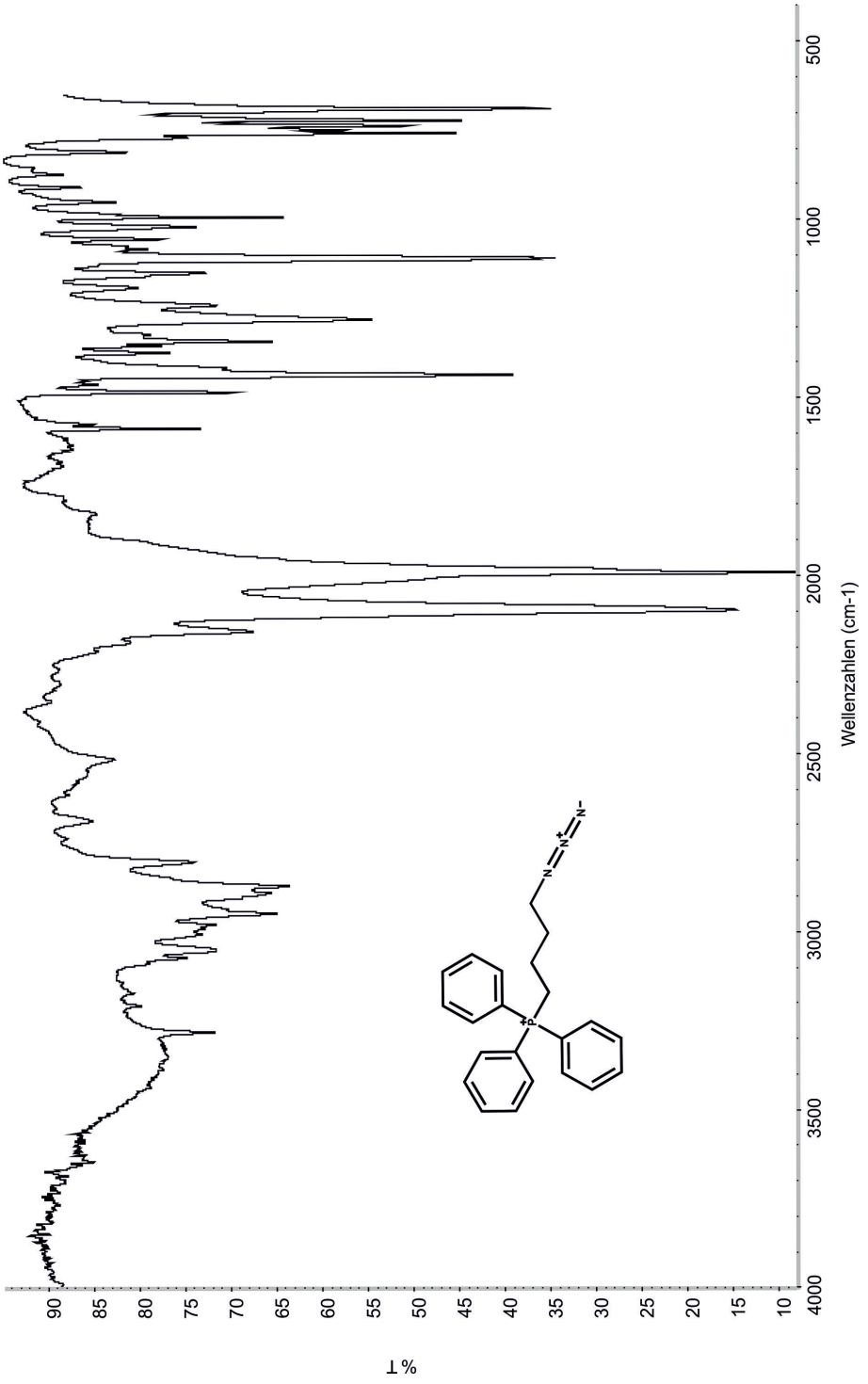

Figure A19: TPP azide IR spectrum

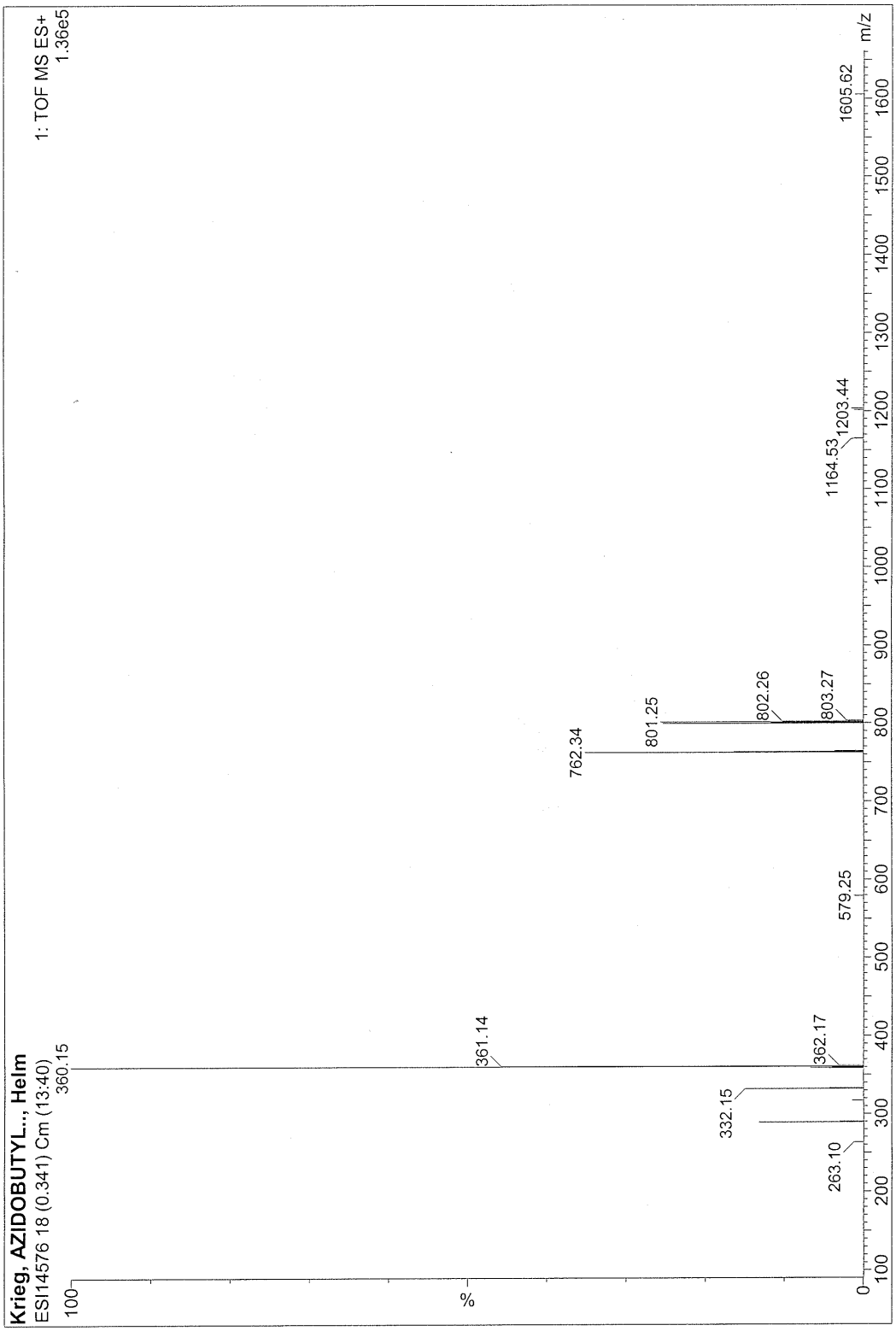

Figure A20: TPP azide HR-ESI-ToF-MS spectrum

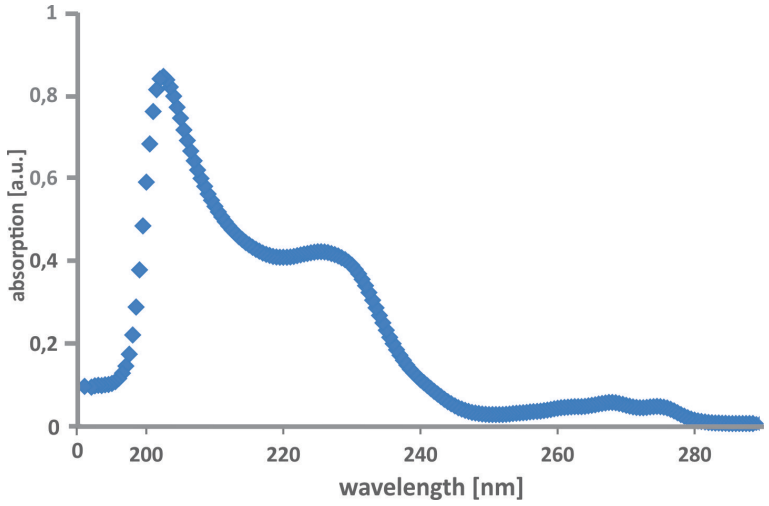

Figure A21: TPP azide absorption spectrum